IMPACT OF Y14 PHOSPHORYLATION OF CAVEOLIN-1 ON ITS BINDING PARTNERS: A PROTEOMIC ANALYSIS

by

Sandeep Saxena

B.tech., Rajasthan Technical University, 2010

A THESIS SUBMITTED IN PARTIAL FULFILLMENT OF

THE REQUIRMENTS FOR THE DEGREE OF

MASTER OF SCIENCE

in

The Faculty of Graduate and Postdoctoral Studies

(Cell and Developmental Biology)

THE UNIVERSITY OF BRITISH COLUMBIA

(Vancouver)

May 2016

ABSTRACT:

Caveolae, a special type of lipid-raft, are cave-like invaginations of plasma-membrane maintained and formed by Caveolins (Cav1, 2 and 3) and Cavin 1 and 2. Caveolae regulate various trafficking and signaling pathways. Cav1, a 178 amino acid protein has a Src-dependent tyrosine-14 phosphorylation site that regulates integrin signaling and focal adhesion dynamics, and a Caveolin Scaffolding Domain (CSD) that physically interacts with multiple proteins.

Glutathione-S-transferase (GST) pull-downs and quantitative proteomics analysis (Maxquant) were performed using lysates from the DU145 prostate cancer cell line and GST-beads tagged with the N-terminal polypeptide of Cav1 (amino acids 1-101) incorporating phosphomimeitic (Y14D) and non-phosphorylatable (Y14F) mutations. Proteomic analysis showed 1.5 fold increased interaction of 196 and 78 proteins with Cav1(1-101)Y14D and Cav1(1-101)Y14F, respectively. Gene Ontology (GO) analysis revealed that Cav1(1-101)Y14D interacted more with proteins that regulate cell stress, proliferation, signal transduction, metabolic processes, apoptosis (Heat shock protein-90 (HSP90)) and focal adhesions, whereas Cav1(1-101)Y14F interacted more with proteins that regulate actin cytoskeleton and RNA processing. Pseudopod-enriched proteome list from DU145 cells revealed 84 proteins overlapping with the Cav1(1-101)Y14D interactome. Comparative proteomics analysis of the CSD mutants (F92A/V94A) suggested that one-third binding proteins of Cav1(1-101)Y14D and Cav1(1-101)Y14F were influenced by this mutation. Binding specificity of Y14 phosphorylation on Cav1 is partially affected by these CSD mutations.

Pseudopod enriched HSP90 was one of the top hits in the Cav1(1-101)Y14D interactome. Inhibition of HSP90 with 17-N-allylamino-17-demethoxygeldanamycin (17AAG) increased expression of Protein Kinase B (also known as AKT) and Cav1 in pCav1 (Y14 phosphorylated

Cav1) expressing DU145 and PC3 prostate cancer cell lines. However, there was no effect of HSP90 inhibition on pCav1 lacking DU145 and Cav1 knocked-down PC3 cells. Reduced cell migration and viability was observed after 17AAG treatment of DU145 (stably expressing various Cav1 mutants) and PC3 in pCav1 dependent manner. This suggests the HSP90 function in regulating cell migration rely on pCav1.

This study reveals that Y14 phosphorylation impacts Cav1 interaction with different proteins and is partially affected by CSD mutants in our study. Also, pCav1 specific interaction with HSP90 decreases prostate cancer cell migration.

PREFACE

This work was conducted at the Life Sciences Institute (LSI), University of British Columbia (UBC) by Sandeep Saxena under the supervision of Dr. Ivan Robert Nabi. All the prostate cancer cell lines are from Nabi lab, extensively used for various projects, originally from ATCC and are mycoplasma negative. Dr. Bharat Joshi helped with the cloning and preparation of the GST-Cav1(1-101) constructs. Dr. Jay Shankar with the GST pulldowns and proteomics analysis and provided the DU145 pseudopod proteomics data. Proteomics samples were processed for Mass Spectrometry (MS) in Dr. Leonard Foster's lab, CHIBI, UBC with the assistance of Jenny Moon.

Contribution in publication: (In preparation)

Regulation of focal adhesion tension and cell migration by tyrosine phosphorylated caveolin-1 requires an intact scaffolding domain.

Fanrui Meng[1], **Sandeep Saxena**[1], Jay Shankar[1], Bharat Joshi[1], Pascal Bernatchez[2] and Ivan R. Nabi[1]*

[1] Cellular and Physiological Sciences, Life Sciences Institute, University of British Columbia, Vancouver, Canada

[2] Department of Anesthesiology, Pharmacology, & Therapeutics, University of British Columbia, Vancouver, Canada

* Corresponding author

SS performed the GST pull down assay, proteomics analysis and western blot validation of vinculin binding of GST constructs.

TABLE OF CONTENTS

LIST OF TABLES

LIST OF FIGURES

(Introduction section)

(Result section)

LIST OF ABBREVIATIONS

17AAG- 17-N-allylamino-17-demethoxygeldanamycin

2D-DIGE— 2-D Fluorescence Difference Gel Electrophoresis

2DE— 2-Dimensional Electrophoresis

BCR— Breakpoint Cluster Region

Cav1—Caveolin 1

CCM— Calcium Concentration Microdomain

ccRCC—Clear Cell Renal Cell Carcinoma

ChoPlas—Choline Plasmogen

CRAC— Cholesterol Recognition Amino acid Consensus

CSD — Caveolin-1 Scaffolding Domain

Csk — C-terminal Src kinase

COX— CyclOXygenase

DRM — Detergent Resistant Membrane

DTCs— Disseminated Tumor Cells

DTX— DoceTaXal

ECM — ExtraCellular Matrix

EGFR — Epidermal Growth Factor Receptor

EMT — Epithelial Mesenchymal Transition

EM — Electron Microscopy

ESI—ElectroSpray Ionization

FA — Focal Adhesion

FAK — FA Kinase

GAP — GTPase Activating Protein

GDP — Guanine DiPhosphate

GEF — Guanine nucleotide Exchange Factor

GO— Gene Ontology

GPI — GlycosyiPhosphatidylInositol

Grb7 — Growth factor receptor-bound protein 7

GST— Glutathione S Transferase

GTP — Guanine TriPhosphate

HCC—HepatoCellular Carcinoma

His — Histone

HSPs— Heat Shock Proteins

HSP90— Heat Shock Proteins-90

HSP70— Heat Shock Proteins-70

ICAT—Isotope Coded Affinity Tags

IEF— IsoElectric Focusing

IMAC—Immobilized Metal ion Affinity Chromatography

iTRAQ—isobaric Tags for Relative and Absolute Quantification

LC-MS—Liquid Chromatography-Mass Spectrometry

MALDI—Matrix-Assisted Laser Desorption/Ionization

MET — Mesenchymal Epithelial Transition

MS—Mass Spectrometery

PANTHER—Protein ANalysis THrough Evolutionary Relationships

PG— ProstaGlandin

PTEN — Phosphatase and Tensin Homolog

PTRF — Polymerase Transcript Release Factor

pCav1 — Tyrosine- 14 phophorylated caveolin- 1

PTM— Post Translational Modifications

ROCK — Rho-ssociated protein Kinase

SH2 — Src Homology 2

shRNA — Short hairpin RiboNucleic Acid

SILAC—Stable Isotope Labeling by Amino acids in Cell culture

siRNA — Small interfering RiboNucleic Acid

TAILS—Terminal Amine Isotopic Labeling of Substrates

TOF— Time Of Flight

VIP21 — Vesicular Integral-membrane Protein of 21 kDa

ACKNOWLEDGEMENTS

Finally, I would like to thank my parents, my elder brother and sister-in-law, the rest of my family, and my wife-to-be, Sruthi Purushothaman, for their love, support and believing in me.

DEDICATION

To my parents

CHAPTER 1: INTRODUCTION

1.1 CANCER

1.1.1 Overview of cancer

Cancer is defined as an abnormal, rapid, uncontrolled growth of cells and has the capacity to spread from one part to other parts of the body and is a leading cause of death globally **(Guan, 2015; Chaffer and Weinberg, 2011)**. The symptoms of cancer include formation of a new mass of tissue, abnormal weight loss and bleeding. Radiation therapy, surgery, chemotherapy and targeted therapy are used to treat cancer **(Vanneman and Dranoff, 2012)**. Till date, there are more than 100 different reported types of cancer. All tumors are not cancerous like the benign tumors that reside at one place and are curable. They include adenomas (tumor of epithelial cells of gland), fibromas (tumor of fibroblast and connective tissue), lipomas (tumor of fat cells) **(Hakim et. al, 2015)** etc. On the other hand malignant tumors spread to distant region and show 6 different hallmarks of cancers: uncontrolled cell division and growth, uninterrupted cell division or growth, evading programmed cell death, unlimited number of cell divisions, increased angiogenesis and capacity to invade and metastasize **(Hanahan and Weinberg, 2000; 2011)**. Commonly all cancers have metastatic potential to form secondary tumors at distant sites **(Zeichner et.al, 2016)** like lung cancer **(Popper, 2016)**, ovarian cancer **(Kyriazi, 2010)**, pancreatic cancer **(Bertucci et.al, 2013)**, prostate cancer etc. Among various cancer types, prostate cancer is slow growing and has no particular symptoms during initial stages and is the second most common type of cancer. It is also the most common cancer in males having less treatment options in advance stages of prostate cancer.

1.1.1.1 Prostate cancer

Prostate cancer is a tumor of the prostate gland (part of the male reproductive system) in men. It is able to metastasize to other body parts and produce secondary tumors mainly in bones and lymph nodes. It was shown that certain kinases such as RAF family members, MERTK, and NTRK2 promote prostate cancer to spread into bone and visceral (**Faltermeiera et.al, 2015**). Prostate cancer usually grows slowly with relatively no initial symptoms but as it progresses, common features of this cancer are urinary dysfunction, pain during urination, blood in urine or pain in pelvis area. Disseminated Tumor Cells (DTCs) have the capacity to remain dormant for a long time (≈ 10 years) and are present in early detection of prostate cancer (**Morgan et. al, 2009; Morrissey et.al, 2015**).

Various genes and proteins are altered or mutated in cancer which help tumor cell to grow and proliferate. Prostate cancer cells silence ZIP1 protein (a metabolic regulator to produce semen) and use the energy (ATP) to grow and divide (**Costello and Franklin, 2006**). p53 inactivation through over expressed MDM2 and p21 transactivation regulates prostate cancer progression (**Osman et. al,, 1999; Muller and Vousden, 2012**). There is a loss of the tumor suppressor proteins PTEN and KAI1 in metastatic prostate cancers (**Ferraldeschi et. al, 2015**). Caveolin 1 (Cav1) protein expression is elevated which helps to reduce Tg stimulated apoptosis (**Karam et.al, 2007**). TGF-β was shown to be an important regulator of tumor cell migration and invasion in prostate cancer via PI3K/AKT signaling by increasing cyclooxygenase (COX)-2 levels and secretion of prostaglandin (PG)E$_2$ (**Vo et. al, 2013**).

1.2 CANCER CELL MIGRATION

Tumor progression consists of various steps that mainly involve the alteration of signaling and metabolic pathways and increase the chance of survival **(Jang et. al, 2013; McCubrey et. al, 2015)**. Metastasis is one of the hallmarks of cancerous cells in which tumor cell migrates from the primary tumor site and invades to other body parts and produces secondary tumors.

Cell migration is the key event in various vital processes like embryogenesis, morphogenesis, neurogenesis, angiogenesis, organogenesis, regeneration, wound healing and inflammation **(Weng et.al, 2009)**. Cancer cell migration involves various cellular events that helps tumor cells spread to other body parts **(Figure 1.1)**.
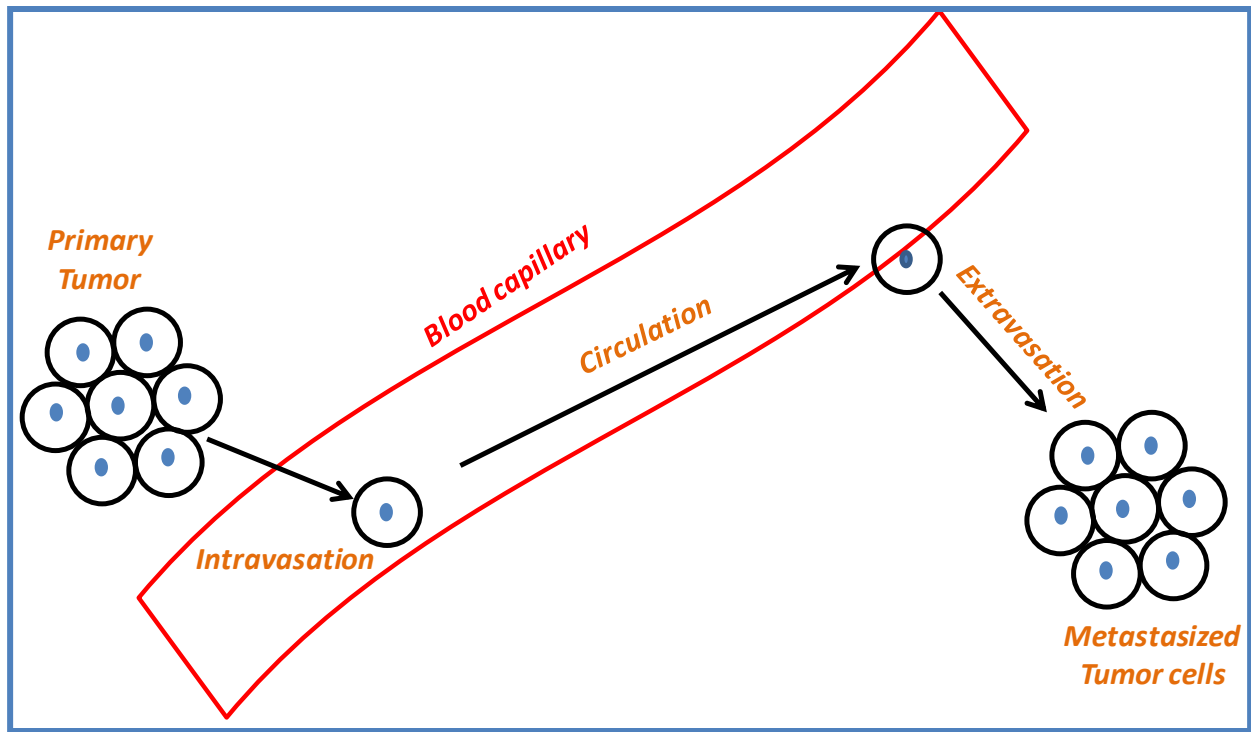
Figure 1.1: Cancer cell metastasis

Cancer cells grow uncontrollably and surround the entire tissue. The cytoskeleton of cancer cells is remodeled and the interaction with cell surface domains/proteins helps them to attach to the extracellular matrix (ECM). In this context, a process known as Epithelial Mesenchymal Transition (EMT) plays an important role where epithelial cells lose their polarity and adhesion and become more migratory and invasive mesenchymal cells **(Heerboth et. al, 2015)**. Studies have also shown the presence of hybrid epithelial/mesenchymal (i.e. partial or intermediate EMT) phenotype having both epithelial and mesenchymal characterestics that helps in collective cell migration **(Lecharpentier et. al, 2011; Jolly et. al, 2015)**. Various EMT markers such as snail family zinc finger 2 (SLUG) and twist family bHLH transcription factor 1 (TWIST) have been analyzed to understand the role of EMT in cancer metastasis **(Grzegrzolka et. al, 2015)**. Upon invading neighboring tissues, tumor cells intravasate into blood or lymphatic vessels and migrate from one place to another through circulating blood, lymphatic system, or via direct extension **(Saykali and El-Sibai, 2014)**. Later at distant locations cancer cells extravasate into the secondary tumor site and multiply to make secondary tumors. Other studies have shown a contradictory phenomenon called Mesenchymal Epithelial Transition (MET) that also stabilizes cancer cells at distant locations **(Yang and Weinberg, 2008; Pattabiraman et. al, 2016)**.

1.2.1 Types of cancer cell migration

Cancer cells migrate individually (mesenchymal and amoeboid) or collectively based on the cell types **(Kawauchi, 2012) (Figure 1.2)**.
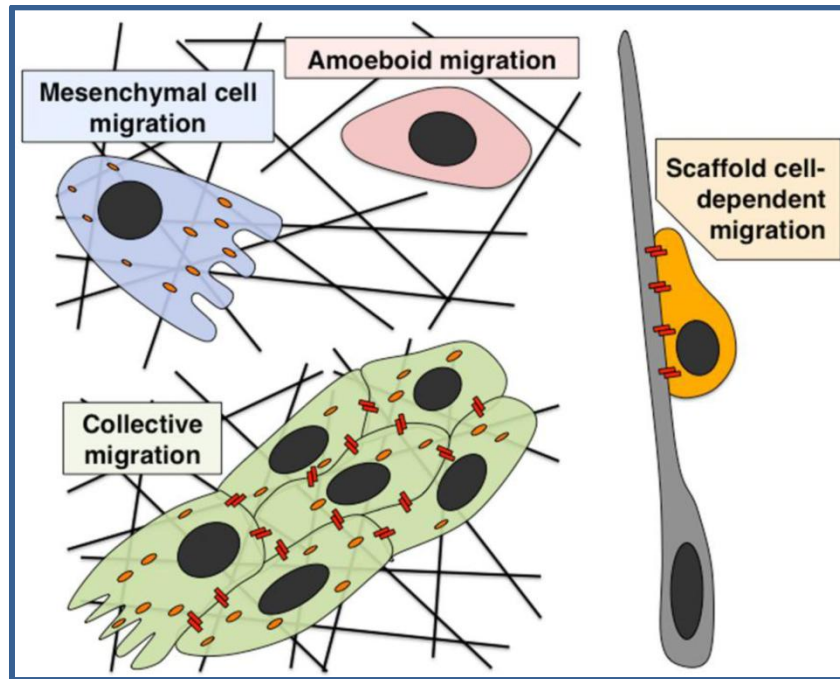
Figure 1.2: Types of cell migration (Kawauchi, 2012)

In the mesenchymal type of migration, epithelial cells transform into mesenchymal cells and increase migratory capacity of cells through EMT. Epithelial cells usually have a tendency to form monolayers and are tightly linked to neighboring cells through specialized junctions, like tight junctions, gap junctions, adherent junctions and desmosomes (**Meng and Takeichi, 2009**). They also possess apical-basal polarity and are tightly associated with basement membrane and only migrate laterally whereas the mesenchymal cells have capacity to invade into surrounding tissue and have front-rear end polarity (**Yang et.al, 2004**). So, during EMT, epithelial cells lose their polarity and inter-cellular contacts and become mesenchymal stem cells having migratory and invasive properties (**Friedl and Wolf, 2003**). These cells form actin-rich pseudopodial protrusions and help cancer cells to metastasize (**Shankar et. al, 2010**).

In amoeboid migration, malignant tumor cells have no polarity as they are round in shape. They are capable of moving at a faster rate (≈ 40 times) than mesenchymal migration (**Clark et. al, 2015; Friedl and Wolf, 2003**). In this type of migration, cancer cells lose their cell-cell adhesion and cell-ECM adhesion (**Liu et. al, 2015**).

In collective cell migration, whole clusters of invasive cells migrate together in a manner similar to mesenchymal migration except that lateral adherent junctions between cells are maintained (**Wolf et. al, 2007; Friedl and Gilmour et. al, 2009**). Essentially, they maintain their cell-cell and cell-ECM adhesion (**Wong et. al, 2014**). It is the slowest type of cell migration.

1.2.2 Mechanisms involved in cell migration

1.2.2.1 Polarization

Polarization of migratory cells shows a clear and defined front and rear ends. There are various modes such as altered chemical and substrate concentration, breakdown of cellular contacts

through which a cancer cell receives the indications to proceed in a particular direction (**Lin et. al, 2015**). In migratory cancer cells, there is an actomyosin contractility where actin polymerizes and there is continuous recycling of the assembly/disassembly of focal contacts at the front end of the cell (**Goetz et al., 2008a**). This actin polymerization helps in driving the cancer cell forward through contraction of cytoskeleton and then detaches from the front end. During this, various cell signaling molecules help to performing this action. Most importantly, the Rho family of GTPases members, Cdc42, Rac1 and RhoA are mainly involved in regulating this actin dynamics (**Joshi et.al, 2008**). These small signaling G protein family members act as a molecular switch where they are continuously interchangeable among an active, GTP-bound state and an inactive, GDP-bound state and hence regulate actin dynamics, cell movement, and other common cellular functions. Various other proteins also play an important role such as guanine nucleotide exchange factors (GEFs), GTPase activating proteins (GAPs) and guanine dissociation inhibitors (GDIs) (**Dorsam and Gutkind, 2007; Van Aelst and D'Souza-Schorey, 1997**). Rac down regulates Rho activity in defining the migratory behavior and cell morphology in fibroblasts (**Parri and Chiarug, 2010**). Extracellular signaling stimulates Rac and Cdc42 which eventually enhances the actin polymerization and formation of focal adhesions (FA's) resulting in the development of actin-based pseudopodial protrusions referred to as filopodia and lamellipodia (**Ridley et. al, 2003**).

These actin rich pseudopod protrusions are membrane extensions in the direction of migration, which help in expanding the plasma membrane, maintaining and forming the backbone structures and also, establishing contacts with the substratum. In metastatic cancer, these pseudopod protrusions control the EMT process and therefore regulate actin cytoskeleton dynamics, tumor migration and invasion (**Nurnberg et. al, 2011**).

1.2.2.2 Adhesions

Cell-cell and cell-ECM adhesions vary in shape, size and function. Integrin receptors are the main components of the substrate adhesions of migratory cells. They are transmembrane proteins which serve as a connecting link between the cells and also, cell and ECM (**Campbell and Humphries, 2011**). Integrins interlink the outside ECM with the cytoskeleton inside the cell. They can interact or bind with different ligands of ECM that initiates signaling events, helps in regulating actin rich protrusions and eventually cell migration (**Chodniewicz and Klemke, 2004**). The adhesion sites are small nascent adhesions/focal complexes or large and elongated FAs (**Lock et. al, 2008**). Focal adhesions present at the front end are small and rapidly assemble/disassemble actin polymerization compared to the ones present further away from migration site.

1.2.2.3 Interaction with ECM and formation of focal contacts

There are various molecules organized into signaling complexes containing kinases and adaptor proteins which help in regulating the actomyosin contractility, microtubule dynamics and integrin signaling. They propel transient signals which help in maintaining the polarity and also, enhance actin polymerization, adhesion, actomyosin contraction and microtubule dynamics (**Gupton and Waterman-Storer, 2006**). The signaling events are regulated through signaling scaffolds, made up of adaptor proteins, membrane lipids or associated proteins which localize kinases and phosphatases at the leading edge of migratory cancer cells (**Worth and Parson, 2008**). Focal adhesion kinases (FAK) and paxillin are two components which regulate the Rho family GTPases and help in adhesion (**Iwanicki et.al, 2008**). Talin, vinculin, and α-actinin are the connecting link between actin to substratum through integrin (**Ciobanasu et. al, 2013**).

1.2.2.4 Cell body translocation and retraction of rear end

Due to these signaling molecules, there is a propelling force to translocate the cell body through contraction of actomyosin complexes and adhesion molecules. Myosin II and other motor proteins like dyenin also help in regulating translocation **(Betapudi, 2009)**. So, for the retraction, it requires a coordinated contraction of actomyosin complex and disassembly of FAs at the rear end **(Parri et. al, 2007)**. The force helping in disassembly of adhesions includes actomyosin contraction, integrin endocytosis, adhesion disassembly and proteolytic cleavage of FA proteins **(Gumbiner, 1996)**. This FA turnover and actomyosin contractility are very complex processes due to the involvement of over about 150 FA associated molecules, cytoskeletal forces and different cell types for cell migration **(Guo and Wang, 2007)**.

ECM and cytoskeleton remodeling and their interaction with growth factor signaling at cell surface helps to regulate cancer cell metastasis **(Teodorczyk and Villalba, 2010)**. As the signaling events between ECM and cytoskeleton are regulated through cell surface receptors or signaling molecules, it is important to study the involvement of cell surface domains in cancer cell motility and its progression **(Dennis et al., 2009; Sotgia et al., 2012; Martinez-Outschoorn et al., 2015)**.

1.3 CELLULAR MICRODOMAINS

Cellular microdomains are the functional microdomains present on the plasma membrane which regulate various signaling or physiological processes. These microdomains are mainly involved in cell signaling, cell adhesion and membrane trafficking. Sometimes, the absence of morphological characters makes it tricky to characterize the organization and composition of various microdomains present on plasma membrane (around 90% in fibroblast) and even doubt

on their existence **(Laude and Prior, 2004).** With growing technology it is getting easier to characterize the composition/morphology of structures such as caveolae and clathrin-coated vesicles through Electron Microscopy (EM), Calcium concentration microdomains (CCMs) through fluorescence microscopy eventually enabling us to the study the role of these microdomains in various signaling events.

1.3.1 Lipid raft domains

1.3.1.1 Lipid rafts

Lipid rafts are dynamic membrane microdomains that exist in a quasi fluid state, floating on the plasma membrane **(Simons and Sampaio, 2011)**. These lipid rafts are composed of sphingolipids and cholesterol in the outside membrane while connected to phospholipids and cholesterol in the inner space of lipid bilayer **(Zajchowski and Robbins, 2002)**. They have saturated hydrocarbon chains of sphingolipids and phospholipids to generate a more ordered and rigid packaging structure **(Ahmed et. al, 1997)**. The Fluid-Mosaic Membrane Model proposed by S. J. Singer and G. L. Nicolson in 1972 explained the protein-lipid thermodynamics within the membrane matrix and helps in characterizing the functional role of cellular membrane **(Singer and Nicolson, 1972; Nicolson, 2014).** This fluid mosaic model has become more complex due to the presence of ordered structures such as lipid raft and cytoskeletal barriers such as septins that obstruct protein diffusion across the membrane **(Vereb et. al, 2003).**

Various proteins change their conformation or oligomerize to alter their affinity with lipid rafts. For eg. palmitoylation stimulates the association of proteins with rafts while depalmitoylation loosens the association **(Levental et. al, 2010)**. Cholesterol plays an important role in the function, biogenesis, and protein association with rafts and maintains the composition of lipid

raft **(Simons and Sampaio, 2011)**. These lipid rafts are insoluble in non-ionic detergents such as Triton X-100 and detergents commonly known as DRMs (detergent resistant membranes) **(Pike, 2004)**. So, when cells or membrane proteins are extracted with Triton X-100 or CHAPS at 4ºC, raft associated lipids or proteins remain insoluble and during separation via sucrose gradient, float in low density fractions.

Membrane proteins are divided into three main categories: the ones present in the raft; the ones present in the liquid (disordered) phase 1 and the ones that are channeled in and out of rafts **(Simons and Ehehalt, 2002)**. There are many receptors or proteins which reside on lipid rafts including Src family tyrosine kinases, glycophosphatidylinositol-anchored (GPI-anchored) proteins, Gα subunit of G protein, PDGF and EGF ligands, endothelial nitrate oxide synthase (eNOS) and various palmitoylated proteins **(Smart et. al, 1999; Brown and Rose, 1992; Song et. al, 1996; Liu et. al, 1995; Mineo et. al, 1996; Chun et. al, 1994; Bickel et. al, 1997; Shaul et. al, 1996; Shenoy-Scaria et. al, 1994)**. The presence of various signaling molecules showed the involvement of lipid raft in signal transduction **(Foster et al., 2003)**.

1.3.1.2 Caveolae

Caveolae are 50-100 nm flask shaped membrane invaginations present on the plasma membrane, known as "little caves" **(Palade, 1953; Yamada, 1955)**. They are special types of lipid rafts and are present in various cell types and tissues like smooth muscle, endothelial cells, fibroblasts and adipocytes. They can be isolated similar to lipid rafts by extracting membrane proteins with Triton X-100 followed by sucrose gradient centrifugation. Caveolae are protein rich but also contain lipid raft-like cholesterol and sphingolipids. Caveolae formation and structure are maintained through crucial proteins like Cav1, Cavin1 known as Polymerase 1 and Transcript

Release Factor (PTRF) and Cavin 2 known as Serum Deprivation Response (SDPR) (**Parton et. al, 2006; Liu and Pilch, 2007; Nabi, 2009; Hansen, et. al, 2012**). In mammalian systems, three homologous forms of Caveolin are present: Cav1, Cav2 and Cav3 (**Razani et. al, 2002**). Around 100 to 200 Cav1 molecules form a caveolae and 15 Cav1 molecules oligomerize to form microdomains known as Cav1 scaffolds (**Chidlow and Sessa, 2010**).

In adipose tissue, Cavin1 co-localizes with Cav1 and it co-distributes with Cav1 in lipid rafts. Cav1 and Cavin1 do not interact directly and mainly rely on actin cytoskeleton and microtubules (**Liu and Pilch, 2008**). Cavin 3 stabilizes caveolae at plasma membrane by forming complexes with Cav1 and Cavin1 subsequently connecting them with the actin cytoskeleton through myosin-1c (**McMahon et. al, 2009; Whitmarsh, 2013**). Caveolae play an essential role in vesicular transport, lipid regulation, signal transduction, calcium signaling, and tumor suppression/progression (**Cohen et. al, 2004; Anderson, 1998; Isshiki and Anderson, 1999; Pani and Singh, 2009**).

1.3.1.3 Cav1 scaffold

Cav1 scaffolds are flat, small (around 5-100nm), stable oligomerized domains on the plasma membrane that do not form caveolae (**Lajoie and Nabi, 2010**). These noncaveolar domains came into consideration after it was shown that Cav1 regulates various functions outside the caveolae such as regulation of EGFR diffusion and signaling and also, CT-b diffusion and endocytosis (**Lajoie et. al, 2009**). Also, these scaffolds are shown to be functionally and structurally different from caveolae through proteomics and subdiffraction limit microscopy (**Zheng et. al, 2011**).

1.3.2 Cav1

Cav1 is a scaffolding protein and the main constituent of caveolae **(Rothberg, 1992)**. Cav1 was identified as a tyrosine phosphorylated substrate in Rous sarcoma virus-transformed chicken fibroblasts and was shown to be a component of the caveolar coat **(Glenney and Soppet, 1992)**. Another group found VIP21 (Vesicular Integral-membrane Protein of 21 kD) from the Golgi apparatus and transported vesicles from the trans-Golgi **(Kurzchalia et. al, 1992)**. It is a 22 kDa protein containing about 178 amino acid residues. Cav1 has two isoforms: Cav1α, which is around 1-178 AA residue long, and Cav1β, which is around 32-178 residues long lacking the first 31 amino acids in Cav1α. *Cav1* gene is transcribed to form a single mRNA that gets translated into two isoforms. The 32nd ATG of gene serves as an internal translation start site and ends up generating the beta-isoform, which is about 3kDa (28 AA) shorter and also lacks Y14. Both isoforms are targeted to the caveolae, form homooligomers and interact with G-proteins. Both the isoforms have significantly different subcellular distribution and it is widely believed that this is due to the phosphorylation of S27. Thus it is this 31-residue difference that decides the cellular fate of each isoform in the context to its cell specific targeting and intracellular destinations **(Li et. al, 2001)**. The Y14 phosphorylation of Cav1α by c-src (and RhoA/Rock) has an established role in focal adhesion dynamics, migration and invasion **(Joshi et al, 2008)**. Therefore, because of the absence of Y14 in Cav1β, we used Cav1α in my study.

Cav1 is localized in caveolae in the plasma membrane in addition to Golgi apparatus and vesicles transported from trans-Golgi and ER **(Ostermeyer et. al, 2001)**. Cav2 and Cav3 lacks tyrosine Y14 phosphorylation site. Cav2 was shown to co-localize and directly interact with Cav1 but lacks the capacity to form caveolae while Cav3 is muscle-specific and functions in a similar way as Cav1 **(Williams and Lisanti, 2004)**. The "Caveolin signature motif"

(FEDVIAEP) is a conserved region present at hydrophilic amino-terminal domains of Caveolin proteins with no functional characterization to date **(Williams and Lisanti, 2004; Scherer, 1996)**.

1.3.2.1 Cav1- Structure and its domains

Cav1 is 1-178 AA long and is a 22 kDa protein **(Glenney and Soppet, 1992)**. Cav1 is present on the plasma membrane and has both cytoplasmic and secretory forms. Cav1 is a ubiquitous protein present in various differentiated cell types such as adipocytes, endothelia, type-I pneumocytes and smooth muscle cells and mainly found in vertebrates, such as human, cow, mouse and also, in *C. elegans* **(Razani et. al, 2002; Tang et. al, 1997)**. Cav1 gene resides on chromosome 7q31.1 in humans **(Hurlstone et. al, 1999; Engelman et. al, 1999)**. Cav1 forms a hairpin-like structure and both amino and carboxyl terminals are cytoplasmic. Cav1 has various modification sites including phosphorylation sites such as a tyrosine residue at amino acid 14, a serine residue at position 80 and 3 cysteine palmitoylation sites localized in the carboxyl terminal **(Figure 1.3)**. It also contains one oligomerization domain forming Cav1 oligomers and one Caveolin scaffolding domain (CSD) that helps Cav1 to interact with other proteins **(Williams and Lisanti, 2004)**.
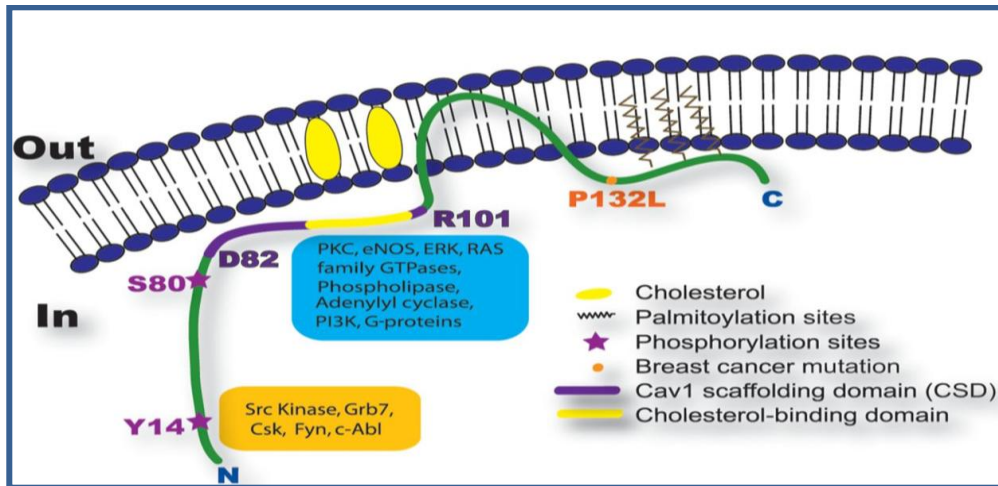
Figure 1.3: Cav1 structure and its domains (Shankar et. al, 2013)

1.3.2.2 CSD

The CSD is located at amino acids 82-101 of Cav1 **(Figure 1.4)**. CSD is known to physically interact with multiple proteins and play an important role in regulating signal transduction through G-proteins, eNOS, src family kinase, epithelial growth factor receptor (EGF-R), PKCα, ERK, Ras family GTPase, PI3K, adenyl cyclase etc **(Bucci et al., 2000; Lisanti et. al, 1994, Lisanti et. al, 1999)**. This domain was shown to play critical role for the oligomerization of Cav1 helping it to form oligomers of 14-16 protein molecules **(Li et. al, 1996)**. Cholesterol is the main component of caveolae, which is required for its formation and function. CSD of Cav1 has Cholesterol recognition/interaction AA consensus (CRAC) motif through which it interacts with cholesterol and positions them in caveolae **(Epand et. al, 2004)**.

Caveolin 1 ①　●　⑧①　[CSD]　⑩①　⑰⑧

Caveolin Scaffolding Domain

↓ contain

Caveolin binding motif (CBM) having a φXφXXXXφ or φXXXXφXXφ or φXφXXXXφXXφ sequence (where φ is F/Y/W amino acid and X is any unspecified amino acid)

↓ Physically interact

eNOS, src family kinase, epithelial growth factor receptor (EGF-R), PKCα, ERK, Ras family GTPase, PI3K, adenyl cyclase

↓ Regulates

Signal transduction

Figure 1.4: CSD, CBM and signaling

The segment, "F92TVT95" of CSD is very important and double point mutations (F92A/V94A) in this region of Cav1 have been well characterized to show the role of CSD in Cav1 binding with other proteins (**Kimura et al., 2002**).

A consensus Caveolin binding motif (CBM) which is recognized through this sequence, $\phi X \phi XXXX\phi$ or $\phi XXXX\phi XX\phi$ or $\phi X \phi XXXX\phi XX\phi$ where ϕ is an aromatic residue (Trp, Phe, or Tyr) and X any unspecified amino acid is known to be present in Caveolin binding partners (**Okamoto et. al, 1998; Cout et. al, 1997**). However some groups have doubted the role of CBM in Cav1 binding. Structural and bioinformatics analysis has shown that the aromatic residues of CBMs are buried inside the protein and rather inapproachable (**Collins et. al, 2012**). Also, sequence and structure based studies showed no characteristics properties present in the CBM which should be present in an interaction motif (**Byrne et. al, 2012**). Further, various other studies have also shown that many Cav1 binding partners lack a CBM. For instance, Sproutyprotein-1 interacts with Cav1 through its conserved cysteine-rich C-terminal domain, hepatocyte Cell Adhesion Molecule (hepaCAM) through its immunoglobulin domain, Protein Kinase A (PKAcat) through its catalytic domain whereas nerve growth factor receptor and sterol carrier protein lack a CBM and yet interact with Cav (**Cabrita et. al, 2006; Moh et. al, 2009; Zhang et. al, 2007**).

1.3.2.3 Y14 phosphorylation

Cav1 Tyrosine-14 (Cav1(1-101)Y14) phosphorylation has been extensively studied in our lab and elsewhere. Cav1(1-101)Y14 phosphorylation was found in chicken embryo fibroblasts and also by another group who showed that stimulation of 3T3-L1 adipocytes with insulin phosphorylates Cav1 at Y14 (**Glenney and Soppet, 1992; Lee et. al, 2000**). The study showed

that the non-receptor protein tyrosine kinase (c-src, c-Yes, Fyn) and tyrosine kinase (Cav, Ras, and GAP) substrates were present in Caveolin rich insoluble hetero-oligomeric complexes and that this Cav1(1-101)Y14 phosphorylation is through src family tyrosine kinase **(Sargiacomo et. al, 1993)**. Y14 phosphorylation of Cav1 has been linked to integrin signaling and focal adhesion dynamics suggesting its vital role in cancer cell migration. Rho/ROCK mediated migration is regulated through FA turnover via Cav1(1-101)Y14 phosphorylation **(Gaus et al., 2006; Joshi et al., 2008)**.

1.3.2.4 Other modification sites (S80, P132 and palmitoylation)

Serine residue at position 80 is another phosphorylation site in Cav1. Phosphorylation at this site changes the configuration of Cav1. It was shown that mutation of serine 80 with glutamate in the ER of fibroblasts loosens Cav1 from Caveolae membranes and makes it a secretory protein product **(Schlegel et. al, 2001)**.

Proline at position 132 is another crucial residue of Cav1. Reports have shown that the *P132L* mutation is predominant in around 16% of breast cancer patients. Studies have shown that this mutation is responsible in forming misfolded Cav1 oligomers and hence Cav1 is not transferred to caveolae or plasma membrane and is retained in the Golgi complex and hence affects Cav1 function in caveolae **(Lee et. al, 2002)**.

Cav1 also has 3 different palmitoylation sites (Cys 133, 143 and 156) residing in the carboxyl terminal and is believed to help CSD domain in the oligomerization of Cav1 **(Dietzen et. al, 1995)**.

1.4 ROLE OF CAV1 IN CANCER

1.4.1 Membrane trafficking

Cav1 CSD has the capacity to physically interact with different proteins having CBMs and regulate the trafficking of various signaling molecules and proteins. Cav1 directly interacts with various receptor kinases such as EGFR, insulin receptor, PDGFR-α and −β etc. and various signaling molecules such as c-src, PKA, eNOS etc, (**Lajoie et al, 2007; Yamamoto et. al, 1999; Garcia-Cardena, et. al, 1997; Li et. al, 1995**). EGFR, PDGFR-Ras-ERK and the whole extracellular signal-regulated kinase cascade are recruited to caveolae and negatively regulated through Cav1 (**Liu et. al, 1996**).

1.4.2 Cell cycle progression

Cav1 plays a dual role in regulating cell cycle progression. It stimulates/inhibits cell proliferation by modulating cell cycle arrest via different signaling pathways.

 siRNA knock down of *Cav1* in RAL and SCLC-R1 cell lines (lung adenocarcinoma) shows reduced expression of cyclin D1 and CDK4 (cell cycle regulators) and eventually decreases cell proliferation (**Pancotti et. al, 2012**). In vivo and in vitro studies have shown direct inhibition of ERK-1/2 through Cav1 and increased activity of ERK-1/2 in *Cav1* null mouse cells and in tissue, enhancing cell cycle arrest and inhibiting cell proliferation (**Cohen et. al, 2003**). Caveolae disruption through cholesterol sequestering agents inhibits PI3K/AKT signaling via inhibition of IL6 and IGF1 suggesting that caveolae and Cav1 are required for proper growth signaling (**Podar et. al, 2003**).

On the other hand, Cav1 was shown to regulate signaling pathway such as Ras-p42/44 MAP kinase and its components such as Neu/ErbB2, EGFR, Ras, Raf-1, MEK-1/2 and ERK-1/2 and inhibit cell growth (**Mineo et. al, 1996; Zhang et. al, 2000**). Hepatoma cells (CBRH7919, HepG2 and SMMC7721) treated with choline plasmalogens (ChoPlas) show increased Cav1 expression and reduced expression of pAkt and Bcl-2 (downstream of P13K/AKT signaling) as well as CDK4, cyclin E and CDK2 (cell cycle regulators), stimulating G1 and G1/S phase transition cell cycle arrest and inhibiting cell proliferation (**Zhan et. al, 2013**).

1.4.3 Apoptosis

Cav1 has a dubious role in apoptosis in cancer as it has been shown to be both pro-apoptotic and anti-apoptotic.

Knockdown of *Cav1* in stable A549/Taxol cell line (lung cancer) inhibits cancer cell proliferation, induces G0/G1 cell cycle arrest and apoptosis in vitro and in vivo (**Han et. al, 2015**). β-carotene downregulates *Cav1* expression that eventually decreases AKT and NF-κB phosphorylation level and increases Bax/Bcl-2 ratio resulting in stimulation of apoptosis, induction of cell cycle G0⁄G1 phase arrest, and inhibition of cell migration (**Zhu et. al, 2016**). Cav1 regulates the cytotoxic activity of docetaxel (DTX) in different subtypes of breast cancer. DTX induces apoptosis in MDA-MB-231 cells (over-expressing *Cav1*) by inactivating Bcl-2 while in MCF-7 cells (with reduced *Cav1* expression) it induces apopotosis through p53 mediated cell cycle arrest (**Kang et. al, 2015**). Cav1 directly interacts with PI3K and expression of Cav1 leads to ceramide induced cell death through PI3K/AKT signaling (**Zundel et. al, 2000**). Stable overexpression of *Cav1* in human glioblastoma-derived cell line U-87MG, downregulates

MAPK, PI3K/AKT and mTOR signaling, while it activates apoptotic pathways **(Quann et. al, 2013)**. These studies support the pro-apoptotic properties of Cav1.

In contrast to this, it was shown that *Cav1* knock down in H9c2 cardiac cells tries to protect the doxorubicin-induced apoptosis and shows an anti-apoptotic effect but Cav1 expression is not enough to alter apoptosis in these cells **(Takaguri et. al, 2015)**. Another group showed that the over expressed *Cav1* retains active AKT through binding and inhibition of PP1 and PP2A (serine/theronine protein phosphatases) **(Li et. al, 2003)**. These studies support the anti-apoptotic properties of Cav1.

1.4.4 Tumor suppressor

Cav1 also plays a dual role in tumor progression/suppression and depends on the tumor type and/or tumor stage.

Cav1 works synergistically with INK4a (which codes for cell cycle regulators such as p16-INK4a and p19-ARF). *INK4a* and *Cav1* null mice produce large tumors in nude mice depicting their tumor suppressor activity **(Williams et. al, 2004)**. Various oncogenes such as *c-Myc*, *HPV E6*, *v-Abl*, *Bcr-Abl*, *H-ras*, *v-src* and *Neu/ErbB2* have been shown to down regulate *Cav1* expression **(Caselli et. al, 2002; Engelman et. al, 1998; Park et. al, 2001)**. PI3K/AKT/mTOR signaling pathways are activated during breast cancer progression. Lack of *Cav1* activates PI3K/AKT, EGFR-MAPK and MAPK signaling in breast and pancreatic cancer **(Feng et. al, 2010; Han et. al, 2009)**. *Cav1* ectopic expression regulated through histone H3 modifiers (H3K4me3, H3K9AcS10P enrichment and H3K9me3 depletion) inhibits the growth of colon cancer cells **(Deb et. al, 2016)**. *Cav1* expression is low in Alveolar RhabdoMyoSarcoma

(ARMS) and expression of *Cav1* in xenografts for in vivo studies leads to aberrant cell growth and proliferation and formation of ARMS (**Huertas-Martínez et. al, 2014**).

P132L mutation is predominant in almost 16% of breast cancer tumors and makes misfolded Cav1 oligomers that reside in the Golgi complex. It was shown that this mutation in Cav1 expressing NIH 3T3 cells, increases growth, invasiveness and chemotactic migration (**Hayashi et. al, 2001**) but later, *P132L* mutation was shown to be absent in breast cancer and other organ cancers making previous results doubtful (**Koike et. al, 2010**).

1.4.5 Tumor promoter

Correlation of *Cav1* expression with pathological tumor-node-metastasis (pTNM) and *FAK* in tissue microarray experiments showed its relationship to cancer progression in gastric cancer (**Nam et. al, 2012**). Overexpressed *Cav1* increased the lung cancer cell proliferation, migration, invasion and also, tumor size that might be through EGFR and ERK signaling (**Luan et. al, 2015**). siRNA knock down of *Cav1* in the breast cancer cell line, BT474 showed reduced cell proliferation, migration and invasion (**Wang et. al, 2014**). FoxM1-Cav1 signaling was shown to promote the EMT, migration, invasion, and metastasis in preclinical models of pancreatic cancer and in human tissue specimens but RNA interference (RNAi) knockdown of *FoxM1* inhibits them (**Huang et. al, 2012**). It was shown that pCav1 regulates Rho/ROCK activation, causing stabilization of FAK in FAs eventually increasing tumor cell migration and invasion (**Joshi et. al, 2008**). Cav1 and Rho-GTPases interactions positively regulate the expression of α5-integrin and also, the Src-dependent activation of p130(Cas)/Rac1, FAK/Pyk2 and Ras/Erk1/2 signaling cascades which eventually promotes cancer progression and metastasis (**Arpaia et. al, 2012**).

pCav1 and Grb7 interaction show increased anchorage independent growth and EGF-stimulated cell migration (**Liu et. al, 2002**). Thus, pCav1 acts like a growth factor receptor, which recruits various SH2-domain containing proteins to the plasma membrane.

It was also shown that in prostate cancer, through serine-80 phosphorylation, the secreted Cav1 exerts its autocrine or paracrine properties rendering tumor promoting function (**Schlegel et. al, 2001**). These studies support the idea of Cav1 functioning as a potential tumor promoter.

1.5 CANCER CELL STRESS

Cav1 has long been associated with the cancer cell stress. During stress conditions, cancer cells modify their metabolic and signaling pathways accordingly channeled through cell surface receptors. Mechanical stress such as cell stretching or swelling shows instant disruption of caveolae due to decreased Cav1 and Cavin 1 expression which helps to buffer the tension (**Sinha et. al, 2011; Parton and Pozo, 2013**). During oxidative stress, expression of Cav1 goes down which leads to altered signaling and endocytic trafficking of caveolae (**Mougeolle et. al, 2015**). In breast cancer, starved cell down regulates *Cav1* expression that enhances autophagy and lysosomal function, degrading proteins and organelles and hence, increases chance of survival (**Shi et. al, 2015**).

On the contrary, pCav1 level has been reported to increase due to mechanical and oxidative stress through activated p38 MAP kinase and c-src kinase. pCav1 has also been shown to localize at FAs as the actin cytoskeleton is disrupted due to stress (**Volonte et. al, 2000**). pCav1 plays an important role during mechanical stress by stimulating the transcriptional activation of *Egr1* via its phosphorylation. This regulates Cav1 and cavin-1 expressions and caveolae biogenesis by promoting transcriptional activation and increasing Cav1 and cavin-1 expression

(**Joshi et. al, 2012**). The activation of a metabolic master switch, 5′ AMP-activated protein kinase (AMPK) leads to the inhibition of oxidative stress by over expressing *pCav1* and stabilization of c-Abl and prdx-1 interaction (**Takeuchi et. al, 2013**). pCav1 disrupts the interaction between Cav1 and the chaperone complex, TCP-1 thereby activating protein folding (**Doucey et. al, 2006**). In hypoxic conditions, HSP90 down regulates Cav1 expression that leads to the activation of Epidermal Growth Factor Receptor (EGFR) eventually enhancing EMT and gastric cancer cell proliferation and survival (**Kannan et. al, 2014**). During stress, cancer cell stimulates the expression of molecular chaperones, which are responsible for fighting against stress and maintaining cellular homeostasis (**Hishiya and Takayama, 2008**).

Immunoprecipitation and GST-Cav1 complex pull down shows that Cav1 interacts with eNOS and HSP90 (**Gratton et. al, 2000**). Also, eNOS dissociation by the addition of CaM, is regulated through Cav1 and stimulated by the presence of HSP90. Thus, Cav1 interaction with HSP90 might have a significant impact on Cav1 functions in cancer.

1.5.1 Role of chaperones in cancer cell stress condition

Many genes and proteins that play crucial roles during embryonic development are either mutated or abnormally expressed in cancerous cells (**Muller and Vousden, 2013**). These mutated proteins change their confirmation and become non-functional. Molecular chaperones are a group of proteins that become hyper-active in cancer cell stress conditions (**Zhang and Burrows, 2004**). They assist proper folding of misfolded proteins, stabilize them and lead to maturation. So, whenever cancer cells detect denatured, misfolded proteins, they elevate production of heat shock proteins (HSPs), which are a group of molecular chaperones (**Schmitt**

et. al, 2007; Zhao and Houry, 2005). They initially try to fold them properly or trigger proteosomal degradation of the misfolded proteins **(Amm et. al, 2014)**.

1.5.2 Heat shock protein 90 (HSP90)

HSP90 is ubiquitously present in various cancer types, and complexes with other chaperones such as HSP70 **(Csermely et. al, 1998)**. HSP90 has two isoforms: HSP90α and HSP90β. It has 3 functional domains: ATP binding, protein binding and dimerizing domains. ATP binding domain has ATPase enzyme activity which makes ATP-bound and ADP-bound states **(Stebbins et. al, 1997; Pearl and Prodromou, 2000)**. Various client proteins of HSP90 bind through its protein-binding domain whereas dimerizing domain is required to form HSP90 dimers. In ATP-bound state, various client proteins are able to bind with HSP90 and get folded properly thus increasing the chances of cancer cell survival and proliferation. On the other hand, in the ADP-bound state, there is no binding with client proteins and they get degraded via the proteosomal degradation route **(Panaretou et. al, 1998; Imai et. al, 2003)**. In cancer cell, HSP90 was shown to stabilize various mutant proteins such as v-Src, fusion oncogene Bcr/Abl, p53, growth factor receptors and signaling molecules such as PI3K and AKT **(Calderwood et al, 2006)**. HSP90 participates in many key processes favorable to cancer cell survival such as responding to growth signals, stabilization of mutant proteins, angiogenesis, and metastasis **(Sawai et al., 2008)**. HSP90 is therefore an important regulator for cellular homeostasis and cancer cell proliferation and hence HSP90 inhibitors might have therapeutic benefits in cancer treatment **(Porter et. al, 2010)**.

1.5.3 17 AAG

To better understand the role of HSP90 in cancer, various inhibitors of the ATP binding pocket of HSP90 have been discovered and characterized such as geldanamycin and 17-N-Allylamino-

17-demethoxygeldanamycin (17 AAG) **(Figure 1.5)**. 17 AAG is a synthetic derivative of geldanamycin and is relatively less toxic **(Dimopoulos et. al, 2011)**. It binds to the ATP binding pocket and stimulates the degradation of client proteins through the proteasome degradation pathway **(Kamal and Burrows, 2004)**. It has anti-tumor properties in xenograft mouse models and is currently in phase II clinical trials. Dose dependent treatment of 17 AAG has shown to induce apoptosis and also has a negative effect on the expression of AKT, pAKT, Her2 and Her3 **(Solit et. al, 2002)**. 17 AAG was shown to inhibit PI3K/AKT signaling causing decrease in survival and inhibiting proliferation of cancer cells **(Ma et. al, 2014)**. Another dose dependent treatment effect of 17 AAG in prostate cancer is inhibition of androgen sensitive and non-sensitive xenografts growth **(Solit et. al, 2002)**.
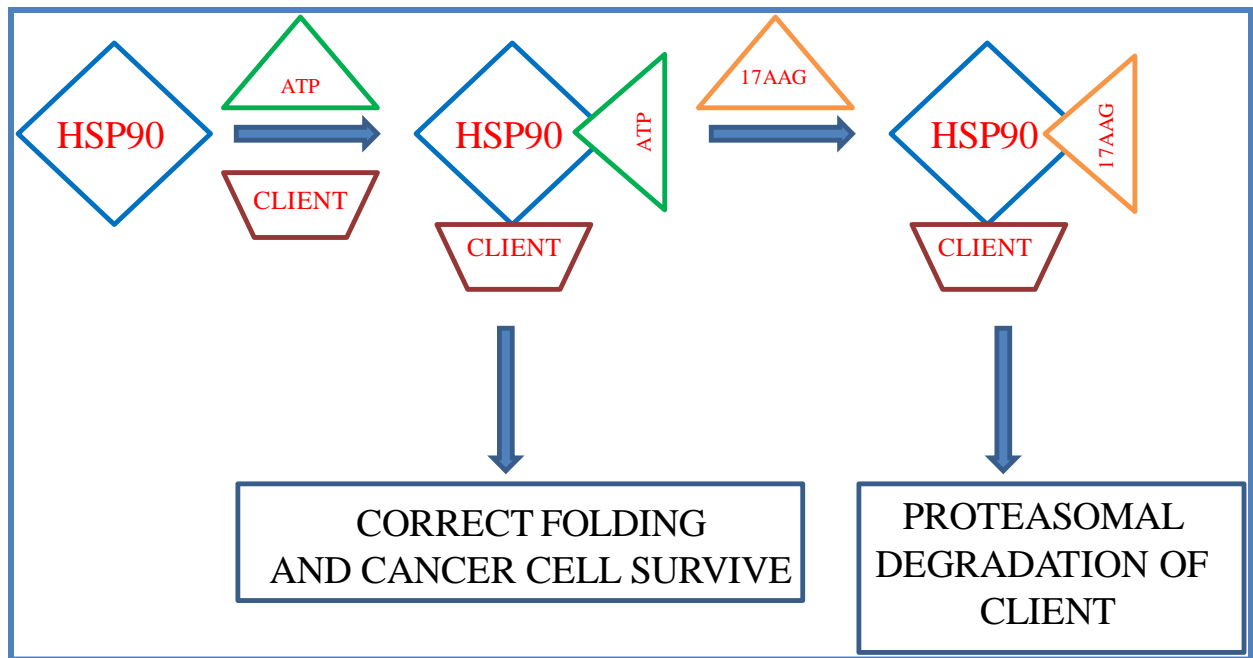
Figure 1.5: Mechanism of action of HSP90 inhibitor

1.6 PROTEOMICS

1.6.1 Overview of quantitative proteomics

As there are limited molecular targets available for cancer treatment and it is difficult to apply basic science research into clinical treatments, a high throughput approach will be an efficient tool. Proteomics would be an excellent approach in the discovery of drugs, inhibitors, biomarkers and therapeutic targets that would help in preventing and curing cancer (**Koomen et. al, 2008; Mesri et. al, 2014; Sallam et. al, 2015**).

Quantitative proteomics helps finding out the differences in the amount of protein in a given sample, such as between control and test groups or healthy and diseased patient samples. While proteomics identifies and helps in characterizing the structure and function of a large scale of proteins, quantitation adds an extra aspect in understanding the proteome (**Ong and Mann, 2005**). There are two major approaches to quantitative proteomics: (1) two-Dimensional Differential In-Gel Electrophoresis (2D-DIGE) using protein samples that are labeled with fluorescent dyes, separated through Two-Dimensional gel Electrophoresis (2-DE) followed by qualitative Mass spectrometry (MS); and (2) labeling digested protein samples with with tags followed by quantitative MS analysis (**Bantscheff et. al, 2007**). In 2D-DIGE, the total protein from different samples are labeled with fluorescent dyes and then separated via Isoelectric focusing (IEF) based on pH differences followed by Two-Dimensional gel Electrophoresis (2-DE) based on molecular weight (**Friedman et. al, 2009**). The 2-DE separated proteins are subjected to in-gel digestion followed by qualitative LC-MS (Liquid Chromatography Mass Spectrometry) run that identifies the charge and mass of intact (quantified) proteins. The basic principle of MS is to ionize the chemical compounds to generate charged molecules or molecular

fragments and measure their mass-to-charge ratios **(Aebersold and Mann, 2003)**. Ionization sources such as Matrix-Assisted Laser Desorption/Ionization (MALDI) use time-of-flight (TOF) analyzer whereas Electrospray Ionization (ESI) source uses Quadrupole mass analyzers and Ion traps (Orbitrap) **(Karas and Kruger, 2003; Fenn et. al, 1989)**. The resulting molecular fragments with specific mass-to-charge ratio are represented as a spectrum, which would further undergo fragmentation via MS/MS run. The final spectra are used to fish out and quantitate the proteins present in different sample sets using the respective databases.

In quantitative MS, different digested samples are quantified by labeling the peptides with different tags such as Isotope-Coded Affinity Tags (ICAT) which uses light, medium and heavy tags, Isobaric Tags for Relative and Absolute Quantitation (iTRAQ), Stable Isotope Labeling with Amino acids in Cell culture (SILAC), and Terminal Amine Isotopic Labeling of Substrates (TAILS) **(Gevaert et. al, 2008; Patel et. al, 2009)**. The differentially labeled samples are pooled and subjected to LC-MS/MS run.

1.6.1.1 Triple Peptide labeling by formaldehyde

In this quantitative proteomics approach, stable isotope labeling strategy is used to differentially quantify proteins in biological samples. Formaldehyde is used to label the N-terminal and α- and ε-amino group of Lysine followed by reductive dimethylation **(Gua et. al, 2007)**. This would give an additional 28 mass units to the labeled peptide and at least 4 mass unit differences between different labels used. In Triple peptide labeling, labels used are CH_2O (light), CD_2O (medium) and $^{13}CD_2O$ (heavy) formaldehyde isotopes, which give +28 Da, +32 Da and +36 Da mass shifts to the peptides respectively **(Boersema et. al, 2009)**. This isotopic labeling is very

rapid, sensitive and easily accessible to any quantitation based proteomics study including proteins from cell, tissues and fluids (**Kovanich et. al, 2012**).

1.6.2 Role of proteomics in cancer cell research

Proteomics is an important tool in defining the structure and functioning of various proteins, protein groups/complexes (formed through protein-protein interaction) or signaling molecules involved in cancer (**Reymond and Schlegel, 2007**). Various drugs, drug inhibitors and biomarkers have been found from quantitative proteomic analysis of normal and cancer patient samples (**Liang et. al, 2012**). In cancer, many genes get mutated and/or proteins undergo post-translational modifications that alter normal signaling and metabolic pathways. Quantitative functional proteomics can define this altered activity, expression levels and post-translational modifications (PTMs) of tumor related proteins (**Zou and Wang, 2007**). The comparative dimethyl labeled quantitative proteomic analysis between clear cell Renal Cell Carcinoma (ccRCC) of FFPE tissue and adjacent non–malignant renal tissue shows the involvement of enhanced glyocolytic enzymes, annexins, ribosomal and proteasomal proteins (**Weisser et. al, 2015**). Quantitative proteomics of human liver cancer cells and normal liver cells showed that 188 proteins were differentially regulated that were involved in metastasis and recurrence of cancer or other pathological processes (**Tang et. al, 2013**). Dimethyl labeled quantitative proteomics between Hepatocellular carcinoma (HCC) patients and normal patients showed around 91 differentially expressed proteins such as microtubule proteins that were down regulated and signal and inflammation responsive proteins that were up regulated (**Huang et. al, 2015**). Pancreatic Ductal Adenocarcinoma and normal mice quantitative proteomic analysis showed 5 differentially expressed protein biomarkers that were present in cancerous mice (**Kuo et. al, 2016**). Tyrosine kinase receptor signaling pathways were analyzed in stimulated A549

lung adenocarcinoma cells with EGF or HGF using SILAC quantitation method. The study found a smal set of HGF and a large set of EGF induced proteins in the cancerous cell (**Hammond et. al, 2009**). Similarly various signaling pathways such as epidermal growth factor receptor (EGFR), ERK and breakpoint cluster region (BCR)–ABL1 networks were analyzed using quantitative proteomics (**Kolch and Pitt, 2010**). Quantitative proteomics along with affinity purification will help to understand the protein-protein interaction and reveal the dynamic changes in various signaling events (**Dengjel et. al, 2010**).

1.6.2.1 Defining interacting partners

Quantitative proteomics helps in understanding protein-protein or protein-complex interactions through affinity purification followed by mass spectrometry (**Tew et. al, 2011**). Various affinity purification methods are available that have different sensitivity and purity, for eg, immunoaffinity, Immobilized Metal ion Affinity Chromatography (IMAC), recombinant proteins tags (Glutathione-S-Transferase (GST), Hexahistidine (His), and Maltose Binding Protein (MBP), Histidine tags) and lectins (**Lichty et. al, 2005**). The PCR generated proteins are fused with GST to make GST-tagged protein beads followed by pulldowns from protein lysates and subsequently subjected to quantitative proteomics analysis (**Luo et. al, 2014**). The GST fusion proteins are used for global or high throughput data analysis and a study purified 5800 individual yeast GST fusion proteins from glutathione-agarose platform (**Zhu et. al, 2001**). GST fusion proteome chip is used to analyze yeast protein kinases for its biochemical activity (**Zhu et. al, 2000**). GST-tagged proteins have been purified through Glutathione modified super paramagnetic nanoparticles and analyzed through mass spectrometry in yeast proteome mixture (**Lee et.al, 2010**). The up regulated genes in genomic data of colorectal cancer (CRC) were tagged to understand protein expression and solubility in *E.coli* (**Sagynaliev et. al, 2005**).

1.6.2.2 Bioinformatics analysis of proteomics data

Quantitative proteomics provides ratio between two different samples, which can be further analyzed to understand its role, biological function, protein class or pathways involved. The testable hypothesis requires performing the functional analysis of our protein group. We therefore link the protein identifier to its Gene Ontology term and hierarchically cluster them (**Ashburner et al, 2000**). The proteins are analyzed for biological processes, molecular function or cellular component and arranged into different groups accordingly (**Yon et. al, 2008**).

GO-term enrichment analysis compares the specific proteins present in one sample with reference dataset (**Malik et. al, 2010**). GO-overrepresentation analyzes specific proteins present in one sample compared to another sample set. This would be statistically significant and have a calculated p-value based on the clustered GO-terms (**Huang et. al, 2009**).

There are other tools which help in analyzing the biological pathways involved in the sample sets that include comprehensive databases such as KEGG, Reactome, Ingenuity Pathway Knowledge Base or BioCarta for interacted proteins in metabolic and signaling pathways, genetic interactions or drug development while some are specific databases such as PANTHER, GenMAPP or PID for signal transduction processes (**Croft et. al, 2011; Kanehisa et. al, 2012; Mi et. al, 2007; Salomonis et. al, 2007**).

To understand the protein-protein interaction in any biological process, the interaction databases such as MINT, BioGRID, IntAct or HRPD are helpful (**Chatraryamontri et. al, 2007; Stark et. al, 2006; Kerrien et. al, 2012**). Some interaction databases are based on the experimental data collected from literature that includes STRING or iRefWeb (**Franceschini et. al, 2013**).

1.6.3 Pseudopod proteome and Cav1

Actin rich pseudopod protrusions are an important aspect of mesenchymal tumor cell migration. These protrusions help them invade and metastasize to secondary tumor sites. The microarray and proteomic analysis of six different metastatic cancer lines showed 384 mRNAs and 64 proteins similar and 19 proteins were characterized for their specificity to pseudopod protrusions **(Shankar et. al, 2010)**. AHNAK, septin-9, eIF4E, and S100A11 proteins were shown to be involved in cancer cell migration and invasion and their knockdown decreased actin cytoskeleton dynamics and cancer cell performs MET **(Shankar et. al, 2010)**. LC-MS analysis of pseudopod proteins from Moloney sarcoma virus (MSV)-Madin-Darby canine kidney (MDCK)-invasive (INV) variant cells showed enrichment of various groups of protein related to actin-regulation, adhesion, glycolysis, protein and RNA translation, ubiquitin-mediated protein degradation, chaperones and signaling **(Jia et. al, 2005)**.

Two-dimensional difference gel electrophoresis followed by MS of whole cells and pseudopodia fractions revealed 46 proteins localized to pseudopodia such as RAB1A, HSP90B, TDRD7, and vimentin which might help in understanding the role of pseudopodia in tumor cell migration **(Ito et. al, 2012)**.

Briefly, in my study, quantitative proteomic analysis of phosphomimetic and non-phosphorylatable mutants of Cav1 shows that various proteins that interacted with phosphorylated Cav1 were pseudopod enriched. GO analysis shows the presence of similar classes of proteins present in pseudopod and phosphorylated Cav1 such as metabolic enzymes, chaperones (HSP90), focal adhesions, etc. Also, after treating the prostate cancer cells lines with

HSP90 inhibitor (17 AAG), we found pCav1-dependent function of HSP90 in regulating cell migration.

1.7 THESIS AIMS AND HYPOTHESIS

Aim 1

Comparative proteomics study/analysis of the binding partners of phosphorylated (Cav1(1-101)Y14D) and non-phosphorylated (Cav1(1-101)Y14F) form of Cav1

Hypothesis

We hypothesize that the phosphorylation of Y14 will differentially regulate the binding of different proteins to Cav1

Aim 2

Comparative proteomics analysis of the CSD mutant (F92A/V94A) of Cav1(1-101)Y14D and Cav1(1-101)Y14F to find the dependency of binding partners on CSD domain

Hypothesis

We hypothesize that the binding specificity of Y14 is dependent on the CSD domain of Cav1

Aim 3

To determine whether pCav1-specific interaction with Hsp90 impacts on Cav1 function in cancer cell migration

Hypothesis

We hypothesize that interaction between pCav1 and Hsp90 could play a crucial role in cancer cell migration.

CHAPTER 2: MATERIALS AND METHODS

2.1. ANTIBODIES AND REAGENTS

The following primary antibodies were used: Anti-Vinculin, Anti-AKT and Anti-p-AKT (Cell Signaling), CST, Anti-HSP90 (Enzolifesciences), Anti-PKM2 (Abnova), Anti Cav1 (BD-Transduction Laboratories) and Anti-β-Actin (Sigma-Aldrich). HRP-conjugated secondary antibodies against mouse or rabbit were purchased from Jackson Immuno-Research Laboratories. Triton X-l00 and Tween-20 were obtained from Fisher Scientific (Ottawa, Ontario, Canada) and ECL Western Blotting Detection Reagent was from EMD-Millipore. 17 AAG (HSP90 inhibitor) was purchased from Selleckchem (USA). Thrombin was a kind gift from one of our collaborators (Pettingen Lab, UBC, LSI). MTT in powder form was purchased from Sigma. Glutathion S-transferase Agarose beads were from GE Healthcare.

2.2 CELL CULTURE

PC3 and DU145 prostate cancer cell lines have been used extensively in Nabi lab. Originally these cell lines were obtained from American Type Culture Collection with appropriate authenticity certificate. Cell lines were tested negative for mycoplasma and cultured in RPMI 1640 medium (Invitrogen-Life Technologies) and supplemented with 1% L-glutamine and 10% heat inactivated Fetal Bovine Serum (FBS) (Gibco, Invitrogen-Life Technologies, Canada). In the past DU145 stables (stably transfected with CavlWT-mRFP, Cav1(1-101)Y14F-mRFP, Cav1(1-101)Y14D-mRFP and DsRed) were generated and characterized in Nabi Lab. They were also cultured in RPMI 1640 complete medium (as stated above) and supplemented with 0.5% G148 antibiotic (Invitrogen-Life Technologies, Canada) to maintain the transgene. Cells were maintained in an incubator (at 37°C and 5% CO_2) with humidity. After thawing, cell were

passaged twice before starting any experiment and when needed, cells were cryopreserved in a mixture of 10% Tissue Culture grade DMSO (Sigma) and 90% FBS, kept overnight at -80°C and stored in liquid nitrogen for long time storage.

2.3 SMALL INTERFERING RNA (siRNA) TRANSFECTIONS

siRNA transfection for PC3 cell lines was performed in 6 well plate (seeded with 200,000 cells/well) and 96 well plate (seeded with 5000 cells/well). Cells were allowed to grow up to 50-60% confluency prior to transfection. Following manufacturer's protocol, cells were transiently transfected with either human Cav1 siRNA or control siRNA using Lipofectamine 2000 transfection reagent and Opti-MEM (Invitrogen-Life Technologies). Transfected cells were incubated for five hours then washed once with 1xPBS (Invitrogen-Life Technologies, Canada), supplied with complete RPMI-medium and cultured further for about 48 h in the incubator.

2.4 DRUG TREATMENT

The DU145 cells (and stables) were seeded in 6 well plate (200,000 cells/well) for 24 h. PC3 cells were seeded, transiently transfected with either human Cav1 siRNA or control siRNA for 24 h (as described above). 17AAG treatment was performed on all the cells in dose dependent manner (5, 10 and 25nM) whereas 0.01% DMSO was used as control. Drug treated cells were incubated for additional 24 h, harvested post two PBS washes and subjected to lysate preparation and western blotting.

In order to perform cell viability assays: About 5000 cells were seeded per well in 96-well plate. Cells were treated with either 17AAG with following dosages (5, 10, 25, 50 and 100nM) or its corresponding concentration of DMSO (as control) for 24 and 48 h for PC3 cells (12 hours post siRNA transfection) and 24, 48 and 72 h for DU145 and its stables.

25nM of 17 AAG and 0.25% DMSO (as control) were used for cell migration assay (50,000 cells/insert in 24-well plate).

2.5 GST TAGGED CONSTRUCT AND BEADS PREPARATION

1-101 AA fragments of Cav1 construct were point mutated to form Cav1(1-101)Y14F and Cav1(1-101)Y14D mutants. These mutants were used as a template to introduce double point mutation (F92A/V94A) in the CSD domain to generate Cav1(1-101)Y14D-CSD and Cav1(1-101)Y14F-CSD mutants by site directed mutagenesis technique. Two sets of PCRs were performed to make the full GST-tagged protein construct. In first set of PCR, the overhang carrying partly thrombin cleavage site and GST linker was added before the ATG, whereas *Eco*RI restriction site was added at the 5' end in second set of PCR. This also added termination codon after 101 AAs and an *Xho*I restriction site at the 3' end of the Cav1. The pGEX-4T1 plasmid (GE Healthcare) was digested with *Eco*RI and *Xho*I restriction enzymes and ligated with corresponding enzyme digested appropriate fragments of Cav1 (1-101). GST, GST-Cav1(1-101)Y14D, GST-Cav1(1-101)Y14F, GST-Cav1(1-101)Y14D-CSD and GST-Cav1(1-101)Y14F-CSD plasmids obtained post colony screening and sequencing were maintained into DH5-alpha *E.coli* strain. Also, the positive plasmid was then transformed into BL21 *E.coli* strain (NEB, a suitable strain normally used for IPTG mediated recombinant protein induction). In order to generate GST-beads, we first induced protein expression and characterized it. Briefly, bacteria carrying appropriate plasmids were inoculated in 6ml LB (Luria Broth) containing ampicillin and cultured overnight at 37ºC in a shaker incubator set at 225rpm. Next day, 2.5ml of the overnight culture was added to 15ml LB containing ampicillin and cultured at 37ºC in a shaker incubator set at 225rpm till OD@600nm reached 0.9-1.0. Bacteria, containing GST, Cav1(1-101)Y14D, Cav1(1-101)Y14F, Cav1(1-101)Y14D-CSD or Cav1(1-101)Y14F-CSD plasmids were induced

with 0.4mM IPTG and at 30ºC in a shaker incubator set at 225rpm for additional 3 h. The induced bacteria were pelleted down at 4000rpm, 4ºC for 20 mins and stored at -80ºC for bead preparation. GST and GST-tagged proteins beads were prepared according to manufacturer's protocol (GE health care). Pellets were lysed in 2ml lysis buffer (1% Tween 20, 1% Triton X-100, 10mM DTT, 0.15mg/ml Lysozyme, one Protease inhibitor tablet added in cold PBS), sonicated (Fisher scientific) @power 4 with 30s pulse (3-5 pulses with 2 mins on ice in-between) and centrifuged (13,000rpm, 4 ºC for 15 mins). The supernatant was incubated with 350µl of GST beads slurry (prepared as per manufacturer's protocol in PBS) and rotated at 4ºC for about 3 h to allow binding. After 3 h, beads were washed five times with wash buffer (1% Tween 20, 1% Triton X-100, 10mM DTT in cold PBS) and then one time with cold PBS. Beads were stored with slurry in cold PBS containing 0.01M DTT at a 1:1 ratio at 4ºC for further use.

2.6 GST PULL DOWN, THROMBIN CLEAVAGE AND PROTEOMICS

Pull-down assays with (GST, GST-Cav1(1-101)Y14D and GST-Cav1(1-101)Y14F), (GST, GST-Cav1(1-101)Y14D and GST-Cav1(1-101)Y14D-CSD) and (GST, GST-Cav1(1-101)Y14F and GST-Cav1(1-101)Y14F-CSD) beads were performed according to previously described protocol (Garcia-Carden et al., 1997). Confluently cultured DU145 cells were scraped off, pelleted and lysed with lysis buffer (150mM NaCl, 10mM NaF, 20mM HEPES, 0.4mM EDTA, 1% Triton X-100, 0.5mM Na_3VO_4, 1mM PMSF, 0.5µg/ml Leupeptin and Protease inhibitor cocktail tablet (Roche) in double-distilled water) by rotating at 4ºC for 30 mins. After centrifugation cell debris was removed and total protein was quantified using Bradford reagent (Bio-Rad). About 15mg of total protein lysate from DU145 cells was incubated with the GST or GST-tagged protein beads on a rotator at 4ºC for 3 h, washed with binding buffer and subjected to Thrombin cleavage (0.1U/reaction) using following buffer: 20 mM Tris-HCl, pH-8.0, 100 mM

NaCl, 0.3mM $CaCl_2$, 1 mM DTT and 0.1% Triton X-100. Reaction mixtures were incubated overnight at 4^oC. The supernatant was collected and subjected to quantitative proteomics analysis using formaldehyde labeling. Collected supernatant was dried completely and dissolved in Digestion Buffer (1% sodium deoxycholate, 50mM NH_4HCO). The protein samples were reduced (using 1mg DTT/50 mg sample protein) for 30 min and alkylated (using 5mg Iodoacetamide/50 mg sample protein) for 20 mins at 37ºC. The samples were trypsin digested for 18-22 h at 37 ºC and desalted. The elution from GST-Cav1(1-101)Y14D pull-downs were labeled with CH_2O (light), GST-Cav1(1-101)Y14F pull-down with CD_2O (medium) and the GST alone pull-down with $^{13}CD_2O$ (heavy) formaldehyde, which gave a +28 Da, +32 Da and +36 Da mass shift to the peptides, respectively. Similarly other sets of elution products from GST-Cav1(1-101)Y14D/ GST-Cav1(1-101)Y14F pull-downs were labeled with CH_2O (light), GST-Cav1(1-101)Y14D-CSD/GSTCav1(1-101)Y14F-CSD pull-downs with CD_2O (medium) and the GST alone pull-downs with $^{13}CD_2O$ (heavy) formaldehyde respectively. All the different labeled samples (with light, medium and heavy formaldehyde) from each set were mixed together, desalted again, completely dried and stored at -80ºC until the MS run. The mass shifts were detected in LC-MS/MS run and quantified using MaxQuant software package designed for analyzing large data sets from quantitative MS.

2.7 WESTERN BLOTTING

Pull-down assays with GST, GST-Cav1(1-101)Y14D or GST-Cav1(1-101)Y14F beads were performed. DU145 lysates were prepared as described above. The beads were incubated overnight with 2mg DU145 protein lysates on a rotator at 4°C. Next day, this was washed with GST pull down lysis buffer, boiled in 1xSDS-PAGE loading buffer, centrifuged, separated on SDS-PAGE and western blotted following standard protocol.

For drug treated samples, the cell pellets were lysed in M2 lysis buffer (20mM Tris-HC1, pH 7.6, 0.5% NP-40, 250mM NaC1, 3mM EDTA, 3mM EGTA (Fisher Scientific)) containing freshly added 2mM DTT, 0.5mM PMSF, 1mM sodium vanadate, 2.5 mM sodium fluoride, and 1µM leupeptin (Sigma-Aldrich) plus protease/phosphatase inhibitor tablet (Roche) and rotated for 30 mins on a rotator at 4°C. The samples were centrifuged at 14,000rpm at 4ºC for 10 mins, supernatants were collected and the total amount of protein was quantified using Bradford method.

GST pull-downs were performed as described above. Samples were boiled and separated by SDS-PAGE, transferred to nitrocellulose membrane and subjected to standard western blotting protocol (**Mahmood and Yang, 2012**). Blots were probed with appropriate primary and HRP-conjugated secondary antibodies following protocols used in our lab. The signal was detected using ECL Western Blotting Detection Reagent and X-ray film (Clonex Corporation, Markham, Ontario, Canada). The expressions of the desired proteins were quantified using Image J software and normalized against β-Actin. Prism Graph-pad was used to assess statistical significance, prepare graphs and compare different samples.

2.8 MIGRATION ASSAY

DU145 and its stables as well as PC3 (+/-siCav1) cells were treated with 17 AAG as mentioned above. After 16 h treatment, cells (50,000 cells/insert) were incubated in serum free media containing 24 well transwell insert (0.8micron pore size) for about an 8 h. The base of well was filled with complete media (RPMI with FBS and L-Glutamine) to encourage cell migration. The cells were treated with 17 AAG (25nM) during the migration assay. After 8 h, cells were washed once with PBS, fixed with PFA and stained using 0.05% crystal violet prepared in 70% EtOH

(for 10 mins). The cells present on top of the filter were swabbed using cotton swab; migrated cells were scored manually, plotted using prism graph-pad and analyzed for significance in changes post treatment with 17 AAG in migration.

2.9 CELL VIABILITY ASSAY

In order to test the cell viability cells were first seeded (5000 cells/well) onto 96-well plate and treated with 17 AAG as described above. The DU145 and its stables were treated for 24, 48 and 72 h whereas PC3 cells were transiently transfected with siCtrl or siCav1 prior to 17AAG treatment for 24 and 48 h. Four hours before the completion of incubation time, cells were supplied with MTT drug (0.5mg/ml) and further incubated for 4 h. The formazan crystals formed within the viable cells were solubilized using solubilization buffer (40% DMF, 2%GAA and 16%SDS) that produces purple coloration. OD was measured at 570nm to ascertain the number of viable cells. Prism graph-pad was used to generate statistical data and plotted as bar graph.

CHAPTER 3: RESULTS

3.1 COMPARATIVE PROTEOMIC ANALYSIS OF THE BINDING PARTNERS OF CAV1(1-101)Y14D (PHOSPHOMIMETIC) AND CAV1(1-101)Y14F (DOMINANT NEGATIVE)

3.1.1 GST-tagged construct

Human Cav1 constructs are available and have been extensively studied in Nabi lab. In order to study binding partners of Y14 Cav1 and later to explore the role of CSD, we decided to use GST pull-down and proteomics approach. First, we set out to generate GST-fused amino terminal, 1-101 AA long cytoplasmic fragment of human Cav1. Cav1-mRFP plasmid was used as template to amplify 1-101 AA cDNA fragments by PCR. Point mutation was introduced at the Y14 residue of Cav1(1-101) cDNA to generate Cav1(1-101)Y14D (phosphomimetic) and Cav1(1-101)Y14F (dominant negative).

The generated fragments were subcloned into pGex-4t1 vector. The first PCR (PCR1) was performed to attach an overhang carrying partly thrombin cleavage site and GST linker at the 5' end of the Cav1 cDNA (for all the variants). Also at 3' end of Cav1, a termination codon and an *Xho*I restriction site were engineered using PCR approach as shown in (**Figure 3.1A**). Second PCR (PCR2) was performed to add the *Eco*RI restriction site at the beginning of the GST linker at 5'end of cDNA (**Figure 3.1A**). These PCR amplified products were purified, digested with *Eco*RI-*Xho*I along with the cloning vector pGEX-4t1, gel extracted and ligated as shown in (**Figure 3.1B & 3.1C**). Positive bacterial clones were identified by PCR amplifying 1-101 cDNA with internal (GST Forward primer) and Cav1 reverse primer set. Positive clones were evident in **Figure 3.1D**. Positive clones in DH5-alpha were sequence verified (as shown below) and

maintained for further use. These clones were retransformed into BL21 (*E.coli* strain) and induced with IPTG to express GST-tagged Cav1 (1-101).
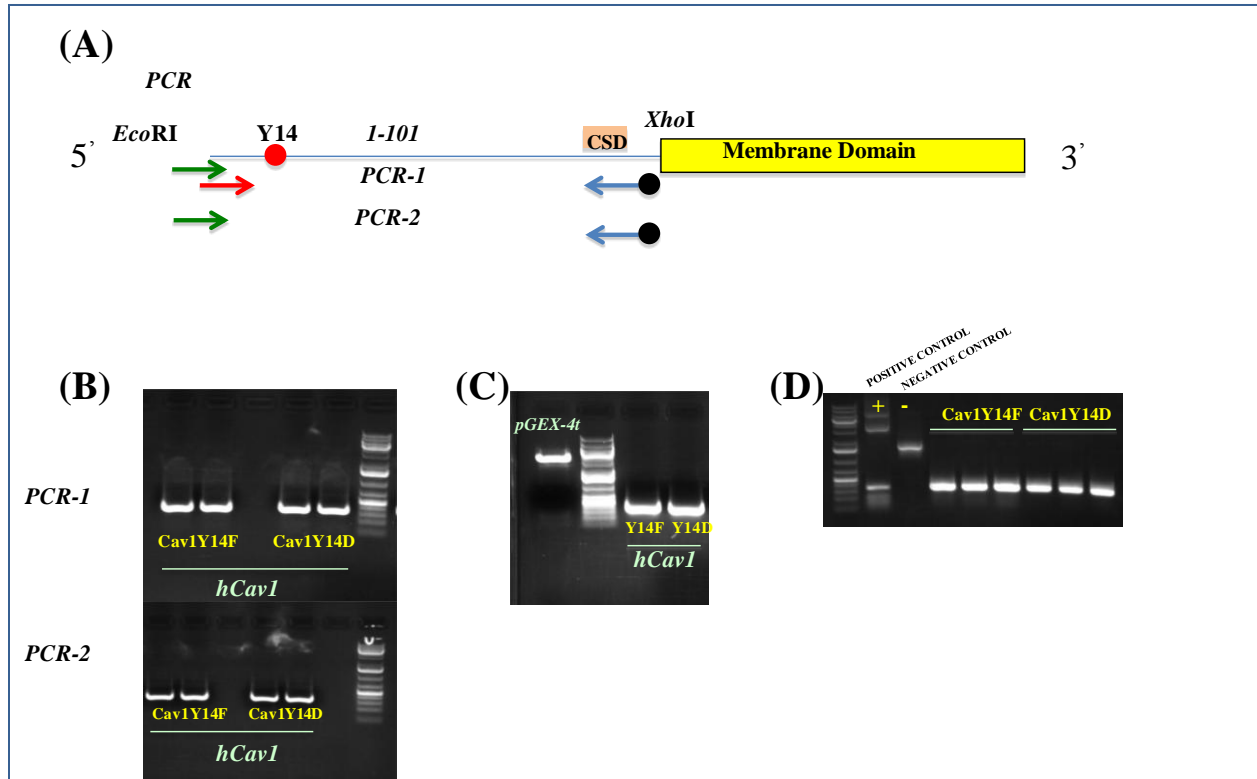
Figure 3.1: PCR generated Cav1(1-101)Y14D and Cav1(1-101)Y14F mutants. *(A) hCav1 (1-101) construct was used to introduce the point mutation at Y14 residue and generate Cav1(1-101)Y14D and Cav1(1-101)Y14F mutants. PCR-1 was performed to attach a overhang carrying partly thrombin cleavage site and GS linker at 5' end and also a termination codon and an XhoI restriction site at 3' end of the constructs. PCR-2 was done to insert an EcoR1 restriction site at the beginning of the GST linker at 5'end and make the full construct. (B) PCR-1 and PCR-2 amplified products of Cav1(1-101)Y14D and Cav1(1-101)Y14F were run on agarose gel. (C) Digested product of Cav1(1-101)Y14D and Cav1(1-101)Y14F along with pGEX-4t vector from EcoRI-XhoI digestion. (D) PCR product analysis of Cav1(1-101)Y14D and Cav1(1-101)Y14F along with positive and negative controls.*

3.1.1.1 Cav1(1-101)Y14D mutant sequence

nnnnnnnnnnaaatcggntctggtt

ccgcgtggatccccggaattcatgggcgacggcggcagcggcggcggcagctctgggggc

 P R G S P E F M G D G G S G G G S S G G

aaatacgtagactcggagggacatctcgacaccgttcccatccgggaacagggcaacatc

 K Y V D S E G H L D T V P I R E Q G N I

tacaagcccaacaacaaggccatggcagacgagctgagcgagaagcaagtgtacgacgcg

 Y K P N N K A M A D E L S E K Q V Y D A

cacaccaaggagatcgacctggtcaaccgcgaccctaaacacctcaacgatgacgtggtc

 H T K E I D L V N R D P K H L N D D V V

aagattgactttgaagatgtgattgcagaaccagaagggacacacagttttgacggcatt

 K I D F E D V I A E P E G T H S F D G I

tggaaggccagcttcaccaccttcactgtgacgaaatactggttttaccgctagctcgag

 W K A S F T T F T V T K Y W F Y R -

3.1.1.2 Cav1(1-101)Y14F mutant sequence

nnnnnnnnnnaaatcggntctggtt

ccgcgtggatccccggaattcatgggcgacggcggcagcggcggcggcagctctgggggc

 P R G S P E F M G D G G S G G G S S G G

aaatacgtagactcggagggacatctcttcaccgttcccatccgggaacagggcaacatc

 K Y V D S E G H L **F** T V P I R E Q G N I

tacaagcccaacaacaaggccatggcagacgagctgagcgagaagcaagtgtacgacgcg

 Y K P N N K A M A D E L S E K Q V Y D A

cacaccaaggagatcgacctggtcaaccgcgaccctaaacacctcaacgatgacgtggtc

H T K E I D L V N R D P K H L N D D V V

aagattgactttgaagatgtgattgcagaaccagaagggacacacagttttgacggcatt

K I D F E D V I A E P E G T H S F D G I

tggaaggccagcttcaccaccttcactgtgacgaaatactggtttaccgctagctcgag

W K A S F T T F T V T K Y W F Y R -

To generate GST, or GST-Cav1 (1-101) variants, BL21 was transformed with positive plasmids. Positive colonies were inoculated into 6ml culture media with ampicillin and incubated overnight at 37ºC in a shaker incubator set at 225rpm. For protein induction 2.5ml of overnight culture was taken and inoculated into 15ml media with ampicillin and cultured at 37ºC in a shaker incubator set at 225rpm till OD@600nm reached to 0.9-1.0. 0.4mM IPTG was added into this culture and incubated at 30ºC in a shaker incubator set at 225rpm for 3 h to induce protein expression for GST, GST-Cav1 (1-101)Y14D and GST-Cav1(1-101)Y14F proteins. An aliquot from uninduced and induced protein samples were separated by SDS-PAGE to check induction. Uninduced samples did not show protein expression of desired size (~35kDa) whereas induced samples showed GST as well as GST tagged Cav1 (1-101) expression as an induced band (**Figure 3.2**). The protein pellets from the large prep were stored at -80ºC for further use.
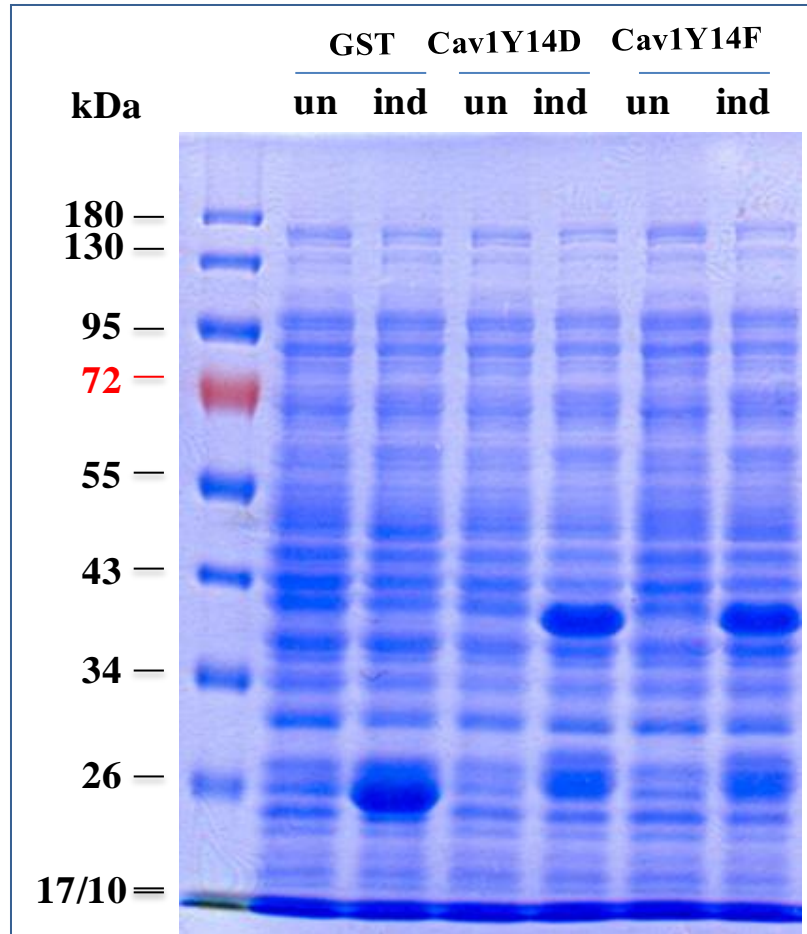
Figure 3.2: Coomassie Blue stained SDS-PAGE Gel for induced GST, Cav1(1-101)Y14D and Cav1(1-101)Y14F proteins. *GST alone, Cav1(1-101)Y14D and Cav1(1-101)Y14F uninduced (un) and induced (ind) protein products separated on SDS-PAGE. Protein marker shows the GST induced protein at 26kDa and Cav1(1-101)Y14D and Cav1(1-101)Y14F induced protein at 40 kDa.*

The protein pellets were used to prepare GST or GST-tagged Cav1 beads. The induced protein pellets were lysed by sonicating thrice and centrifuged. Aliquots of this pre binding sample were stored. The supernatants were incubated with Glutathione-agarose beads (Sigma-Aldrich) on rotator at 4ºC for 3 h and post binding aliquots were stored. The GST alone and GST-tagged construct agarose beads were first washed with wash buffer, then with PBS and subsequently stored in PBS (containing 10mM DTT) at 4ºC for further use. The purified beads along with pre binding and post binding protein samples were separated on SDS-PAGE. As shown in **Figure 3.3A,** lysates of either GST or GST fused Cav1 variants show presence of the protein which disappears post binding with glutathione beads from the lysates and remain bound with beads. Beads alone show purified proteins bound with bead. This was further confirmed by performing western blotting and probing the blot with GST and Cav1 antibody, also confirming bead purity (**Figure 3.3B & 3.3C)**
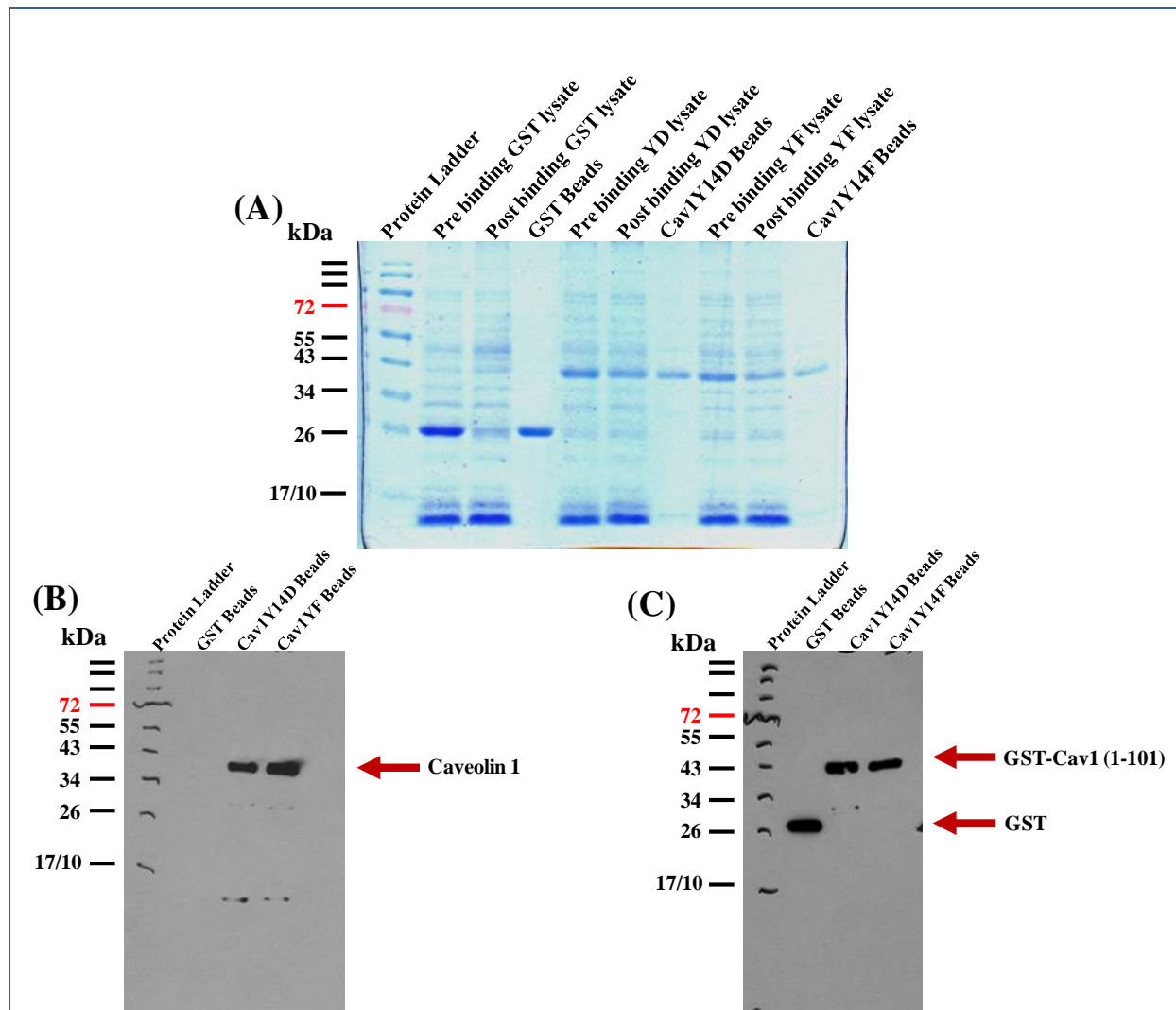
Figure 3.3: Preparation of GST, GST-Cav1(1-101)Y14D and GST-Cav1(1-101)Y14F beads and validation. (A) GST, Cav1 (1-101)Y14D and Cav1 (1-101)Y14F induced protein were tagged to GST beads. Coomassie blue stained gel shows the SDS-PAGE of pre binding, post binding, purified GST alone, GST-Cav1 (1-101)Y14D and GST-Cav1 (1-101)Y14F beads. (B) & (C) Purity of the prepared beads was confirmed through western blotting and probed for (B) Cav1 (40kDa) and (C) GST (GST-26kDa and GST-Cav1-43kDa).

3.1.2 Pull down assay and proteomics

GST pull down assay was performed using GST alone (5µl) as a negative control, GST-Cav1 (1-101)Y14D (10µl) and GST-Cav1 (1-101)Y14F (10µl) beads. DU145 cell lysate was used for pull down assay. DU145 cells from a confluent plate were lysed using the GST lysis buffer (pH-7.4), centrifuged and total protein concentration was measured using Bradford method. About 15mg of total protein was used for pull down. The lysate was incubated with the beads for 3 h at 4ºC on a rotator to encourage the interaction of the proteins with its binding domains (Cav1 variants). The beads were washed and subjected to the thrombin (0.1U) cleavage overnight for cleaving off Cav1 and its interactome from GST beads. The supernatant was collected and further processed for quantitative proteomics. Samples were vacuum dried and after reduction (with DTT) and alkylation (with IAA), trypsinized for 18-22 h at 37ºC. The trypsinized samples were desalted and formaldehyde labeled as follows: Cav1(1-101)Y14D with CH2O (light), Cav1(1-101)Y14F with CD2O (medium) and GST with 13CD2O (heavy) formaldehydes, which gave +28 Da, +32Da and +36 Da mass shift to the peptides respectively. Post mixing, the sample was desalted again to remove any impurity. The samples were loaded onto the plate for Mass spectrometry run and were analyzed against human database using MaxQuant software package designed for analyzing large data sets from quantitative MS **(Schaab et. al, 2012)**. Quantitative ratios of interacting partners with GST alone, Cav1(1-101)Y14D and Cav1(1-101)Y14F were obtained. Proteins having ≥2 peptides **(as shown below in Table 3.1)** were considered for further bioinformatics analysis. Around 17 proteins (refer IDs in **Table 3.1** marked as *) such as Annexin A2, Coronin-1C, Drebrin, Flotillin-2 from the Cav1(1-101)Y14D and Cav1(1-101)Y14F list have been previously shown to interact with Cav1 **(Byrne et. al, 2012; Lian et. al, 2013, Ji et.al, 2007; Hein et. al, 2015; Boettcher et. al, 2010)**.

ID	Detail	Log_Mean Cav1(1-101)Y14F/ Cav1(1-101)Y14D	Log_SD Cav1(1-101)Y14F/ Cav1(1-101)Y14D	Number of observations
P06733	Alpha-enolase	-2.3743	0.0314	3
P04083	Annexin A1	-2.1238	0.1220	4
P04075	Fructose-bisphosphate aldolase A	-2.0849	0.1486	4
P29401	Transketolase	-2.0844	0.1140	3
E7ERW2	Aspartate aminotransferase	-2.0481	0.0354	2
E7EQR4	Ezrin	-2.0132	0.0211	2
P10809	60 kDa heat shock protein, mitochondrial	-1.9726	0.0695	3
P62937	Peptidyl-prolyl cis-trans isomerase A	-1.9394	0.5378	4
E9PIR7	Thioredoxin reductase 1, cytoplasmic	-1.9175	0.0533	2
P18206	Isoform 1 of Vinculin	-1.8954	0.1552	2
P25705	ATP synthase subunit alpha, mitochondrial	-1.8734	0.1531	3
B4DLR8	NAD(P)H dehydrogenase [quinone] 1	-1.8645	0.1463	2
P06576	ATP synthase subunit beta, mitochondrial	-1.8610	0.1318	2
P60174	Isoform 2 of Triosephosphate isomerase	-1.8595	0.6562	4
P22392	Nucleoside diphosphate kinase B	-1.8422	0.1515	3
P43490	Nicotinamide phosphoribosyltransferase	-1.8311	0.1283	3
P27797	Calreticulin	-1.8225	0.0902	2
P07737	Profilin-1	-1.7964	0.1507	3
P00441	Superoxide dismutase [Cu-Zn]	-1.7892	0.1804	2
E7EUT4	Glyceraldehyde-3-phosphate dehydrogenase	-1.7853	0.4248	5
P13667	Protein disulfide-isomerase A4	-1.7693	0.3647	3
P07237	Protein disulfide-isomerase	-1.7659	0.1205	4
O60701	UDP-glucose 6-dehydrogenase	-1.7404	0.3694	3
P07900*	Heat shock protein HSP 90-alpha	-1.7328	0.2041	3
P61026	Ras-related protein Rab-10	-1.7274	0.5453	3
F5GX11	Proteasome subunit alpha type-1	-1.6838	0.2467	2
P05362	Intercellular adhesion molecule 1	-1.6778	0.1503	3
E7EUJ8	Creatine kinase B-type	-1.6687	0.3431	3
P40926	Malate dehydrogenase, mitochondrial	-1.6553	0.9398	3
P14314	Isoform 2 of Glucosidase 2 subunit beta	-1.6493	0.0464	2
C9J8F3	Fructose-bisphosphate aldolase C (Fragment)	-1.6407	0.1645	2
B7Z7A9	Phosphoglycerate kinase	-1.6374	0.6823	2
F5H0T1	Stress-induced-phosphoprotein 1	-1.5947	0.1040	2
Q9H3N1	Thioredoxin-related transmembrane protein 1	-1.5654	0.7402	3
P12763	Alpha-2-HS-glycoprotein precursor	-1.5456	0.6061	2
P14618	Pyruvate kinase isozymes M1/M2	-1.5317	0.8127	8
O94925	Isoform 2 of Glutaminase kidney isoform, mitochondrial	-1.5056	0.5835	3
Q06830	Peroxiredoxin-1	-1.5008	0.0450	3

ID	Detail	Log_Mean Cav1(1-101)Y14F/ Cav1(1-101)Y14D	Log_SD Cav1(1-101)Y14F/ Cav1(1-101)Y14D	Number of observations
P61978	Heterogeneous nuclear ribonucleoprotein K	-1.4953	0.6991	5
P60842	Eukaryotic initiation factor 4A-I	-1.4902	0.0988	3
P08758	Annexin A5	-1.4738	0.6780	3
P14625	Endoplasmin	-1.4338	0.0891	3
E9PMW7	Elongation factor 1-delta	-1.4075	0.0654	3
G3V1A4	Cofilin 1 (Non-muscle)	-1.3803	0.1553	3
P08238	Heat shock protein HSP 90-beta	-1.3662	0.3738	5
Q9NZM1	Isoform 6 of Myoferlin	-1.3587	0.0211	3
P06744	Glucose-6-phosphate isomerase	-1.3574	0.6987	2
Q5TCU6	Talin 1	-1.3569	0.1519	3
P34932	Heat shock 70 kDa protein 4	-1.3427	0.4763	2
P63104	14-3-3 protein zeta/delta	-1.3411	0.4488	3
Q86UY0	TXNDC5 protein	-1.3411	0.1100	4
B4DEM7	T-complex protein 1 subunit theta	-1.3405	0.2581	2
P08729	Keratin, type II cytoskeletal 7	-1.3223	0.2046	4
P37802	Transgelin-2	-1.3219	0.9508	3
P09936	Ubiquitin carboxyl-terminal hydrolase isozyme L1	-1.3168	0.8381	3
P05787*	Keratin, type II cytoskeletal 8	-1.3091	0.2354	5
O43707	Alpha-actinin-4	-1.3039	0.0540	3
B3KQT9	Protein disulfide-isomerase A3	-1.2832	0.5641	5
B7Z254	Protein disulfide-isomerase A6	-1.2688	0.4939	3
P13639	Elongation factor 2 OS=Homo sapiens	-1.2648	0.3133	4
P61604	10 kDa heat shock protein, mitochondrial	-1.2640	0.0669	2
E9PH38	Serine/threonine-protein phosphatase 2A 65 kDa regulatory subunit A alpha isoform	-1.2518	0.0941	2
Q6IQ15	EEF1A1 protein	-1.2491	0.0650	3
Q9UJZ1	Stomatin-like protein 2	-1.2478	0.0750	3
P08727	Keratin, type I cytoskeletal 19	-1.2469	0.1879	4
Q5HY54	Filamin-A	-1.2423	0.1091	5
Q8IVF2	Isoform 3 of Protein AHNAK2	-1.2348	0.2380	3
P31946	Isoform Short of 14-3-3 protein beta/alpha	-1.2305	0.4880	2
Q9BVK6	Transmembrane emp24 domain-containing protein 9	-1.2293	0.2372	2
P27695	DNA-(apurinic or apyrimidinic site) lyase	-1.2283	0.0874	2
P05783	Keratin, type I cytoskeletal 18	-1.2147	0.1648	5
Q58FF8	Putative heat shock protein HSP 90-beta 2	-1.2089	0.3989	2
Q04637	Isoform E of Eukaryotic translation initiation factor 4 gamma 1	-1.2030	0.1359	3
Q14697	Neutral alpha-glucosidase AB	-1.1960	0.6227	3

ID	Detail	Log_Mean Cav1(1-101)Y14F/ Cav1(1-101)Y14D	Log_SD Cav1(1-101)Y14F/ Cav1(1-101)Y14D	Number of observations
P11021	78 kDa glucose-regulated protein	-1.1850	0.0992	4
P68371	Tubulin beta-4B chain	-1.1818	0.0323	4
P35613*	Isoform 2 of Basigin	-1.1740	0.0780	3
Q14974	Importin subunit beta-1	-1.1720	0.1324	2
O75369-2	Isoform 2 of Filamin-B OS=Homo sapiens	-1.1695	0.1232	4
Q92688	Isoform 2 of Acidic leucine-rich nuclear phosphoprotein 32 family member B	-1.1670	0.6337	3
E9PPU1	40S ribosomal protein S3	-1.1555	0.1609	2
Q9UHB6-4	Isoform 4 of LIM domain and actin-binding protein 1	-1.1473	0.9301	2
B7Z4V2	Stress-70 protein, mitochondrial	-1.1401	0.3801	4
P27348	14-3-3 protein theta	-1.1350	0.0182	3
P68363	Tubulin alpha-1B chain	-1.1240	0.6655	2
Q13509	Tubulin beta-3 chain	-1.1228	0.1689	2
F5H634	D-3-phosphoglycerate dehydrogenase	-1.1139	0.0270	2
P42704	Leucine-rich PPR motif-containing protein, mitochondrial	-1.0937	0.3676	3
P24752	Acetyl-CoA acetyltransferase, mitochondrial	-1.0665	0.6315	3
P35232	Prohibitin	-1.0396	0.0625	4
P16403	Histone H1.2	-1.0336	0.3945	3
Q9BQE3	Tubulin alpha-1C chain	-1.0301	0.5019	3
B4E3S0*	Coronin-1C	-1.0270	1.0995	2
E7EM48	DNA replication licensing factor MCM4	-1.0115	0.0955	2
Q5JP53	Tubulin beta chain	-0.9981	0.3012	3
G3XAM7	Catenin (Cadherin-associated protein), alpha 1, 102kDa, isoform CRA_a	-0.9904	0.0841	2
P11142	Heat shock cognate 71 kDa protein	-0.9782	0.1529	5
F5GY37	Prohibitin-2	-0.9758	0.1392	4
P07355*	Annexin A2	-0.9750	0.0620	3
P49411	Elongation factor Tu, mitochondrial	-0.9624	0.0442	4
Q09666	Neuroblast differentiation-associated protein AHNAK	-0.9483	0.0702	3
B4DIT7	Protein-glutamine gamma-glutamyltransferase 2	-0.9477	0.7956	2
F8WCJ1	Eukaryotic translation initiation factor 5A-2	-0.9349	0.5546	3
O43795-2*	Isoform 2 of Unconventional myosin-Ib	-0.9241	0.5751	3
B4E2Z3	4F2 cell-surface antigen heavy chain	-0.9221	0.8094	3
P62258	14-3-3 protein epsilon	-0.9215	0.2564	2
Q15149	Isoform 7 of Plectin	-0.9202	0.2668	4
P26196	Probable ATP-dependent RNA helicase DDX6	-0.9170	0.2666	2
P34955	Alpha-1-antiproteinase precursor	-0.9142	0.4411	2

ID	Detail	Log_Mean Cav1(1-101)Y14F/ Cav1(1-101)Y14D	Log_SD Cav1(1-101)Y14F/ Cav1(1-101)Y14D	Number of observations
P62851	40S ribosomal protein S25	-0.9066	0.0689	3
P08107	Heat shock 70 kDa protein 1A/1B	-0.9021	0.2991	3
P49756	RNA-binding protein 25	-0.9008	0.5851	3
Q13263	Isoform 2 of Transcription intermediary factor 1-beta	-0.8893	0.0168	2
P13010	X-ray repair cross-complementing protein 5	-0.8814	0.0726	4
P09874	Poly [ADP-ribose] polymerase 1	-0.8803	0.4354	3
P02786	Transferrin receptor protein 1	-0.8703	0.5549	3
Q9P2E9	Isoform 2 of Ribosome-binding protein 1	-0.8563	0.1161	2
P05141	ADP/ATP translocase 2	-0.8526	0.4697	2
B7Z3U6	ATPase, Na+/K+ transporting, alpha 1 polypeptide, isoform CRA_a	-0.8473	0.2938	5
P18124	60S ribosomal protein L7	-0.8412	0.5883	3
P05556	Integrin beta-1	-0.8399	0.7351	3
P78527	DNA-dependent protein kinase catalytic subunit	-0.8045	0.0787	2
P06703	Protein S100-A6	-0.7909	0.9328	3
P08670	Vimentin	-0.7853	0.1828	4
P30040	Endoplasmic reticulum resident protein 29	-0.7807	0.5531	3
B0QYK1	Ewing sarcoma breakpoint region 1	-0.7743	0.1158	2
E9PNX1	Serpin H1 (Fragment)	-0.7670	0.0956	3
Q9NX58	Cell growth-regulating nucleolar protein	-0.7583	0.4291	2
P60660	Myosin light polypeptide 6	-0.7482	0.6558	2
Q14152	Eukaryotic translation initiation factor 3 subunit A	-0.7476	0.2351	2
P16152	Carbonyl reductase [NADPH] 1	-0.7432	0.1218	3
P60953*	Cell division control protein 42 homolog	-0.7384	0.3903	3
B3KX72	Heterogeneous nuclear ribonucleoprotein U	-0.7308	0.0440	3
B4DUR8	T-complex protein 1 subunit gamma	-0.7292	0.4371	3
D6RF44	Heterogeneous nuclear ribonucleoprotein D0 (Fragment)	-0.7284	0.2211	3
E7EWT1	Dolichyl-diphosphooligosaccharide--protein glycosyltransferase 48 kDa subunit	-0.7267	0.2742	2
Q5VTE0	Putative elongation factor 1-alpha-like 3	-0.7199	0.5029	2
P55072	Transitional endoplasmic reticulum ATPase	-0.7173	0.1419	4
Q9Y265	RuvB-like 1	-0.7117	0.1207	2
G3V529	ATP-dependent RNA helicase DDX24	-0.7066	0.4151	2
P98179	Putative RNA-binding protein 3	-0.7018	0.0652	2
O94832	Unconventional myosin-Id	-0.7017	0.4474	2
P42166	Lamina-associated polypeptide 2, isoform alpha	-0.7015	0.4065	2
Q00688	Peptidyl-prolyl cis-trans isomerase	-0.6910	0.0866	3
P32119	Peroxiredoxin-2	-0.6899	0.0514	2

ID	Detail	Log_Mean Cav1(1-101)Y14F/ Cav1(1-101)Y14D	Log_SD Cav1(1-101)Y14F/ Cav1(1-101)Y14D	Number of observations
P61247	40S ribosomal protein S3a	-0.6894	0.6080	3
P26641	Elongation factor 1-gamma	-0.6850	0.1396	3
A8MW50	L-lactate dehydrogenase (Fragment)	-0.6823	0.1166	2
P60903	Protein S100-A10	-0.6813	0.6511	2
P04843	Dolichyl-diphosphooligosaccharide--protein glycosyltransferase subunit 1	-0.6754	0.4362	2
P23396	40S ribosomal protein S3	-0.6724	0.7895	2
Q00839	Heterogeneous nuclear ribonucleoprotein U	-0.6719	0.8244	2
P21266	Glutathione S-transferase Mu 3	-0.6601	0.3372	3
P16615	Isoform 5 of Sarcoplasmic/endoplasmic reticulum calcium ATPase 2	-0.6586	0.4450	3
B4E2W0	3-ketoacyl-CoA thiolase	-0.6560	0.1073	4
P15880	40S ribosomal protein S2	-0.6274	0.4030	2
B8ZZQ6	Prothymosin alpha	-0.6157	0.0827	2
P04899*	Guanine nucleotide-binding protein G(i) subunit alpha-2	-0.6007	0.0966	3
P62873	Guanine nucleotide-binding protein G(I)/G(S)/G(T) subunit beta-1	-0.6006	0.2105	2
Q15365	Poly(rC)-binding protein 1	-0.6000	0.5127	4
B4DW94	Ras-related protein Rap-1b	-0.5969	0.1748	2
Q658Y7	Bromodomain containing 2, isoform CRA_a	-0.5933	0.0178	2
P62081	40S ribosomal protein S7	-0.5913	0.1487	3
P09488	Glutathione S-transferase Mu 1	-0.5854	0.1943	4
F8WC15	Solute carrier family 2, facilitated glucose transporter member 1	-0.5843	0.2618	3
P27824	Calnexin	-0.5801	0.6507	4
P17066	Heat shock 70 kDa protein 6	-0.5796	0.4730	2
Q5TCJ4	Lamin A/C	-0.5772	0.1991	3
B4DHG0	Dihydrolipoyl dehydrogenase, mitochondrial	-0.5713	0.1845	2
P23528	Cofilin-1	-0.5713	0.5241	2
B4DLV4	Serine hydroxymethyltransferase	-0.5677	0.1360	2
O75083	WD repeat-containing protein 1	-0.5581	0.4852	2
P23284	Peptidyl-prolyl cis-trans isomerase B	-0.5571	0.7291	2
Q14573*	Inositol 1,4,5-trisphosphate receptor type 3	-0.5568	0.2964	2
B7Z9S8	Sodium/potassium-transporting ATPase subunit beta-1	-0.5361	0.6585	2
Q9NQX4	Unconventional myosin-Vc	-0.5300	0.4874	3
P26038	Moesin	-0.5238	0.7365	4
Q9UQ80	Proliferation-associated protein 2G4	-0.5202	0.2874	3
Q9Y6N5	Sulfide:quinone oxidoreductase, mitochondrial	-0.5198	0.3706	4

ID	Detail	Log_Mean Cav1(1-101)Y14F/ Cav1(1-101)Y14D	Log_SD Cav1(1-101)Y14F/ Cav1(1-101)Y14D	Number of observations
Q07021	Complement component 1 Q subcomponent-binding protein, mitochondrial	-0.5185	0.7967	3
P00338	L-lactate dehydrogenase A chain	-0.5154	0.1178	3
P20618	Proteasome subunit beta type-1	-0.5055	0.1524	2
Q9BSJ8	Extended synaptotagmin-1	-0.4948	0.6105	4
F8VWB4	Protein phosphatase 1 regulatory subunit 12A	-0.4919	0.1198	2
O75947	ATP synthase subunit d, mitochondrial	-0.4869	0.6282	4
P18669	Phosphoglycerate mutase 1	-0.4830	0.1571	3
P40227	T-complex protein 1 subunit zeta	-0.4733	0.1168	2
P46940	Ras GTPase-activating-like protein IQGAP1	-0.4721	0.1878	3
B4DV79	Eukaryotic translation initiation factor 3 subunit B	-0.4561	0.0900	2
P63244	Guanine nucleotide-binding protein subunit beta-2-like 1	-0.4539	0.0382	2
P05198	Eukaryotic translation initiation factor 2 subunit 1	-0.4504	0.0559	2
Q13501*	Isoform 2 of Sequestosome-1	-0.4451	0.1884	4
O43491	Band 4.1-like protein 2	-0.4294	0.2141	4
H0YB56	Protein LYRIC (Fragment)	-0.4119	0.3729	2
P46781	40S ribosomal protein S9	-0.4104	0.2407	3
E7EUY0	DNA-dependent protein kinase catalytic subunit	-0.4084	0.3155	2
E9PED3	Ankycorbin	1.4597	1.7209	3
P0426*	Keratin, type II cytoskeletal 1	0.9935	0.1425	2
E9PNW4	CD59 glycoprotein	0.9115	0.4333	2
P09497	Isoform Non-brain of Clathrin light chain B	0.8704	0.1612	2
P35052	Glypican-1	0.7158	0.5555	2
P12956	X-ray repair cross-complementing protein 6	0.7010	0.7579	3
P0CW22	40S ribosomal protein S17-like	0.6719	0.0359	2
P62158	Calmodulin	0.6600	0.2209	5
H0YHC3	Nucleosome assembly protein 1-like 1 (Fragment)	0.6531	1.1008	3
Q03135	Caveolin-1	0.6417	0.5777	4
Q8WXF1	Isoform 2 of Paraspeckle component 1	0.6396	0.5806	2
E9PIZ3	60S ribosomal protein L8	0.6187	0.3957	2
Q07065	Cytoskeleton-associated protein 4	0.6038	0.3215	2
P62280	40S ribosomal protein S11	0.5861	0.3520	2
E9PLL6	60S ribosomal protein L27a	0.5857	0.2735	2
P84098	60S ribosomal protein L19	0.5753	0.2869	3
P05386	60S acidic ribosomal protein P1	0.5730	0.1137	3
P47914	60S ribosomal protein L29	0.5556	0.1953	2
Q5QNZ2	ATP synthase subunit b, mitochondrial	0.5532	0.0945	2
Q7Z406	Myosin-14	0.5527	0.1798	4

ID	Detail	Log_Mean Cav1(1-101)Y14F/ Cav1(1-101)Y14D	Log_SD Cav1(1-101)Y14F/ Cav1(1-101)Y14D	Number of observations
P62424	60S ribosomal protein L7a	0.5336	0.2188	3
P05387	60S acidic ribosomal protein P2	0.5331	0.0363	4
P30050	60S ribosomal protein L12	0.5232	0.1233	3
Q9Y3U8	60S ribosomal protein L36	0.5215	0.0791	2
Q16643*	Drebrin	0.5124	0.3817	3
F5H8M4	Gelsolin	0.5119	0.2415	3
P62263	40S ribosomal protein S14	0.5085	0.1286	2
Q92614	Isoform 4 of Unconventional myosin-XVIIIa	0.5073	0.0941	4
P17844	Probable ATP-dependent RNA helicase DDX5	0.4930	0.2774	3
E9PMP7	LIM domain only protein 7 (Fragment)	0.4856	0.1092	4
F8VQE1*	LIM domain and actin-binding protein 1	0.4835	0.0794	4
C9JXB8	60S ribosomal protein L24	0.4815	0.1631	3
F8W1R7	Myosin light polypeptide 6	0.4801	0.1288	4
P67936	Tropomyosin alpha-4 chain	0.4765	0.1381	4
Q9NYL9	Tropomodulin-3	0.4759	0.1786	4
D6RD46	LIM and calponin homology domains-containing protein 1	0.4748	0.2511	2
F8W181	60S ribosomal protein L6 (Fragment)	0.4747	0.2843	2
P67809	Nuclease-sensitive element-binding protein 1	0.4695	0.1886	3
Q14254*	Flotillin-2	0.4691	0.1553	4
Q9Y281	Cofilin-2	0.4668	0.2616	2
P52272	Isoform 2 of Heterogeneous nuclear ribonucleoprotein M	0.4667	0.1440	4
P62906	60S ribosomal protein L10a	0.4649	0.1201	4
H7BYY1	Tropomyosin 1 (Alpha), isoform CRA_m	0.4621	0.0155	2
Q9UBI6	Guanine nucleotide-binding protein G(I)/G(S)/G(O) subunit gamma-12	0.4590	0.1819	2
E7EQV9	Ribosomal protein L15 (Fragment)	0.4569	0.2415	2
H0YEN5	40S ribosomal protein S2 (Fragment)	0.4519	0.4427	2
P61353	60S ribosomal protein L27	0.4516	0.2154	2
D6RAN4	60S ribosomal protein L9 (Fragment)	0.4510	0.0335	3
C9J8U1	Cytospin-A (Fragment)	0.4508	0.0061	2
O00161	Synaptosomal-associated protein 23	0.4487	0.4713	2
P35908	Keratin, type II cytoskeletal 2 epidermal	0.4472	0.4038	5
Q07157	Tight junction protein ZO-1	0.4471	0.7842	2
P35580	Myosin-10	0.4460	0.0739	4
P80723	Brain acid soluble protein 1	0.4409	0.4930	3
Q13813	Spectrin alpha chain, brain	0.4402	0.3200	4
Q99880	Histone H2B type 1-L	0.4372	0.2409	3

ID	Detail	Log_Mean Cav1(1-101)Y14F/ Cav1(1-101)Y14D	Log_SD Cav1(1-101)Y14F/ Cav1(1-101)Y14D	Number of observations
Q5JR95	40S ribosomal protein S8	0.4347	0.2488	2
P25398	40S ribosomal protein S12	0.4346	0.0483	2
P09493	Isoform 3 of Tropomyosin alpha-1 chain	0.4344	0.0647	3
P61254	60S ribosomal protein L26	0.4328	0.3131	2
Q14126*	Desmoglein-2	0.4324	0.2344	3
P18621	60S ribosomal protein L17	0.4309	0.1464	3
E7EWF1	60S ribosomal protein L4	0.4284	0.1096	4
Q9ULV4*	Coronin-1C	0.4260	0.0862	4
P83111	Serine beta-lactamase-like protein LACTB, mitochondrial	0.4252	0.1912	3
P35579	Myosin-9	0.4234	0.2000	4
Q96AG4	Leucine-rich repeat-containing protein 59	0.4224	0.3515	4
P26373	60S ribosomal protein L13	0.4184	0.1239	4
P14384	Carboxypeptidase M	0.4165	0.2318	3
P13645	Keratin, type I cytoskeletal 10	0.4138	0.2906	4
P06753	Isoform 2 of Tropomyosin alpha-3 chain	0.4131	0.0753	4
P45880	Voltage-dependent anion-selective channel protein 2	0.4119	0.1577	4
P21589	5-nucleotidase	0.4114	0.1803	4
P05388	60S acidic ribosomal protein P0	0.4108	0.0484	4
D6RG13	40S ribosomal protein S3a (Fragment)	0.4103	0.1311	4
Q12797	Aspartyl/asparaginyl beta-hydroxylase	0.4083	0.2635	2
P52597	Heterogeneous nuclear ribonucleoprotein F	0.4063	0.1530	3
B3KTM6	60S ribosomal protein L5	0.4060	0.1662	3

Table 3.1: *Analyzed list of Quantitative Proteomics showing Cav1(1-101)Y14D and Cav1(1-101)Y14F interactome having ≥ 1.5 fold change (Number of experiments=6). * shows proteins whose interaction with Cav1 were previously reported in the literature.*

3.1.2.1 Proteomic Data analysis

The proteins were subjected to Quantitative Proteomics P-value Calculator (QPCC) from University of Queensland ("UQ"), which provided the significance for the interacting proteins **(Chen et. al, 2014)**. Proteins were filtered through two stages. In Stage 1 raw peptide ratio was taken as input which uses a distribution-free permutation method based on replicated log (ratio). In stage 2, the specific filter generated the significantly altered proteins list based on p-value with ratio of fold-change or standard deviation from the mean. Proteins having more than 1.5 fold change were kept as a criterion.

There were about 428 proteins detected based on Orbitrap MS/MS analysis, which interacted differentially with Cav1(1-101)Y14D and Cav1(1-101)Y14F having peptide $\geq$ 2. *After considering the cutoff of 1.5 fold change,* 196 proteins showed higher interaction with Cav1(1-101)Y14D and 78 proteins with Cav1(1-101)Y14F as shown in Venn diagram (**Figure 3.4**). This shows that phosphorylation of Cav1(1-101)Y14 has a higher interacting capacity compared to non-phosphorylated form of Cav1(1-101)Y14.
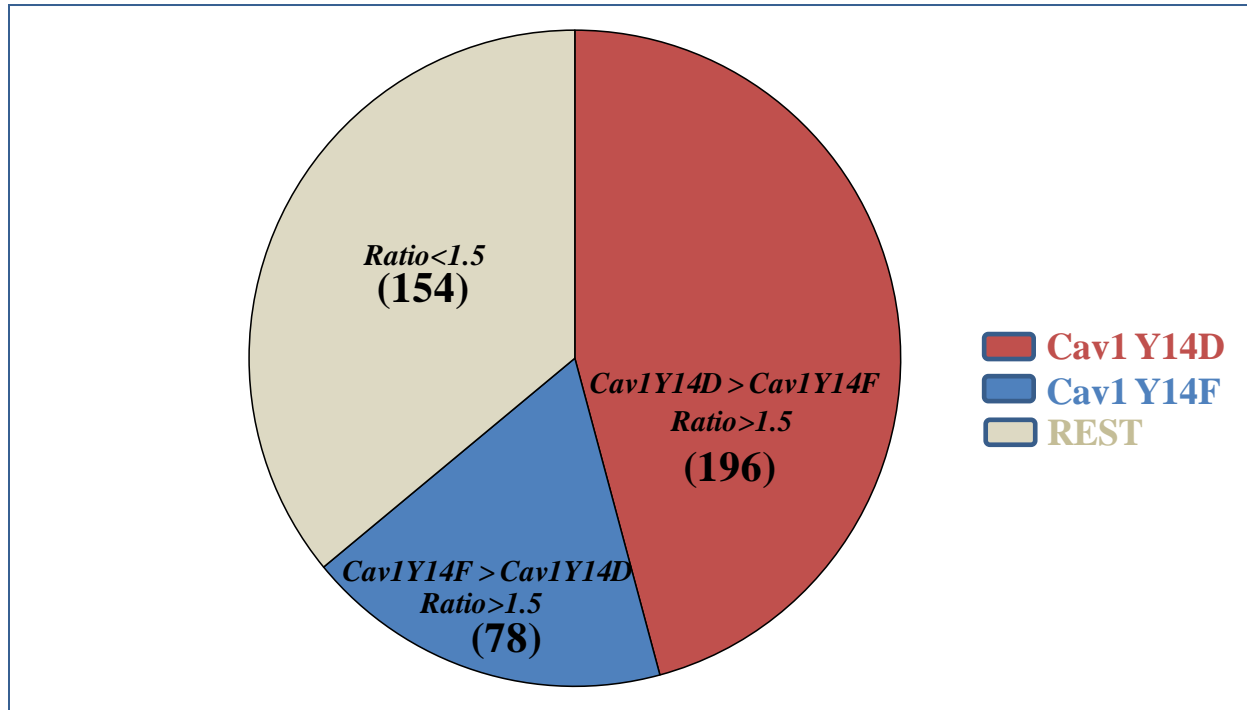
Figure 3.4: Pie chart showing interacting protein partners from quantitative proteomic of Cav1(1-101)Y14D and Cav1(1-101)Y14F (number of experiments = 6). Quantitative proteomics of Cav1(1-101)Y14D and Cav1(1-101)Y14F found 428 differential interacting partners (number of observations ≥2). After considering the cutoff of 1.5 fold change, 154 proteins were filtered out. Following fold change cutoff around 196 proteins are shown interacting specifically to Cav1(1-101)Y14D and 78 proteins with Cav1(1-101)Y14F. Quantitative proteomics p-value calculator (QPPC) was used to filter the significantly altered proteins based on p-value with ratio fold-change ≥1.5.

The PANTHER (Protein ANalysis THrough Evolutionary Relationships) Classification System is an important tool for GO analysis (**Mi et. al, 2013**). PANTHER classifies high throughput proteomics data into family and subfamily and reveals the molecular functions, biological processes and pathways involved. Statistical overrepresentation test of PANTHER compares the interacting proteins within two different groups. The analysis is based on binomial statistical tool and has Bonferroni correction which tests every individual hypothesis, "N" having a statistical significance level (x) at "x/N time" to the required overall significance level. It provides the observed fold enrichment of the genes, significant p-Value. + or − sign indicates over-presentation or under-presentation respectively. The list of Cav1(1-101)Y14D and Cav1(1-101)Y14F interactome were used for analysis and each protein identifier received a GO term and was clustered. PANTHER's Statistical overrepresentation test was used to compare and classify the interactome as it provided the statistical significance (p-value) for the test. First Cav1(1-101)Y14D was used as test file and Cav1(1-101)Y14F as reference file, (**Figure 3.5A**). This showed that according to GO biological process in Cav1(1-101)Y14D, proteins involved in regulation of cellular stress (HSP70), cell proliferation, signal transduction, metabolic process (**PKM2**) and apoptosis (**HSP90**) were interacting more. Then, Cav1(1-101)Y14F was used as test file and Cav1(1-101)Y14D as reference file, (**Figure 3.5B)** which showed that with Cav1(1-101)Y14F in GO biological process, proteins that regulate actin cytoskeleton and RNA processing have elevated interaction. This further showed that the Cav1(1-101)Y14D and Cav1(1-101)Y14F interactome was different from each other.
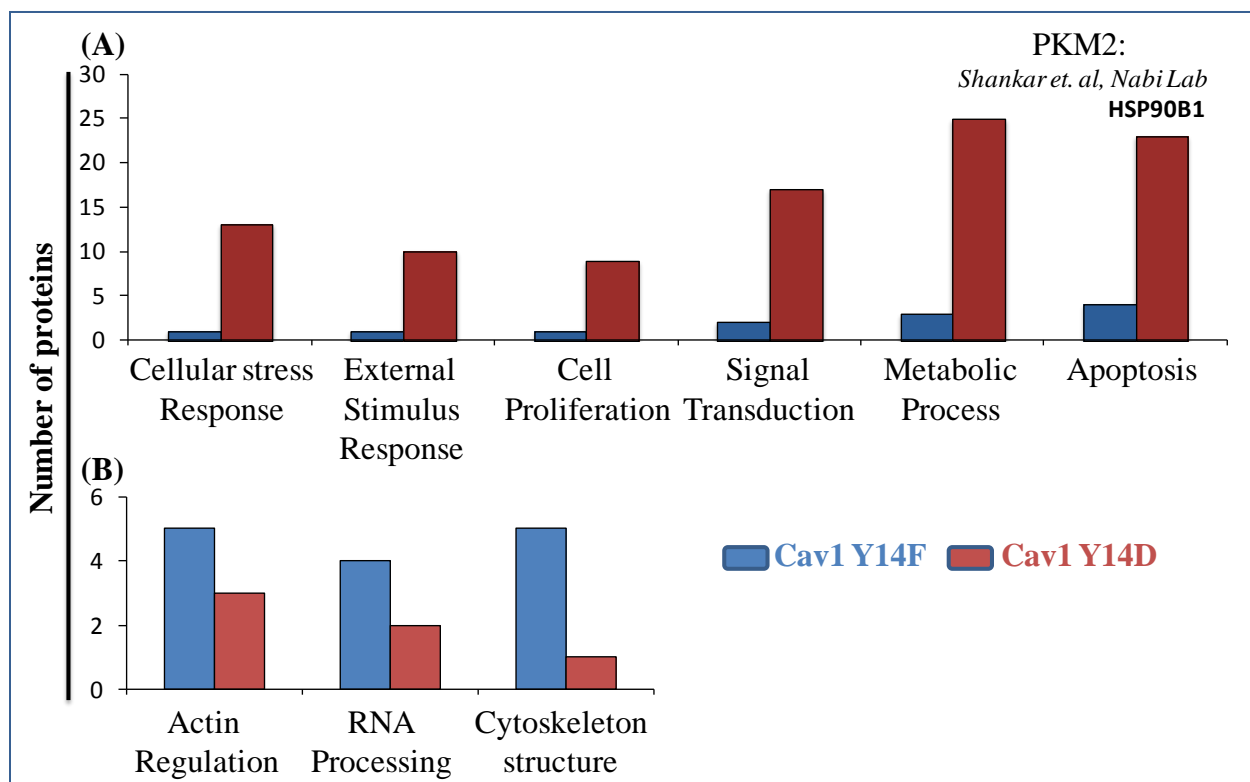
Figure 3.5: PANTHER Classification System for GO Biological Process analysis of Cav1(1-101)Y14D and Cav1(1-101)Y14F interactome. PANTHER (Protein ANalysis THrough Evolutionary Relationships) classification system from Gene Ontology (GO) Consortium was used to analyze the proteomics data for function, ontology, pathways and statistical analysis (lists of proteins were statistically analyzed by Bonferroni correction). GO Biological Process shows different groups/classes of proteins interacting with (A) Cav1(1-101)Y14D interactome (analyzed file) to Cav1(1-101)Y14F interactome (reference file) and (B) Cav1(1-101)Y14F interactome (analyzed file) to Cav1(1-101)Y14D interactome (reference file).

PANTHER search analysis also showed different classes based on GO Cellular Process. Similarly, Cav1(1-101)Y14D was used as test file and Cav1(1-101)Y14F as reference file first as shown, (**Figure 3.6A**). Cav1(1-101)Y14D interacted more with proteins involved in regulation of focal adhesion (**Vinculin**), cell junction, microtubule cytoskeleton and chromosome. Later, Cav1(1-101)Y14F was used as test file and Cav1(1-101)Y14F as reference file, (**Figure 3.6B**). This showed that Cav1(1-101)Y14F interacts more with proteins that regulates the actomyosin complex, actin filament bundle and ribonucleoprin.
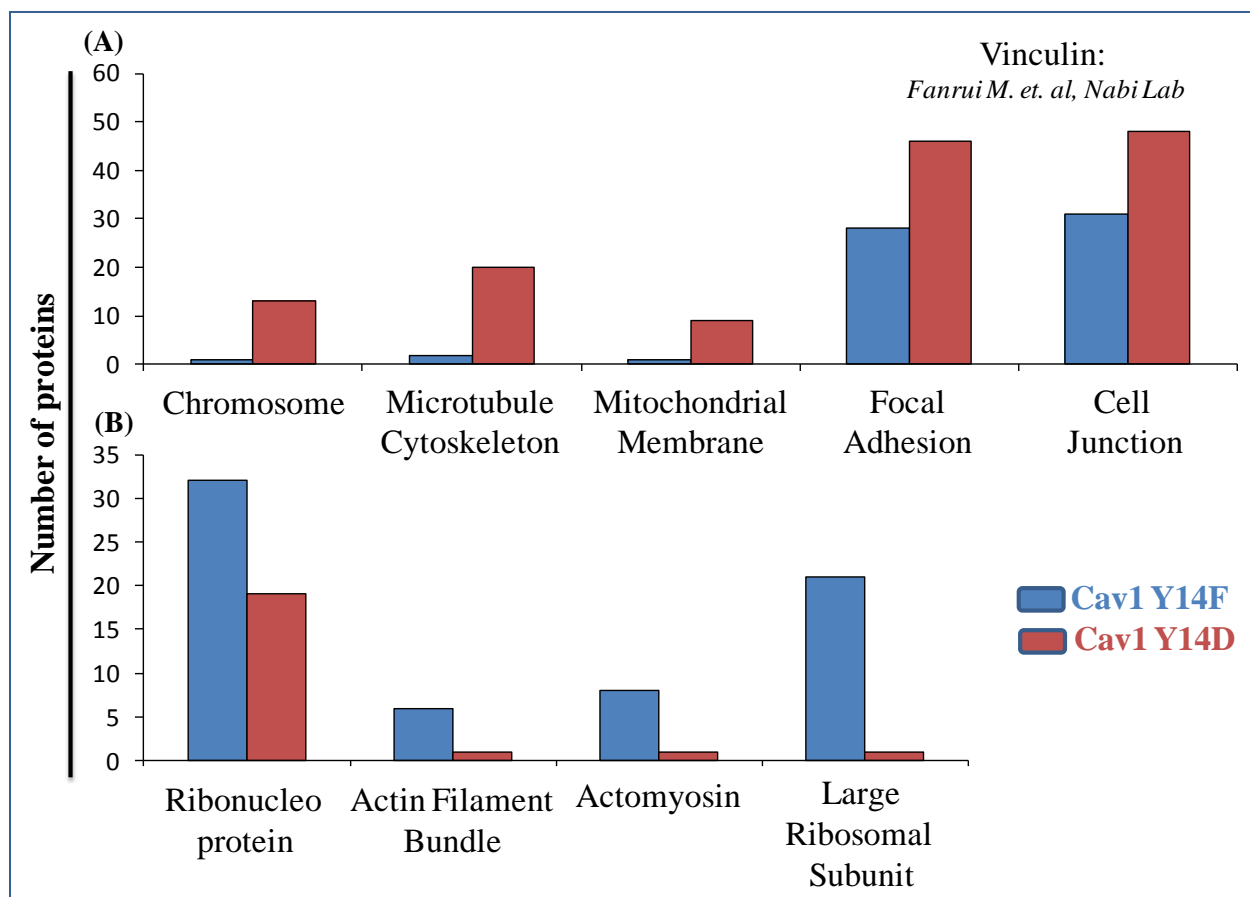
Figure 3.6: PANTHER Classification System for GO Cellular Process analysis of Cav1(1-101)Y14D and Cav1(1-101)Y14F interactome. Over-representation test in PANTHER classification system for GO Cellular Process (Bonferroni correction) shows different groups/classes of proteins interacting with (A) Cav1(1-101)Y14D interactome (analyzed file) to Cav1(1-101)Y14F interactome (reference file) and (B) Cav1(1-101)Y14F interactome (analyzed file) to Cav1(1-101)Y14D interactome (reference file).

As various proteins interacting with Cav1(1-101)Y14D are involved in cell proliferation, metabolism and focal adhesion, we compared it with our previously generated DU145 pseudopod list (a work done by previous post-doc in our lab, Jay Shankar). As expected, comparing the Cav1-Y14D and Cav1-Y14F interactome with DU145 pseudopod proteomics list gave some interesting results. Approximately 84 differential interacting proteins from Cav1(1-101)Y14D were enriched in pseudopod proteome while only 24 proteins were enriched from Cav1(1-101)Y14F (**Figure 3.7**). This showed that various proteins interacting with Cav1(1-101)Y14D interactome were indeed enriched in pseudopod.
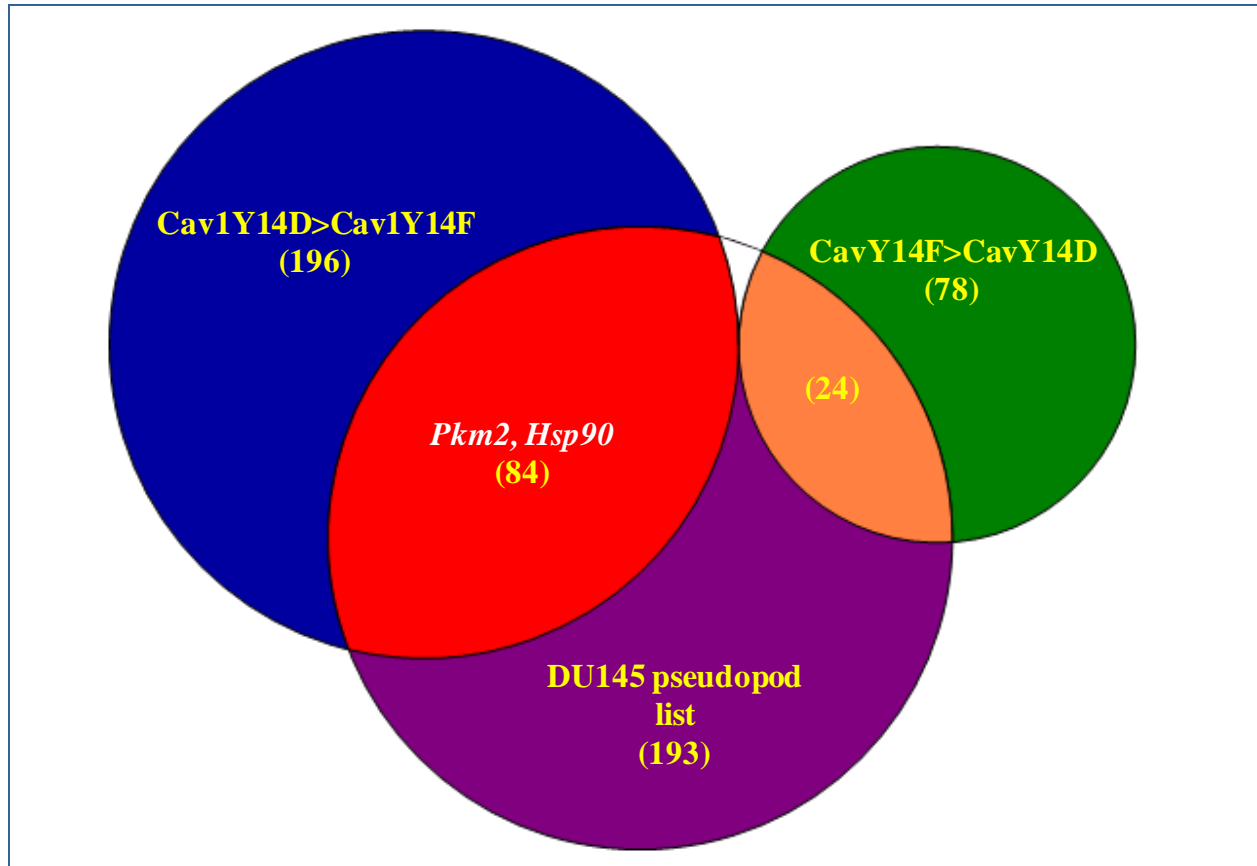
Figure 3.7: Venn diagram showing comparison of Cav1(1-101)Y14D and Cav1(1-101)Y14F interactome with DU145 pseudopod list. *The proteins interacting with Cav1(1-101)Y14D>Cav1(1-101)Y14F (196 proteins) v.s. Cav1(1-101)Y14F>Cav1(1-101)Y14D (78 proteins) v.s. DU145 pseudopod lists (193 proteins) were analyzed. Maximum number of proteins from Cav1(1-101)Y14D interactome (84 proteins) were pseudopod enriched compared to Cav1(1-101)Y14F interactome (24 proteins).*

PANTHER search analysis was performed for pseudopod enriched proteins in Cav1(1-101)Y14D interactome (84 proteins) and Cav1(1-101)Y14F (24 proteins). First, Cav1(1-101)Y14D was used as test file and Cav1(1-101)Y14F as reference file first for GO Biological process. As evident (**Figure 3.8A**), it showed various proteins involved in apoptosis, proteins responding to cell stimulus/stress, cell modification and metabolic processes were present in Cav1(1-101)Y14D pseudopod enriched list. Using Cav1(1-101)Y14F as test file and Cav1(1-101)Y14D as reference file for GO Biological process showed proteins involved in translation and ribonucleoprotein biogenesis were present in Cav1(1-101)Y14F pseudopod enriched list (**Figure 3.8B**).
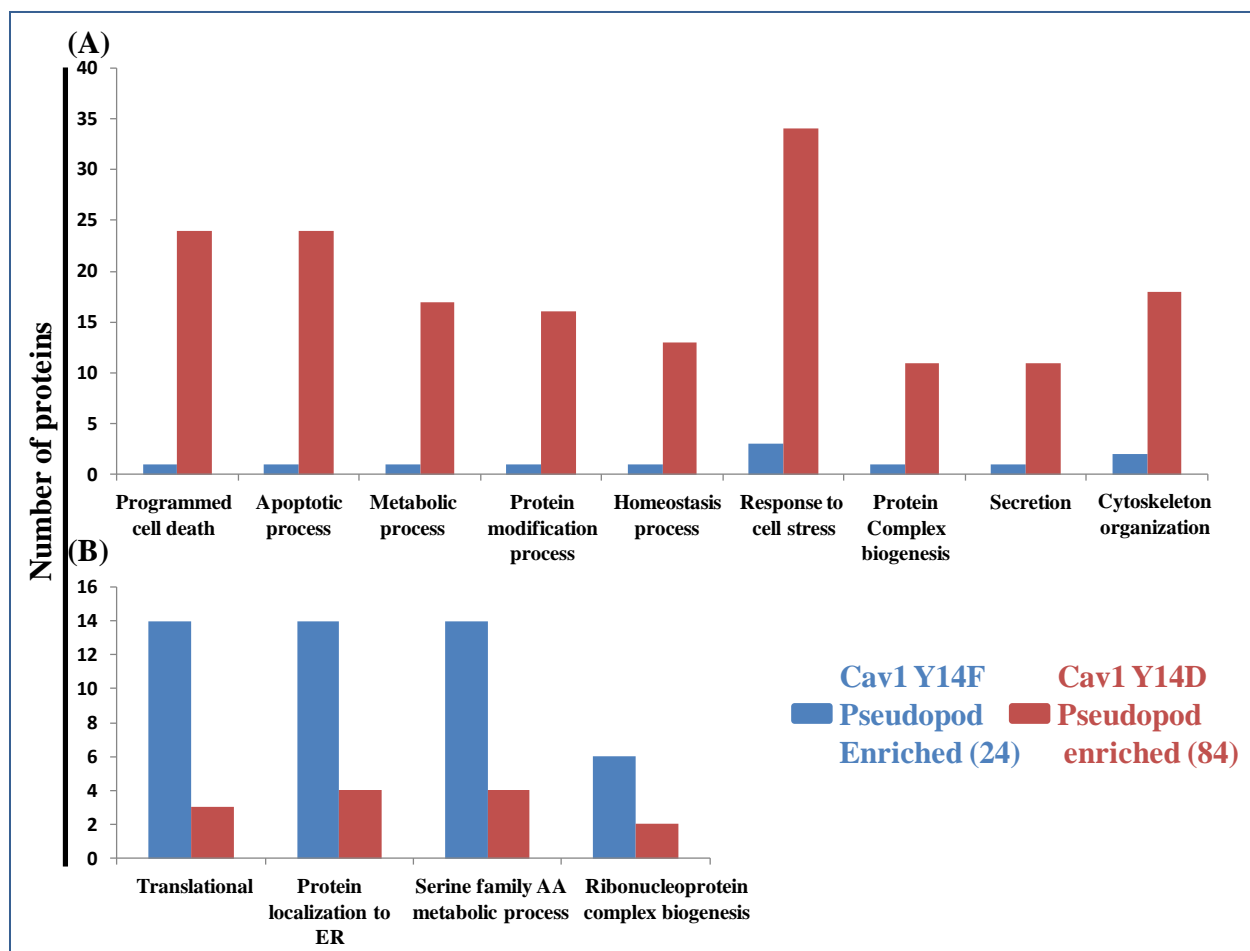
Figure 3.8: PANTHER Classification System for GO Biological Process analysis of pseudopod enriched Cav1(1-101)Y14D and Cav1(1-101)Y14F. Over-representation test in PANTHER classification system for GO Biological Process (Bonferroni correction) was used to compare Cav1(1-101)Y14D interactome (84 proteins) with pseudopod enriched Cav1(1-101)Y14F interactome (24 proteins) for GO biological function. (A) Comparison between Cav1(1-101)Y14D interactome (analyzed file) to Cav1(1-101)Y14F interactome (reference file) and (B) comparison between Cav1(1-101)Y14F interactome (analyzed file) to Cav1(1-101)Y14D interactome (reference file) showing different classes of proteins.

PANTHER search analysis for GO cellular components also showed different classes of proteins binding to pseudopod enriched list of Cav1(1-101)Y14D and Cav1(1-101)Y14F. Cav1(1-101)Y14D interactome (analyzed file) was compared with Cav1(1-101)Y14F interactome (reference file) (**Figure 3.9A)** based on Go cellular components. This showed that proteins involved in cell surface protein complex, cell junction and focal adhesions were present in Cav1(1-101)Y14D enriched pseudopod list. Cav1(1-101)Y14F interactome (analyzed file) was compared with Cav1(1-101)Y14D interactome (reference file) (**Figure 3.9B)**, which showed that the proteins involved in ribosomal subunits were present in Cav1(1-101)Y14F enriched pseudopod list.
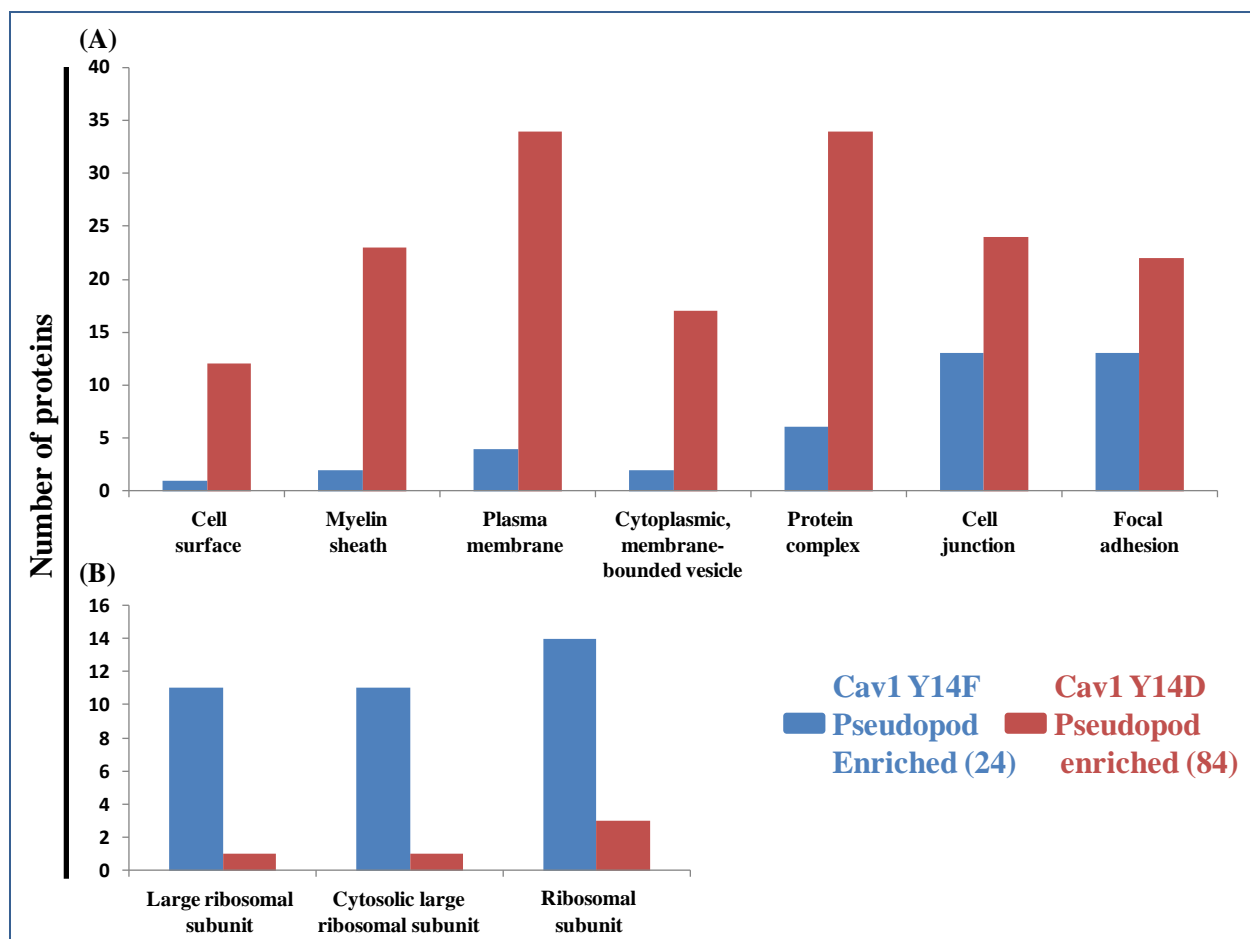
Figure 3.9: PANTHER Classification System for GO Cellular Process analysis of pseudopod enriched Cav1(1-101)Y14D and Cav1(1-101)Y14F. Over-representation test in PANTHER classification system was used for GO cellular components (Bonferroni correction). (A) Comparison between Cav1(1-101)Y14D interactome (analyzed file) and Cav1(1-101)Y14F interactome (reference file) and (B) comparison between Cav1(1-101)Y14F interactome (analyzed file) and Cav1(1-101)Y14D interactome (reference file) showing different classes of proteins.

3.1.2.3 Validations

Of the proteomics list, few of the candidate proteins were selected for further validation. Our lab studies FAs and Cav1 phosphorylation (**Joshi et.al, 2008; Meng et. al, 2015**). We have also found PKM2 interacting with Cav1(1-101)Y14D (Jay Shankar). Thus, Vinculin and PKM2 proteins interacting with Cav1(1-101)Y14D (**Figure 3.10A)**, as show in table, were obvious choices to validate.

In vitro GST pull down assay and western blotting was performed. **Figure 3.10B** reveals very strong interaction PKM2 and evident interaction of Vinculin with GST-Cav1(1-101)Y14D.

Quantification of these results showed that Cav1(1-101)Y14D interaction with PKM2 and Vinculin were indeed significant (**Figure 3.10C & 3.10D)**.

(A)

Accession	# Peptides	Cav1Y14F/Y14D	Description
P18206-2	2	0.1502	Isoform 1 of Vinculin
H3BTN5	4	0.2161	Pyruvate kinase
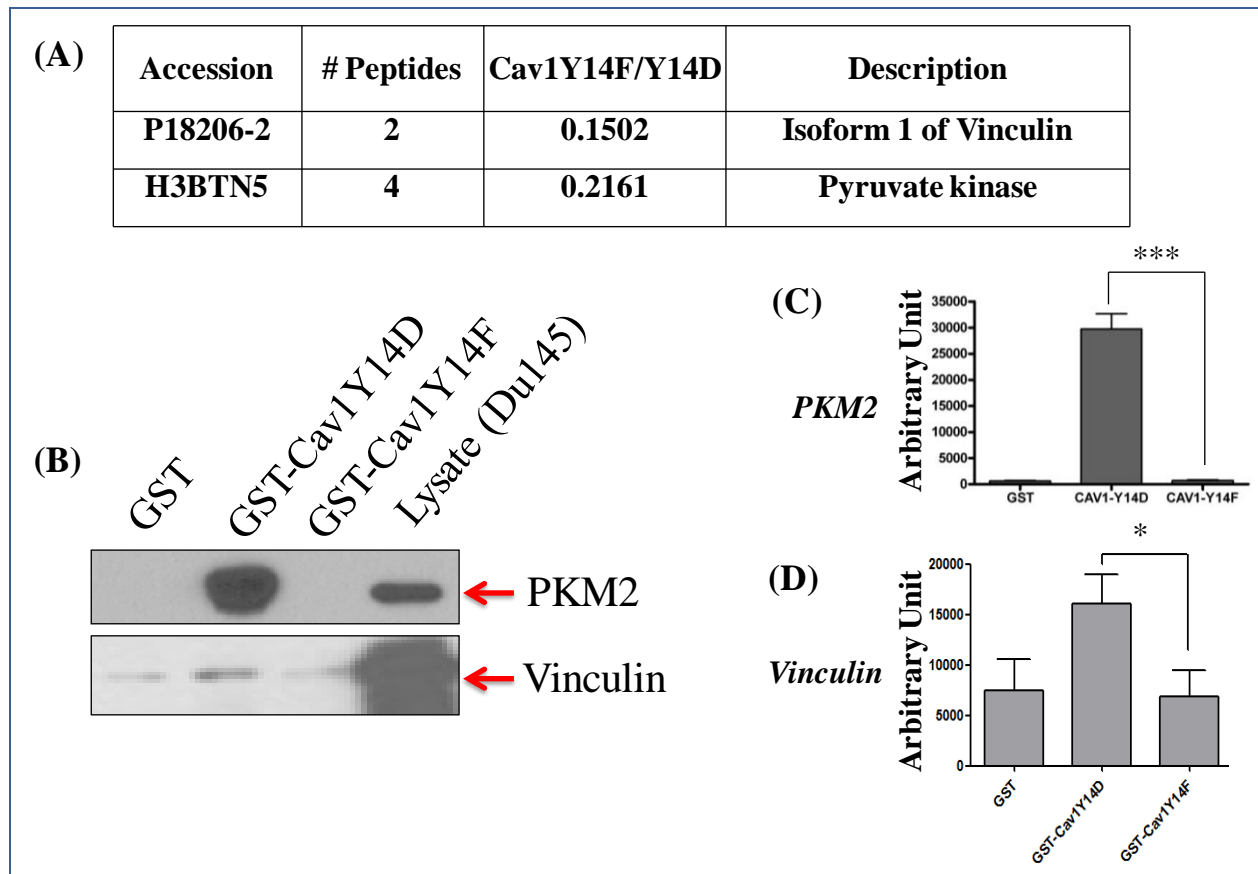
Figure 3.10: Validation of Cav1(1-101)Y14D interaction with PKM2 and Vinculin by GST pull down and western blotting (number of experiment=3). *(A) Proteomics data for Vinculin and PKM2 shows more interaction with Cav1(1-101)Y14D compared to Cav1(1-101)Y14F. (B) GST pull down and western blotting to probe for PKM2 and Vinculin. (C) Blots analyzed to show the Statistical significance through One-way ANNOVA where * means P<0.05 and *** means P<0.001.*

3.2 COMPARATIVE PROTEOMICS ANALYSIS OF THE CSD MUTANT (F92A/V94A) OF CAV1(1-101)Y14D AND CAV1(1-101)Y14F TO FIND THE DEPENDENCY OF BINDING PARTNERS ON CSD DOMAIN

3.2.1 GST-tagged construct

Double point mutations (at F92A/V94A) were incorporated in the CSD domain of Cav1(1-101)Y14D and Cav1(1-101)Y14F constructs by site-directed mutagenesis. These double point mutations have been well characterized to elucidate the role of CSD in Cav1 binding with other proteins. The PCR product was transformed into DH5-alpha (*E.coli* strain). Few colonies were sequence verified and positives were transformed into BL21, (*E.coli* strain) for induction. Sequencing results are as below:

3.2.1.1 Cav1(1-101)Y14F-CSD construct sequence

5'3' Frame 3

nnnnnnnnnnaaatcggntctggtt

ccgcgtggatccccggaattcatgggcgacggcggcagcggcggcggcagctctgggggc

 P R G S P E F M G D G G S G G G S S G G

aaatacgtagactcggagggacatctcttcaccgttcccatccgggaacagggcaacatc

 K Y V D S E G H L **F** T V P I R E Q G N I

tacaagcccaacaacaaggccatggcagacgagctgagcgagaagcaagtgtacgacgcg

 Y K P N N K A M A D E L S E K Q V Y D A

cacaccaaggagatcgacctggtcaaccgcgaccctaaacacctcaacgatgacgtggtc

 H T K E I D L V N R D P K H L N D D V V

aagattgactttgaagatgtgattgcagaaccagaagggacacacagttttgacggcatt

 K I D F E D V I A E P E G T H S F D G I

tggaaggccagcttcaccaccgccactgcgacgaaatactggttttaccgctagctcgag

W K A S F T T A T A T K Y W F Y R -

3.2.1.2 Cav1(1-101)Y14D-CSD construct sequence

nnnnnnnnnncanncggntctggttccgcgtggatccccggaattcatg

X X X X X X X X X L V P R G S P E F M

ggcgacggcggcagcggcggcggcagctctgggggcaaatacgtagactcggagggacat

G D G G S G G G S S G G K Y V D S E G H

ctcgacaccgttcccatccgggaacagggcaacatctacaagcccaacaacaaggccatg

L D T V P I R E Q G N I Y K P N N K A M

gcagacgagctgagcgagaagcaagtgtacgacgcgcacaccaaggagatcgacctggtc

A D E L S E K Q V Y D A H T K E I D L V

aaccgcgaccctaaacacctcaacgatgacgtggtcaagattgactttgaagatgtgatt

N R D P K H L N D D V V K I D F E D V I

gcagaaccagaagggacacacagttttgacggcatttggaaggccagcttcaccaccgcc

A E P E G T H S F D G I W K A S F T T A

actgcgacgaaatactggttttaccgctagctcgagcggccgcatcgtgactgactgacg

T A T K Y W F Y R -

The proteins for GST, Cav1 (1-101)Y14D-CSD and Cav1 (1-101)Y14F-CSD mutants were induced as discusssed before. BL21 bacterial cells containing verified plasmids were innoculated in 6 ml culture media and cultured overnight at 37 ℃ , 225rpm shaker, and 2.5 ml was used for induction in 15 ml culture next day. 0.4mM IPTG was used and the cultures were maintained at 250 rpm, 30℃ for 3 h to induce protein expression. An aliquot from uninduced and induced protein samples were separated by SDS-PAGE to check the induction. As evident, uninduced

lanes did not show protein expression whereas induced proteins are visible in IPTG added lane,

(**Figure 3.11).** The protein pellets from large preps were stored at -80ºC for further use.
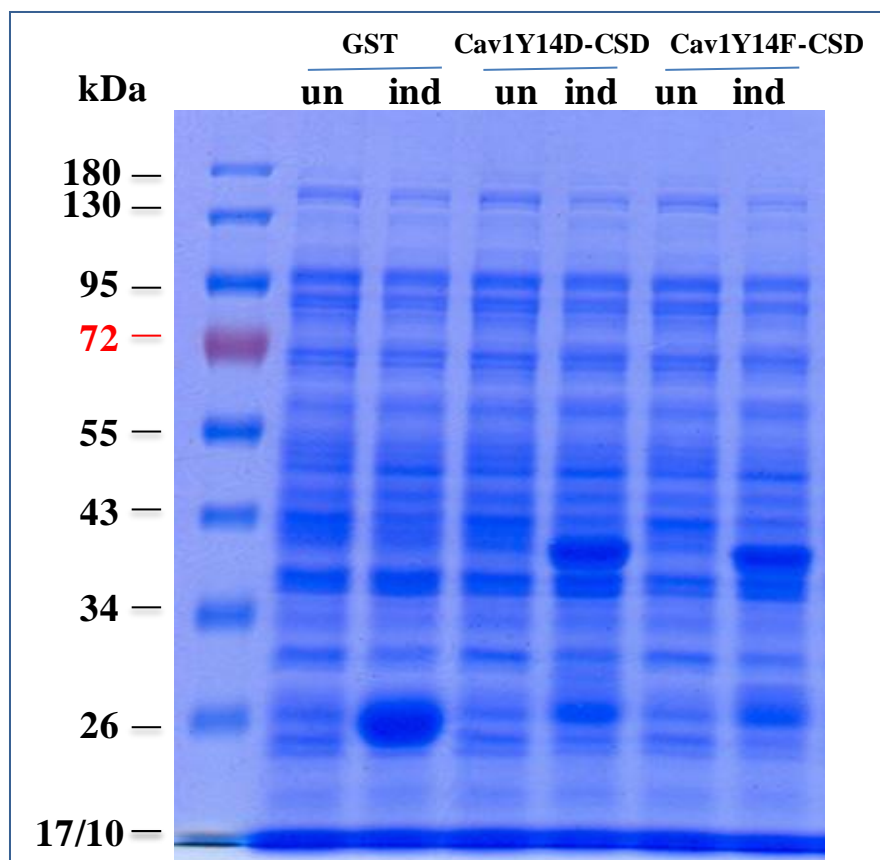
Figure 3.11: Coomassie Blue stained SDS-PAGE Gel for uninduced (un) and induced (ind) GST, Cav1 (1-101)Y14D-CSD and Cav1 (1-101)Y14F-CSD mutant proteins. Commassie stained gel showing Induced and uninduced proteins from GST, Cav1 (1-101)Y14D-CSD and Cav1 (1-101)Y14F-CSD mutants were separated on SDS-PAGE.

Similarly, the induced protein pellet for GST, Cav1 (1-101)Y14D-CSD and Cav1 (1-101)Y14F-CSD mutants were lysed and incubated with GST beads for 3 h at 4ºC rotator. The beads were washed and stored in PBS with 10mM DTT for later use. The pre binding, post binding and purified beads protein were separated on SDS-PAGE (**Figure 3.12**).
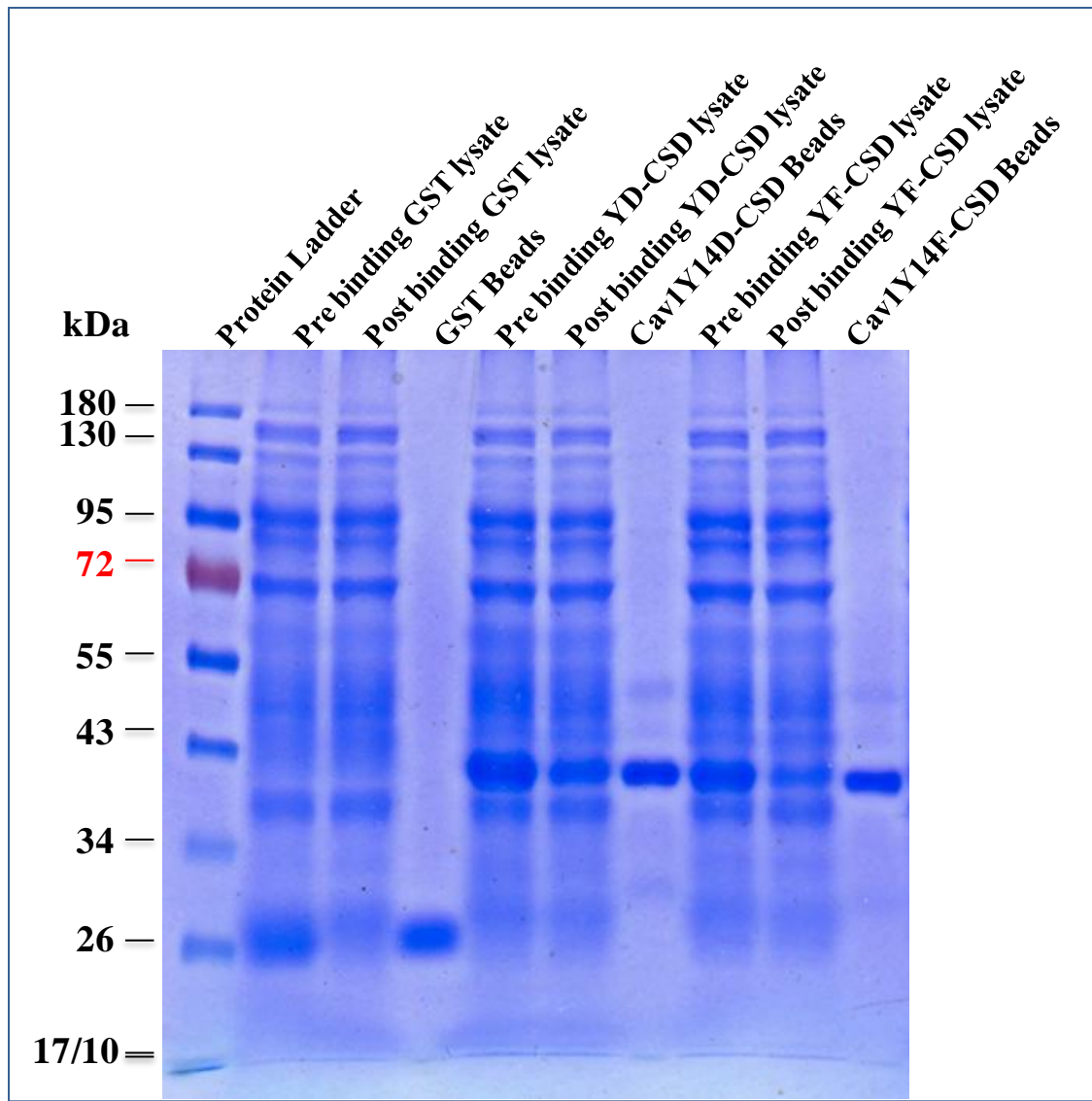
Figure 3.12: Preparation of GST, GST-Cav1 (1-101)Y14D-CSD and GST-Cav1 (1-101)Y14F-CSD beads. *GST beads were prepared from induced protein of GST, Cav1 (1-101)Y14D-CSD and Cav1 (1-101)Y14F-CSD mutants. Pre binding, post binding and purified beads protein were separated on SDS-PAGE for the GST, GST-Cav1 (1-101)Y14D-CSD and GST-Cav1 (1-101)Y14F-CSD beads and gel was commassie stained.*

The purified GST, GST-Cav1 (1-101)Y14D-CSD and GST-Cav1 (1-101)Y14F-CSD beads proteins were separated on SDS-PAGE, transferred onto nitrocellulose membrane and subjected to western blotting. The blots were probed for Cav1 and GST antibodies to check purity of the beads. GST blots show expression of GST and GST fused Cav1 variants (**Figure 3.13A)** and when probed with anti-Cav1 antibody, only GST fused Cav1 variants showed a band at ~40kDa size, confirming specificity and expression of right protein (**Figure 3.13B)**.
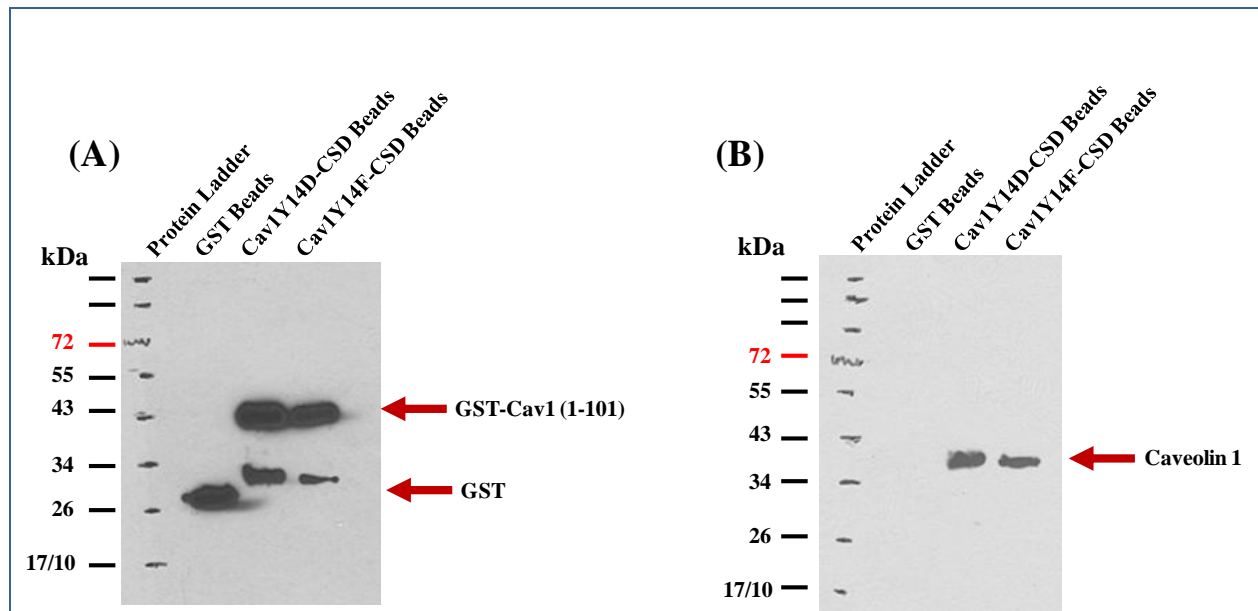
Figure 3.13: GST, GST-Cav1 (1-101)Y14D-CSD and GST-Cav1 (1-101)Y14F-CSD beads purification and validation by western blotting. *The purity of GST, GST-Cav1 (1-101)Y14D-CSD and GST-Cav1 (1-101)Y14F-CSD prepared beads was confirmed by western blotting and probed for (A) GST (GST-26kDa and GST-Cav1-43kDa) and (B) Cav1 (40kDa).*

3.2.2 Pull down assay and proteomics

The GST pull down assays were performed for two separate sets of samples: one set contained GST alone, GST-Cav1 (1-101)Y14D and GST-Cav1 (1-101)Y14D-CSD beads whereas another set contained GST alone, GST-Cav1 (1-101)Y14F and GST-Cav1 (1-101)Y14F-CSD. GST beads were incubated with 15mg total proteins of DU145 cell lysate for 3 h, washed and thrombin cleaved. The supernatant was used to perform quantitative proteomics as discussed earlier. We labeled Cav1(1-101)Y14D with light, Cav1(1-101)Y14D-CSD with medium and GST alone with heavy formaldehyde and in another set, Cav1(1-101)Y14F with light, Cav1(1-101)Y14F-CSD with medium and GST alone with heavy formaldehyde. The proteins having peptides≥2 for Cav1(1-101)Y14D and Cav1(1-101)Y14D-CSD group **(as shown below in Table 3.2)** and for Cav1(1-101)Y14F and Cav1(1-101)Y14F-CSD group **(as shown below in Table 3.3)** were considered for further bioinformatics analysis. We found 6 proteins from Cav1(1-101)Y14D and Cav1(1-101)Y14D-CSD list whereas 11 proteins from Cav1(1-101)Y14F and Cav1(1-101)Y14F-CSD list (refer IDs in **Table 3.2** and **Table 3.3** marked as *) whose interactions with Cav1 were previously reported in the literature. Our proteomics data did not reveal many of the previously found Cav1 interacting proteins. One of the possible reasons for this could be because we used phosphorylated and non- phosphorylated, and also CSD mutant forms of Cav1. Another reason could be because proteomics analyses filter out most of the low abundant proteins.

ID	Detail	Log_Mean Cav1(1-101)Y14D-CSD/ Cav1(1-101)Y14D	Log_SD Cav1(1-101)Y14D-CSD/ Cav1(1-101)Y14D	Number of observations
P02533	Keratin, type I cytoskeletal 14	-1.1771	0.6407	2
O00159	Isoform 2 of Unconventional myosin-Ic	-1.0608	0.1220	2
Q99880	Histone H2B type 1-L	-1.0025	0.8127	2
P05388	60S acidic ribosomal protein P0	-0.9663	0.5448	2
O60841	Eukaryotic translation initiation factor 5B	-0.9492	0.1023	2
O43795*	Isoform 2 of Unconventional myosin-Ib	-0.9380	0.9072	2
P39019	40S ribosomal protein S19	-0.8914	0.5196	2
Q9Y4I1	Unconventional myosin-Va	-0.8842	0.5407	3
Q9Y3U8	60S ribosomal protein L36	-0.8515	0.6922	2
Q9UPN4	Isoform 3 of 5-azacytidine-induced protein 1	-0.8258	0.3700	2
P09493	Isoform 3 of Tropomyosin alpha-1 chain	-0.8181	0.5857	2
P62424	60S ribosomal protein L7a	-0.8149	0.4895	4
P09488	Glutathione S-transferase Mu 1	-0.8055	0.3553	2
Q9UNX3	60S ribosomal protein L26-like 1	-0.7958	0.0165	2
P0CW22	40S ribosomal protein S17-like	-0.7872	0.4158	2
Q07065	Cytoskeleton-associated protein 4	-0.7801	0.3715	4
P16403	Histone H1.2	-0.7677	0.7051	3
P62805	Histone H4	-0.7534	0.8962	3
F8W181	60S ribosomal protein L6 (Fragment)	-0.7499	0.3883	4
P41091	Eukaryotic translation initiation factor 2 subunit 3	-0.7474	0.2986	2
C9JXB8	60S ribosomal protein L24	-0.7443	0.5396	2
P07355*	Annexin A2	-0.7406	0.2322	4
P61353	60S ribosomal protein L27	-0.7403	0.4222	4
E7EQV9	Ribosomal protein L15 (Fragment)	-0.7392	0.5132	3
Q3B7A4	60S acidic ribosomal protein P0	-0.7373	0.5058	2
P49756	RNA-binding protein 25	-0.7367	0.0003	2
B4E3S0*	Coronin-1C	-0.7322	0.3956	2
P17096	Isoform HMG-Y of High mobility group protein HMG-I/HMG-Y	-0.7298	0.4329	2
P13647	Keratin, type II cytoskeletal 5	-0.7233	0.5401	2
P60866	40S ribosomal protein S20	-0.7231	0.0159	2
B4DR70	RNA-binding protein FUS	-0.7215	0.3823	3
O43290	U4/U6.U5 tri-snRNP-associated protein 1	-0.7051	0.7059	2
Q9P2E9	Isoform 1 of Ribosome-binding protein 1	-0.7026	0.1306	3
E9PKZ0	60S ribosomal protein L8	-0.6949	0.5528	3
P04264*	Keratin, type II cytoskeletal 1	-0.6884	0.3531	2
E7ESE0	60S ribosomal protein L9 (Fragment)	-0.6873	0.6627	2
Q96AG4	Leucine-rich repeat-containing protein 59	-0.6865	0.4745	4

ID	Detail	Log_Mean Cav1(1-101)Y14D-CSD/ Cav1(1-101)Y14D	Log_SD Cav1(1-101)Y14D-CSD/ Cav1(1-101)Y14D	Number of observations
H0Y2W2	ATPase family AAA domain-containing protein 3A (Fragment)	-0.6846	0.2097	2
P30050	60S ribosomal protein L12	-0.6845	0.5687	2
P05198	Eukaryotic translation initiation factor 2 subunit 1	-0.6802	0.3971	3
P61247	40S ribosomal protein S3a	-0.6723	0.4676	2
P11940	Isoform 2 of Polyadenylate-binding protein 1	-0.6699	0.1347	2
O60832	H/ACA ribonucleoprotein complex subunit 4	-0.6650	0.1311	3
P67809	Nuclease-sensitive element-binding protein 1	-0.6642	0.4138	4
Q9NQX4	Unconventional myosin-Vc	-0.6618	0.6000	2
Q09666	Neuroblast differentiation-associated protein	-0.6616	0.2035	3
Q5SSJ5	Heterochromatin protein 1-binding protein 3	-0.6558	0.6380	2
P62854	40S ribosomal protein S26	-0.6553	0.4506	2
E5RI99	60S ribosomal protein L30 (Fragment)	-0.6535	0.7597	2
P62906	60S ribosomal protein L10a	-0.6436	0.4262	4
Q9NR30	Nucleolar RNA helicase 2	-0.6388	0.2818	4
B4DM74	60S ribosomal protein L18a	-0.6365	0.5725	2
P62750	60S ribosomal protein L23a	-0.6289	0.3848	3
I3L1L3	Myb-binding protein 1A (Fragment)	-0.6257	0.3032	2
Q8NE71	ATP-binding cassette sub-family F member 1	-0.6139	0.4196	3
D6RAF8	Heterogeneous nuclear ribonucleoprotein D0 (Fragment)	-0.6091	0.5483	2
P23246	Splicing factor, proline- and glutamine-rich	-0.6040	0.0593	3
O94832	Unconventional myosin-Id	-0.6023	0.6297	2
P62899	60S ribosomal protein L31	-0.6017	0.4439	3
Q7Z406	Myosin-14	-0.5896	1.1511	4
P48047	ATP synthase subunit O, mitochondrial	-0.5843	0.2515	2
P62277	40S ribosomal protein S13	-0.5836	0.4709	4
Q86V81	THO complex subunit 4	-0.5798	0.7749	2
O60884	DnaJ homolog subfamily A member 2	-0.5785	0.4448	2
B4DJB1	AP-2 complex subunit mu	-0.5643	0.2066	2
P26373	60S ribosomal protein L13	-0.5574	0.3836	4
P14618	Pyruvate kinase isozymes M1/M2	-0.5573	0.1083	3
P23396	40S ribosomal protein S3	-0.5569	0.1705	3
P46940	Ras GTPase-activating-like protein	-0.5539	0.2641	3
Q5VTE0	Putative elongation factor 1-alpha-like 3	-0.5520	0.3259	2
P18621	60S ribosomal protein L17	-0.5516	0.2632	4
P46087	Isoform 2 of Putative ribosomal RNA methyltransferase	-0.5443	0.2894	2
Q86UE4	Protein LYRIC	-0.5442	0.1065	2

ID	Detail	Log_Mean Cav1(1-101)Y14D-CSD/ Cav1(1-101)Y14D	Log_SD Cav1(1-101)Y14D-CSD/ Cav1(1-101)Y14D	Number of observations
P18124	60S ribosomal protein L7	-0.5433	0.4227	3
Q4V9L5	ATP-dependent RNA helicase DDX24	-0.5396	0.2864	2
P35268	60S ribosomal protein L22	-0.5336	0.3874	4
Q9UQE7	Structural maintenance of chromosomes protein 3	-0.5281	0.4812	4
P40429	60S ribosomal protein L13a	-0.5279	0.4358	3
P62280	40S ribosomal protein S11	-0.5254	0.3186	4
B7Z6B8	2,4-dienoyl-CoA reductase, mitochondrial	-0.5225	0.3557	4
P12956	X-ray repair cross-complementing protein 6	-0.5189	0.3342	3
Q9UKS6	Protein kinase C and casein kinase substrate in neurons protein 3	-0.5179	0.5991	2
P02545	Prelamin-A/C	-0.5171	0.0781	4
P39023	60S ribosomal protein L3	-0.5151	0.3680	4
P15880	40S ribosomal protein S2	-0.5138	0.3085	2
P20042	Eukaryotic translation initiation factor 2 subunit 2	-0.5114	0.3244	3
P51116	Fragile X mental retardation syndrome-related protein 2	-0.5103	0.3016	4
O75083	WD repeat-containing protein 1	-0.5091	0.1295	3
P83111	Serine beta-lactamase-like protein LACTB, mitochondrial	-0.5085	0.2141	2
P14678	Isoform SM-B of Small nuclear ribonucleoprotein-associated proteins B and B	-0.5072	0.1754	2
F8VTY8	Proliferation-associated protein 2G4	-0.5068	0.2743	3
P08754	Guanine nucleotide-binding protein G(k) subunit alpha	-0.5041	0.1103	2
P35527	Keratin, type I cytoskeletal 9	-0.4969	1.3970	4
F8VPD4	Dihydroorotase	-0.4950	0.0909	2
Q12905	Interleukin enhancer-binding factor 2	-0.4918	0.5796	4
Q9P0L0	Vesicle-associated membrane protein-associated protein A	-0.4875	0.0154	2
P46782	40S ribosomal protein S5	-0.4830	0.3900	3
O75477	Erlin-1	-0.4812	0.0744	2
E7EWF1	60S ribosomal protein L4	-0.4722	0.4263	4
F5H667	Aspartyl/asparaginyl beta-hydroxylase	-0.4683	0.5069	4
P46783	40S ribosomal protein S10	-0.4641	0.0928	4
O75369	Isoform 2 of Filamin-B	-0.4638	0.1119	3
Q9UHB6	Isoform 4 of LIM domain and actin-binding protein 1	-0.4616	0.6484	4
Q9NX58	Cell growth-regulating nucleolar protein	-0.4594	0.2179	4
P62263	40S ribosomal protein S14	-0.4563	0.4088	2
P62249	40S ribosomal protein S16	-0.4559	0.4140	4
Q12906	Interleukin enhancer-binding factor 3	-0.4531	0.3169	3
P07948	Isoform 2 of Tyrosine-protein kinase Lyn	-0.4513	0.0856	2

ID	Detail	Log_Mean Cav1(1-101)Y14D-CSD/ Cav1(1-101)Y14D	Log_SD Cav1(1-101)Y14D-CSD/ Cav1(1-101)Y14D	Number of observations
P61978	Isoform 3 of Heterogeneous nuclear ribonucleoprotein K	-0.4489	0.3136	2
Q7Z451	AP-2 complex subunit beta	-0.4477	0.3589	4
P26641	Elongation factor 1-gamma	-0.4423	0.2764	2
Q00839	Heterogeneous nuclear ribonucleoprotein U	-0.4365	0.2407	2
P13010	X-ray repair cross-complementing protein 5	-0.4348	0.2430	4
P04899*	Guanine nucleotide-binding protein G(i) subunit alpha-2	-0.4346	0.0533	2
P14866	Heterogeneous nuclear ribonucleoprotein L	-0.4339	0.4893	3
B3KX72	Heterogeneous nuclear ribonucleoprotein U	-0.4310	0.6664	2
P19338	Nucleolin	-0.4256	0.5312	3
P68363	Tubulin alpha-1B chain	-0.4248	0.1439	2
Q9UKD2	mRNA turnover protein 4 homolog	-0.4243	0.2306	2
B3KTM6	60S ribosomal protein L5	-0.4232	0.3036	4
O95425	Isoform 2 of Supervillin	-0.4221	0.2661	2
P07814	Bifunctional glutamate/proline--tRNA ligase	-0.4196	0.1304	3
C9JB50	60S ribosomal protein L28	-0.4136	0.5708	2
H0YFC7	Cytosine-specific methyltransferase	-0.4129	0.2564	2
F5H1H6	Cytospin-A	-0.4094	0.7460	2
Q13501*	Sequestosome-1	-0.4082	0.3615	3
H0YDD8	60S acidic ribosomal protein P2 (Fragment)	1.1846	0.7924	2
F5H3X9	Serine/threonine-protein phosphatase 2A 65 kDa regulatory subunit A alpha isoform	0.9316	0.7174	2
P09382	Galectin-1	0.9148	1.1761	2
O96008	Mitochondrial import receptor subunit TOM40 homolog	0.8691	0.2872	2
P62937	Peptidyl-prolyl cis-trans isomerase A	0.8469	1.0813	2
G3V1A4	Cofilin 1 (Non-muscle), isoform CRA_a	0.8245	0.4915	2
P10620	Microsomal glutathione S-transferase 1	0.8174	0.4439	2
Q5STU3	HLA-B associated transcript 1	0.8165	0.2413	2
P14927	Cytochrome b-c1 complex subunit 7	0.7968	0.7706	2
Q86UY0	TXNDC5 protein	0.7946	0.7516	2
P00403	Cytochrome c oxidase subunit 2	0.7922	0.6153	2
P49748	Isoform 2 of Very long-chain specific acyl-CoA dehydrogenase, mitochondrial	0.7603	0.2016	2
P07737	Profilin-1	0.7239	0.5697	3
P31930	Cytochrome b-c1 complex subunit 1, mitochondrial	0.6835	0.3926	2
E9PK01	Elongation factor 1-delta (Fragment)	0.6805	0.5405	2
Q9NUQ2	1-acyl-sn-glycerol-3-phosphate acyltransferase epsilon	0.6604	0.0506	2
F8W1R7	Myosin light polypeptide 6	0.6297	1.0797	2

ID	Detail	Log_Mean Cav1(1-101)Y14D-CSD/ Cav1(1-101)Y14D	Log_SD Cav1(1-101)Y14D-CSD/ Cav1(1-101)Y14D	Number of observations
O94925	Isoform 3 of Glutaminase kidney isoform, mitochondrial	0.6194	0.2385	2
P02765	Alpha-2-HS-glycoprotein precursor	0.6149	1.0428	2
P04075	Fructose-bisphosphate aldolase A	0.6043	0.3577	2
Q1RMN8	Similar to Immunoglobulin lambda-like polypeptide 1	0.5896	0.6277	2
P10809	60 kDa heat shock protein, mitochondrial	0.5761	0.2787	3
Q92945	Far upstream element-binding protein 2	0.5738	0.4519	2
P26368	Isoform 2 of Splicing factor U2AF 65 kDa subunit	0.5630	0.4645	2
Q9Y6C9	Mitochondrial carrier homolog 2	0.5627	0.2325	2
E7EQT4	Apoptotic chromatin condensation inducer in the nucleus	0.5625	0.0501	2
Q14651	Plastin-1	0.5495	0.2014	2
B7Z6M1	Plastin-3	0.5414	0.5903	2
P27824	Calnexin	0.5268	0.6050	2
E7EUT5	Glyceraldehyde-3-phosphate dehydrogenase	0.5146	0.2701	3
P27348	14-3-3 protein theta	0.5057	0.1156	2
Q96C19	EF-hand domain-containing protein D2	0.5039	0.0811	2
P35908	Keratin, type II cytoskeletal 2 epidermal	0.4817	0.5859	3
H0YD13	CD44 antigen (Fragment)	0.4782	0.8183	2
P10412	Histone H1.4	0.4743	1.6795	2
Q9UJZ1	Stomatin-like protein 2	0.4700	0.6302	2
P13073	Cytochrome c oxidase subunit 4 isoform 1, mitochondrial	0.4668	0.5633	3
P13667	Protein disulfide-isomerase A4	0.4589	0.3715	3
P00338	L-lactate dehydrogenase A chain	0.4536	0.4632	2
P09211	Glutathione S-transferase P	0.4532	0.0082	2
A2BDY9	HLA class I histocompatibility antigen, A-3 alpha chain	0.4486	0.2610	2
P22392	Isoform 3 of Nucleoside diphosphate kinase B	0.4478	0.5105	2
Q3MHN5	Vitamin D-binding protein precursor	0.4476	0.5158	2
O14979	Isoform 3 of Heterogeneous nuclear ribonucleoprotein D-like	0.4420	1.4061	2
B7Z9S8	Sodium/potassium-transporting ATPase subunit beta-1	0.4409	0.5172	2
P06733	Alpha-enolase	0.4381	0.5458	3
Q8IZ68	Metaxin 2	0.4342	0.5235	2
E9PDB2	Malate dehydrogenase, mitochondrial	0.4304	0.3223	3
P00978	AMBP protein precursor	0.4282	0.3010	3
P25705	ATP synthase subunit alpha, mitochondrial	0.4269	0.3634	3
F8W8V7	Zinc finger protein 185	0.4237	0.6134	2

ID	Detail	Log_Mean Cav1(1-101)Y14D-CSD/ Cav1(1-101)Y14D	Log_SD Cav1(1-101)Y14D-CSD/ Cav1(1-101)Y14D	Number of observations
Q1RMK2	IGHM protein	0.4175	0.4066	3
F5GWZ7	Serine/arginine repetitive matrix protein 2	0.4080	0.7122	2

Table 3.2: *Analyzed list of Quantitative Proteomics analyzed list showing Cav1(1-101)Y14D and Cav1(1-101)Y14D-CSD interactome having ≥ 1.5 fold change (Number of experiments=4). * shows proteins whose interaction with Cav1 were previously reported in the literature.*

ID	Detail	Log_Mean Cav1(1-101)Y14F-CSD/ Cav1(1-101)Y14F	Log_SD Cav1(1-101)Y14F-CSD/ Cav1(1-101)Y14F	Number of observations
P35579	Myosin-9	-1.4085	0.9909	2
P35580	Myosin-10	-1.1457	1.0031	2
Q9Y4I1-2	Isoform 2 of Unconventional myosin-Va	-1.0768	0.1997	2
O00159	Isoform 2 of Unconventional myosin-Ic	-0.9996	1.0706	2
O75475	PC4 and SFRS1-interacting protein	-0.9086	0.7407	2
E9PDF6	Unconventional myosin-Ib	-0.8701	1.0522	2
F8W181	60S ribosomal protein L6 (Fragment)	-0.7785	0.8231	2
P00761	Trypsin	-0.7243	0.0661	2
O43795*	Isoform 2 of Unconventional myosin-Ib	-0.6881	1.3886	2
P30050	60S ribosomal protein L12	-0.6760	0.8664	2
C9JB50	60S ribosomal protein L28	-0.6614	0.7637	2
P62277	40S ribosomal protein S13	-0.6023	0.5914	2
P19105	Myosin regulatory light chain 12A	-0.5370	0.5977	2
Q3B7A4	60S acidic ribosomal protein P0	-0.5297	0.7695	2
F8W1R7	Myosin light polypeptide 6	-0.5259	0.8058	2
Q92614-4	Isoform 4 of Unconventional myosin-XVIIIa	-0.5235	0.4560	2
Q9ULV4*	Coronin-1C	-0.4924	0.6565	2
Q7Z451	AP-2 complex subunit beta	-0.4610	0.2753	2
Q16643*	Drebrin	-0.4475	0.4102	2
Q08211	ATP-dependent RNA helicase A	-0.4343	0.3283	2
Q9UM54-6	Isoform 6 of Unconventional myosin-VI	-0.4083	0.4869	3
Q9NX58	Cell growth-regulating nucleolar protein	2.7626	0.4120	2
P12956	X-ray repair cross-complementing protein 6	2.4126	2.0230	3
Q8NAK9	Serine/arginine-rich-splicing factor 2	2.2222	0.8772	2
P06753	Isoform 2 of Tropomyosin alpha-3 chain	2.0181	0.5209	2
P0CW22	40S ribosomal protein S17-like	1.9956	0.0497	2
F8VR82	Serine/threonine-protein phosphatase	1.9293	0.6641	2
P46778	60S ribosomal protein L21	1.9008	0.6846	2
P50402	Emerin	1.8121	0.0722	2
P05198	Eukaryotic translation initiation factor 2 subunit 1	1.6704	0.7079	2
Q7Z406-6	Isoform 6 of Myosin-14	1.6640	0.5936	2
P16403	Histone H1.2	1.6597	0.3296	2
Q5JR95	40S ribosomal protein S8	1.6541	0.8847	2
P61254	60S ribosomal protein L26	1.6278	0.5378	2
Q13509	Tubulin beta-3 chain	1.6017	0.6920	2
P62805	Histone H4	1.5891	0.1460	2
Q00839	Heterogeneous nuclear ribonucleoprotein U	1.5834	0.8337	2
O43290	U4/U6.U5 tri-snRNP-associated protein 1	1.5740	1.2831	2

ID	Detail	Log_Mean Cav1(1-101)Y14F-CSD/ Cav1(1-101)Y14F	Log_SD Cav1(1-101)Y14F-CSD/ Cav1(1-101)Y14F	Number of observations
E9PLL6	60S ribosomal protein L27a	1.5026	0.0807	2
Q7Z2T5	TRMT1-like protein	1.5015	0.7099	2
P05388	60S acidic ribosomal protein P0	1.4986	0.0644	2
P62081	40S ribosomal protein S7	1.4781	0.8259	2
O75477	Erlin-1	1.4171	1.9610	2
Q8IY81	Putative rRNA methyltransferase 3	1.3885	0.4752	2
P62280	40S ribosomal protein S11	1.3735	1.0874	2
P08779	Keratin, type I cytoskeletal 16	1.3689	0.9721	2
O00567	Nucleolar protein 56	1.3549	0.2810	2
P62899	60S ribosomal protein L31	1.3378	0.5558	2
P11387	DNA topoisomerase 1	1.3351	1.1563	2
B4E3S0*	Coronin-1C	1.3112	1.4658	2
P11142	Heat shock cognate 71 kDa protein	1.2782	1.2931	3
O76021	Ribosomal L1 domain-containing protein 1	1.2566	0.0983	2
O60716	Isoform 3A of Catenin delta-1	1.2539	0.6714	2
O00571	Isoform 2 of ATP-dependent RNA helicase	1.2397	0.1045	2
Q96AG4	Leucine-rich repeat-containing protein 59	1.2395	0.6119	2
D6RD46	LIM and calponin homology domains-containing protein 1	1.2341	0.2973	2
Q01082-3	Isoform 2 of Spectrin beta chain, brain 1	1.2288	0.7187	2
O94832	Unconventional myosin-Id	1.1672	1.0115	2
Q9BQG0	Myb-binding protein 1A	1.1663	1.2054	2
P46783	40S ribosomal protein S10	1.1633	1.2950	3
P62847	Isoform 2 of 40S ribosomal protein S24	1.1588	0.2829	2
P16152	Carbonyl reductase [NADPH] 1	1.1555	1.3892	2
H0Y8P7	Pre-mRNA 3-end-processing factor FIP1 (Fragment)	1.1275	1.4581	2
P11021	78 kDa glucose-regulated protein	1.1158	0.5997	3
P09211	Glutathione S-transferase P	1.1091	1.0250	2
Q9BUF5	Tubulin beta-6 chain	1.0812	0.1534	2
P09874	Poly [ADP-ribose] polymerase 1	1.0765	1.2172	4
P49411	Elongation factor Tu, mitochondrial	1.0698	1.5607	4
Q03013-2	Isoform 2 of Glutathione S-transferase Mu 4	1.0636	1.2950	2
P01966	Hemoglobin subunit alpha	1.0624	1.3611	2
Q5VTE0	Putative elongation factor 1-alpha-like 3	1.0611	0.7431	2
I3L397	Eukaryotic translation initiation factor 5A-1 (Fragment)	1.0491	0.7230	2
P09651	Heterogeneous nuclear ribonucleoprotein A1	1.0483	1.0983	4
P55265	Isoform 5 of Double-stranded RNA-specific adenosine deaminase	1.0446	0.3041	2

ID	Detail	Log_Mean Cav1(1-101)Y14F-CSD/ Cav1(1-101)Y14F	Log_SD Cav1(1-101)Y14F-CSD/ Cav1(1-101)Y14F	Number of observations
P05976	Isoform MLC3 of Myosin light chain 1/3, skeletal muscle isoform	1.0397	0.9770	4
P02545	Prelamin-A/C	1.0248	1.3117	4
P07900*	Heat shock protein HSP 90-alpha	1.0224	1.1373	3
Q03135	Caveolin-1	1.0153	0.6864	4
P21266	Glutathione S-transferase Mu 3	1.0050	1.1577	2
P24534	Elongation factor 1-beta	0.9948	0.7953	2
P52597	Heterogeneous nuclear ribonucleoprotein F	0.9863	0.9469	3
C9JJV6	Myeloid-associated differentiation marker (Fragment)	0.9781	0.8649	2
P16615	Isoform 5 of Sarcoplasmic/endoplasmic reticulum calcium ATPase 2	0.9610	0.9200	2
P26641	Elongation factor 1-gamma	0.9543	1.0016	4
Q13751	Laminin subunit beta-3	0.9459	0.6391	2
Q9UDY4	DnaJ homolog subfamily B member 4	0.9413	0.6387	2
P09488	Glutathione S-transferase Mu 1	0.9201	1.1587	2
P07814	Bifunctional glutamate/proline--tRNA ligase	0.9173	0.8642	4
Q9Y265	RuvB-like 1	0.8857	1.3383	3
Q13501*	Sequestosome-1	0.8819	1.0483	4
O75083	WD repeat-containing protein 1	0.8786	1.2723	3
P29317	Ephrin type-A receptor 2	0.8765	1.2779	2
P08107	Heat shock 70 kDa protein 1A/1B	0.8750	0.9096	4
P60866	40S ribosomal protein S20	0.8471	0.5114	2
P62829	60S ribosomal protein L23	0.8421	0.7973	2
P61978	Isoform 3 of Heterogeneous nuclear ribonucleoprotein K	0.8416	1.0824	4
Q5JP53	Tubulin beta chain	0.8403	0.7630	3
F8W7C6	60S ribosomal protein L10	0.8322	1.2913	4
Q07955-3	Isoform ASF-3 of Serine/arginine-rich splicing factor 1	0.8318	1.3814	2
Q07065	Cytoskeleton-associated protein 4	0.8280	0.7451	3
P62269	40S ribosomal protein S18	0.8178	0.9325	3
Q9Y281	Cofilin-2	0.8117	0.9602	4
O95425	Isoform 2 of Supervillin	0.8091	0.8063	3
O43707	Alpha-actinin-4	0.8089	0.5496	3
Q13045	Protein flightless-1 homolog	0.7997	0.5617	2
O75369	Isoform 2 of Filamin-B	0.7939	0.5515	5
O95782	Isoform B of AP-2 complex subunit alpha-1	0.7902	1.4405	2
P13010	X-ray repair cross-complementing protein 5	0.7794	0.5135	3
Q9P2E9-2	Isoform 1 of Ribosome-binding protein 1	0.7709	1.1739	3

ID	Detail	Log_Mean Cav1(1-101)Y14F-CSD/ Cav1(1-101)Y14F	Log_SD Cav1(1-101)Y14F-CSD/ Cav1(1-101)Y14F	Number of observations
P62136*	Serine/threonine-protein phosphatase PP1-alpha catalytic subunit	0.7686	0.3715	2
P68363	Tubulin alpha-1B chain	0.7678	0.8156	3
B1APM4	Sterol O-acyltransferase (Acyl-Coenzyme A: cholesterol acyltransferase) 1 (Fragment)	0.7576	1.3597	2
Q1RMN8	Similar to Immunoglobulin lambda-like polypeptide 1	0.7573	0.5076	2
P55072	Transitional endoplasmic reticulum ATPase	0.7541	0.8375	4
P60842	Eukaryotic initiation factor 4A-I	0.7541	0.8337	4
F8W111	Carboxypeptidase M (Fragment)	0.7529	0.0613	2
P02533	Keratin, type I cytoskeletal 14	0.7482	0.6790	4
P02769	Bovine serum albumin precursor	0.7433	0.6305	4
P05783	Keratin, type I cytoskeletal 18	0.7416	0.8629	4
C9JXB8	60S ribosomal protein L24	0.7368	1.3202	2
P12236	ADP/ATP translocase 3	0.7327	0.9659	2
P15880	40S ribosomal protein S2	0.7296	0.6957	3
Q9ULT8	E3 ubiquitin-protein ligase	0.7272	0.7512	4
P13639	Elongation factor 2	0.7262	0.7253	4
P08238	Heat shock protein HSP 90-beta	0.7257	0.6463	3
E7EPB3	60S ribosomal protein L14	0.7252	1.1962	4
P22695	Cytochrome b-c1 complex subunit 2, mitochondrial	0.7235	0.6522	3
Q15233	Non-POU domain-containing octamer-binding protein	0.7212	0.8844	4
P63244	Guanine nucleotide-binding protein subunit beta-2-like 1	0.7208	0.9933	4
H7BXY5	Nexilin (Fragment)	0.7155	1.8291	2
P46781	40S ribosomal protein S9	0.7092	1.5782	3
Q9UHB6-4	Isoform 4 of LIM domain and actin-binding protein 1	0.7006	1.4764	4
E7EUT5	Glyceraldehyde-3-phosphate Dehydrogenase	0.6940	0.8781	4
F5H667	Aspartyl/asparaginyl beta-hydroxylase	0.6935	1.0420	4
Q13813	Spectrin alpha chain, brain	0.6916	0.6896	4
H0Y4A6	Valine--tRNA ligase (Fragment)	0.6892	0.8539	2
Q9H4L5-6	Isoform 2b of Oxysterol-binding protein-related protein 3	0.6872	1.1607	3
B7Z3U6	ATPase, Na+/K+ transporting, alpha 1 polypeptide, isoform CRA_a	0.6764	0.9949	2
O60437	Periplakin	0.6721	0.3077	2
B7Z5W8	Dihydrolipoyllysine-residue succinyltransferase component of 2-oxoglutarate dehydrogenase complex, mitochondrial	0.6714	0.7032	2

ID	Detail	Log_Mean Cav1(1-101)Y14F-CSD/ Cav1(1-101)Y14F	Log_SD Cav1(1-101)Y14F-CSD/ Cav1(1-101)Y14F	Number of observations
P08754	Guanine nucleotide-binding protein G(k) subunit alpha	0.6667	0.6450	3
P07355*	Annexin A2	0.6607	1.4070	4
F5H8M4	Gelsolin	0.6582	1.2495	2
Q05639	Elongation factor 1-alpha 2	0.6578	0.7528	2
O96008	Mitochondrial import receptor subunit TOM40 homolog	0.6573	0.3969	2
P14618	Pyruvate kinase isozymes M1/M2	0.6568	0.6555	2
Q6NZI2	Polymerase I and transcript release factor	0.6562	0.8470	4
Q04637-5	Isoform D of Eukaryotic translation initiation factor 4 gamma 1	0.6555	0.4112	2
B3KTM6	60S ribosomal protein L5	0.6496	0.8419	4
P10809	60 kDa heat shock protein, mitochondrial	0.6495	0.5693	4
B4DUR8	T-complex protein 1 subunit gamma	0.6448	0.6024	3
P23246	Splicing factor, proline- and glutamine-rich	0.6395	0.7654	4
P08670	Vimentin	0.6191	0.5756	2
P35052	Glypican-1	0.6170	0.7644	4
Q9UBS4	DnaJ homolog subfamily B member 11	0.6140	0.3679	3
P13645	Keratin, type I cytoskeletal 10	0.6137	0.4330	4
B7Z4V2	Stress-70 protein, mitochondrial	0.6137	0.6177	4
P00387	Isoform 2 of NADH-cytochrome b5 reductase 3	0.6064	0.7717	2
P62158	Calmodulin	0.6019	0.9750	4
P12814	Alpha-actinin-1	0.6008	0.1702	4
Q86YZ3	Hornerin	0.5937	0.3180	3
B4E2W0	3-ketoacyl-CoA thiolase	0.5914	0.9715	4
Q13505-3	Isoform 3 of Metaxin-1	0.5906	0.6399	2
P45880	Voltage-dependent anion-selective channel protein 2	0.5903	0.8568	4
Q5HY54	Filamin-A	0.5875	0.7164	4
B7Z254	Protein disulfide-isomerase A6	0.5858	0.7871	3
P49748	Isoform 2 of Very long-chain specific acyl-CoA dehydrogenase, mitochondrial	0.5836	0.4938	2
P35527	Keratin, type I cytoskeletal 9	0.5791	0.5522	4
P63104	14-3-3 protein zeta/delta	0.5720	0.8266	4
B4DJ10	Leucine--tRNA ligase, cytoplasmic	0.5669	0.5815	3
Q96RT1-6	Isoform 6 of Protein LAP2	0.5658	0.7274	3
Q9NUQ2	1-acyl-sn-glycerol-3-phosphate acyltransferase epsilon	0.5514	0.4601	2
Q07157	Tight junction protein ZO-1	0.5488	0.7618	4
F5H4F4	similar to Complement C4-A precursor	0.5440	0.4439	4
P02786	Transferrin receptor protein 1	0.5423	0.6610	3

ID	Detail	Log_Mean Cav1(1-101)Y14F-CSD/ Cav1(1-101)Y14F	Log_SD Cav1(1-101)Y14F-CSD/ Cav1(1-101)Y14F	Number of observations
P62070	Ras-related protein R-Ras2	0.5415	0.5532	2
P62753	40S ribosomal protein S6	0.5402	1.2996	3
Q27J81-2	Isoform 2 of Inverted formin-2	0.5300	0.3952	2
F8VPV9	ATP synthase subunit beta	0.5285	0.2159	2
P06748	Isoform 2 of Nucleophosmin	0.5226	0.9706	3
P04259	Keratin, type II cytoskeletal 6B	0.5165	0.5994	2
O75306	NADH dehydrogenase [ubiquinone] iron-sulfur protein 2, mitochondrial	0.5164	0.4493	2
P25205	DNA replication licensing factor MCM3	0.5152	1.0063	2
B7Z6B8	2,4-dienoyl-CoA reductase, mitochondrial	0.5124	0.7918	4
P40939	Trifunctional enzyme subunit alpha, mitochondrial	0.5122	0.7030	4
P62913	60S ribosomal protein L11	0.5112	0.9118	4
Q12792	Twinfilin-1	0.5109	0.5625	3
Q9UM00-2	Isoform 2 of Transmembrane and coiled-coil domain-containing protein 1	0.5097	0.1209	2
P00403	Cytochrome c oxidase subunit 2	0.5062	0.7217	3
Q9UQE7	Structural maintenance of chromosomes protein 3	0.5052	0.6985	4
H0Y390	Microtubule-actin cross-linking factor 1, isoforms 1/2/3/5 (Fragment)	0.5039	0.1105	2
P42166	Lamina-associated polypeptide 2, isoform alpha	0.5039	0.7527	4
P62249	40S ribosomal protein S16	0.5020	0.6948	4
F5H4V4	Antigen KI-67	0.5006	0.9017	4
Q14126*	Desmoglein-2	0.4959	0.6854	4
Q5JR07	Ras homolog gene family, member C (Fragment)	0.4921	0.5651	2
P04843	Dolichyl-diphosphooligosaccharide--protein glycosyltransferase subunit 1	0.4920	0.8184	4
Q14204	Cytoplasmic dynein 1 heavy chain 1	0.4914	0.3921	2
Q9P0L0	Vesicle-associated membrane protein-associated protein A	0.4897	0.8122	3
P09669	Cytochrome c oxidase subunit 6C	0.4865	0.8186	2
E9PKZ0	60S ribosomal protein L8	0.4857	1.2200	4
Q13428-2	Isoform 2 of Treacle protein	0.4851	0.4297	2
P68104	Elongation factor 1-alpha 1	0.4789	0.6895	2
Q6WCQ1	Myosin phosphatase Rho-interacting protein	0.4764	0.8017	4
P42704	Leucine-rich PPR motif-containing protein, mitochondrial	0.4694	0.4248	4
P68371	Tubulin beta-4B chain	0.4674	0.4311	3
P52907	F-actin-capping protein subunit alpha-1	0.4619	1.2214	3
E9PMS6	LIM domain only protein 7	0.4607	0.4810	4
P46940	Ras GTPase-activating-like protein IQGAP1	0.4597	0.6309	4
P08729	Keratin, type II cytoskeletal 7	0.4585	0.7496	6

ID	Detail	Log_Mean Cav1(1-101)Y14F-CSD/ Cav1(1-101)Y14F	Log_SD Cav1(1-101)Y14F-CSD/ Cav1(1-101)Y14F	Number of observations
Q14254*	Flotillin-2	0.4574	0.6989	4
O00151	PDZ and LIM domain protein 1	0.4557	0.1044	2
C9J9K3	40S ribosomal protein SA (Fragment)	0.4545	0.4879	3
F8W8V7	Zinc finger protein 185	0.4543	0.2288	2
P13667	Protein disulfide-isomerase A4	0.4514	0.4568	3
P49327	Fatty acid synthase	0.4465	0.7881	2
Q14573*	Inositol 1,4,5-trisphosphate receptor type 3	0.4447	0.5994	4
P05787*	Keratin, type II cytoskeletal 8	0.4301	0.5557	4
Q12906	Interleukin enhancer-binding factor 3	0.4255	0.6166	2
Q8NE71	ATP-binding cassette sub-family F member 1	0.4210	1.1877	4
P14625	Endoplasmin	0.4177	0.3851	3
P26038	Moesin	0.4161	0.6268	3
P52272	Heterogeneous nuclear ribonucleoprotein M	0.4120	1.0671	3
Q06830	Peroxiredoxin-1	0.4115	0.3390	3

Table 3.3: *Analyzed list of Quantitative Proteomics analyzed list showing Cav1(1-101)Y14F and Cav1(1-101)Y14F-CSD interactome having ≥ 1.5 fold change (Number of experiments=4). * shows proteins whose interaction with Cav1 were previously reported in the literature.*

3.2.2.1 Proteomics Data analysis

The cut off limit of 1.5 fold change was kept and number of peptides was ≥2. As evident from the Pie chart we found around 516 differentially interacting proteins for Cav1(1-101)Y14D and Cav1(1-101)Y14D-CSD, out of which around 126 proteins interacted more with Cav1(1-101)Y14D compared to Cav1(1-101)Y14D-CSD while 53 proteins interacted more with Cav1(1-101)Y14D-CSD in comparison to Cav1(1-101)Y14D (**Figure 3.14A**). Similarly for another set of Cav1(1-101)Y14F and Cav1(1-101)Y14F-CSD, around 461 differentially interacting proteins were found. After applying a cut off of > 1.5 fold change it was found that 21 interacted more with Cav1(1-101)Y14F while 203 had higher interaction with CavY14F-CSD (**Figure 3.14B**). The large number of proteins interacting with Cav1(1-101)Y14F-CSD was surprising to us.
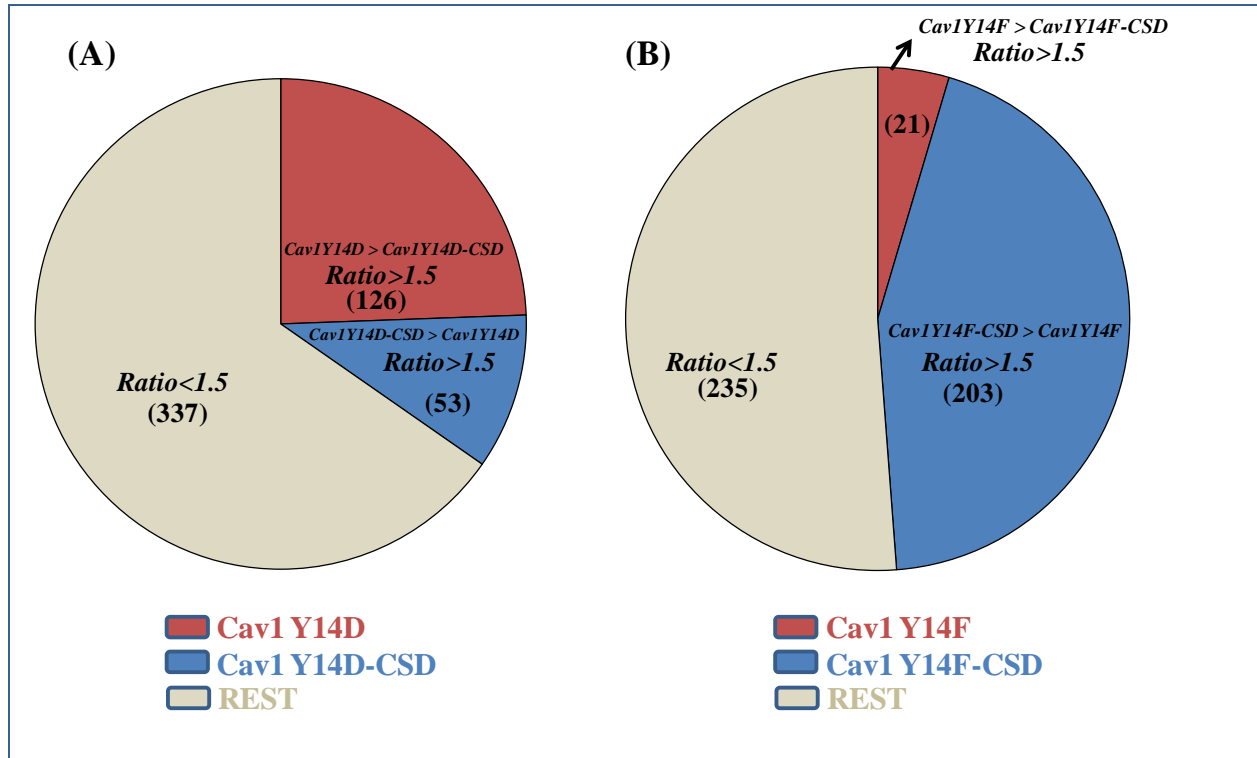
(A)

Cav1Y14D > Cav1Y14D-CSD
Ratio>1.5
(126)

Cav1Y14D-CSD > Cav1Y14D
Ratio>1.5
(53)

Ratio<1.5
(337)

■ **Cav1 Y14D**
■ **Cav1 Y14D-CSD**
□ **REST**

(B)

Cav1Y14F > Cav1Y14F-CSD
Ratio>1.5
(21)

Cav1Y14F-CSD > Cav1Y14F
Ratio>1.5
(203)

Ratio<1.5
(235)

■ **Cav1 Y14F**
■ **Cav1 Y14F-CSD**
□ **REST**

Figure 3.14: Pie chart showing the interacting protein partners from quantitative proteomic analysis of Cav1(1-101)Y14D and Cav1(1-101)Y14D-CSD or Cav1(1-101)Y14F and Cav1(1-101)Y14F-CSD analyzed through QPCC (number of experiment=4). (A) The interacting protein partners from quantitative proteomic of Cav1(1-101)Y14D and Cav1(1-101)Y14D-CSD were analyzed and found 516 differential interacting partners. After considering the cutoff of 1.5 fold change, 337 proteins were filtered out leaving behind 126 proteins having 1.5 fold that interacted specifically with Cav1(1-101)Y14D and 53 proteins with Cav1(1-101)Y14D-CSD. (B) Similarly Cav1(1-101)Y14F and Cav1(1-101)Y14F-CSD group had 461 differential interacting partners. After applying 1.5 fold change filter, 235 proteins were left out and around 21 proteins showed their interaction specifically with Cav1(1-101)Y14F and 203 proteins with Cav1(1-101)Y14F-CSD.

In addition, we compared different proteins groups using Venn diagram. The interacting partners of Cav1(1-101)Y14D>Cav1(1-101)Y14F (196 proteins) compared to Cav1(1-101)Y14D>Cav1(1-101)Y14D-CSD (126 proteins) and Cav1(1-101)Y14D-CSD>Cav1(1-101)Y14D (53 proteins) are represented in **Figure 3.15**. As it appears, the overlap of number of proteins was very less showing that the specificity of CSD domain in Cav1 interaction with other proteins had a lesser impact.
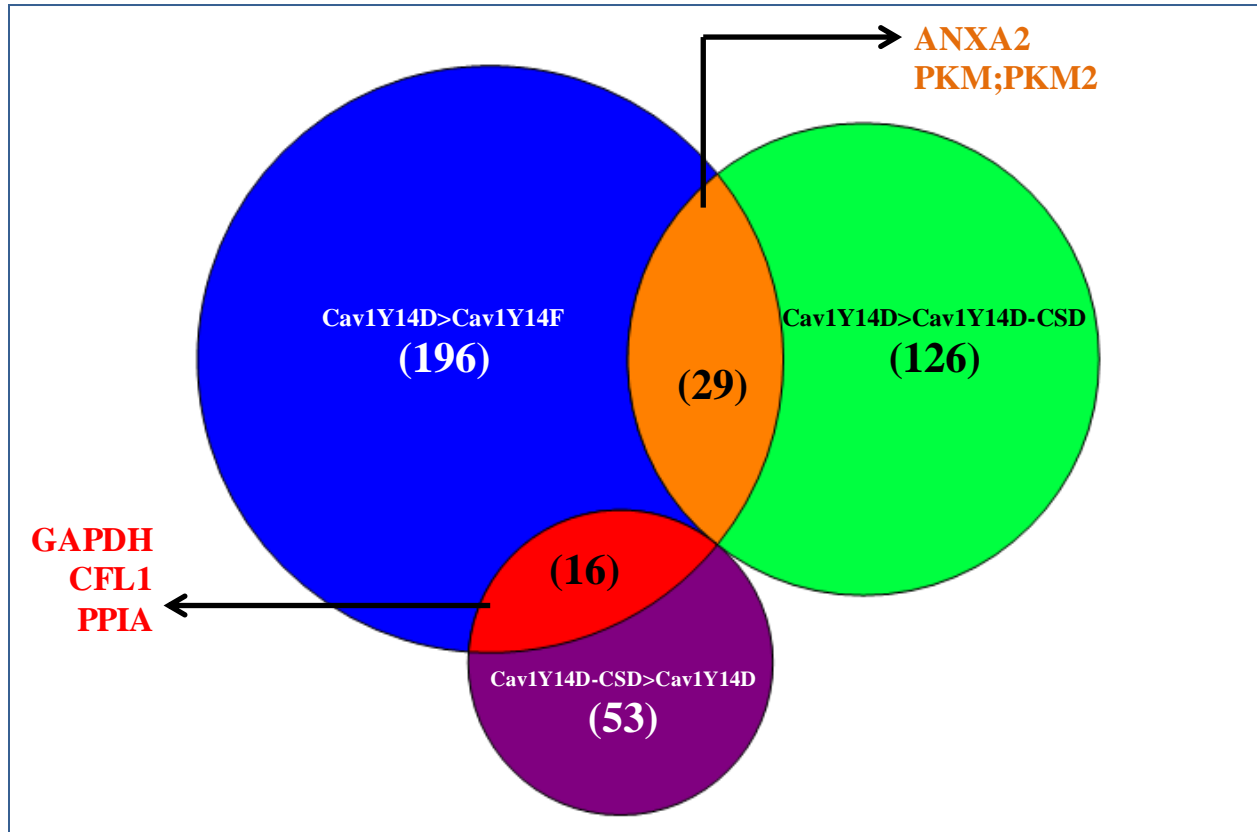
Figure 3.15: Comparative analysis of Cav1(1-101)Y14D and Cav1(1-101)Y14F interactome with Cav1(1-101)Y14D and Cav1(1-101)Y14D-CSD interactome. The interacting partners between Cav1(1-101)Y14D>Cav1(1-101)Y14F (196 proteins) v.s. Cav1(1-101)Y14D>Cav1(1-101)Y14D-CSD (126 proteins) v.s. Cav1(1-101)Y14D-CSD>Cav1(1-101)Y14D (53 proteins) shows 16 common proteins between Cav1(1-101)Y14D>Cav1(1-101)Y14F and Cav1(1-101)Y14D>Cav1(1-101)Y14D-CSD, and 29 between Cav1(1-101)Y14D>Cav1(1-101)Y14F and Cav1(1-101)Y14D>Cav1(1-101)Y14F.

Similarly another set of samples was analyzed for comparison. The number of interacting partners of Cav1(1-101)Y14F>Cav1(1-101)Y14D (78 proteins) compared to Cav1(1-101)Y14F>Cav1(1-101)Y14F-CSD (21 proteins) and Cav1(1-101)Y14F-CSD>Cav1(1-101)Y14F (203 proteins) are represented in **Figure 3.16**.

Proteomics analysis data suggest that about one-third binding proteins to Cav1(1-101)Y14D or Cav1(1-101)Y14F were influenced by mutation (F92A/V94A) in CSD domain. Also, phosphorylation and CSD might also work in concert in determining the selective binding of Cav1. In the absence of phosphorylation or intact CSD, Cav1 binding specificity might get influenced that may increase the number of proteins binding to YF-CSD.
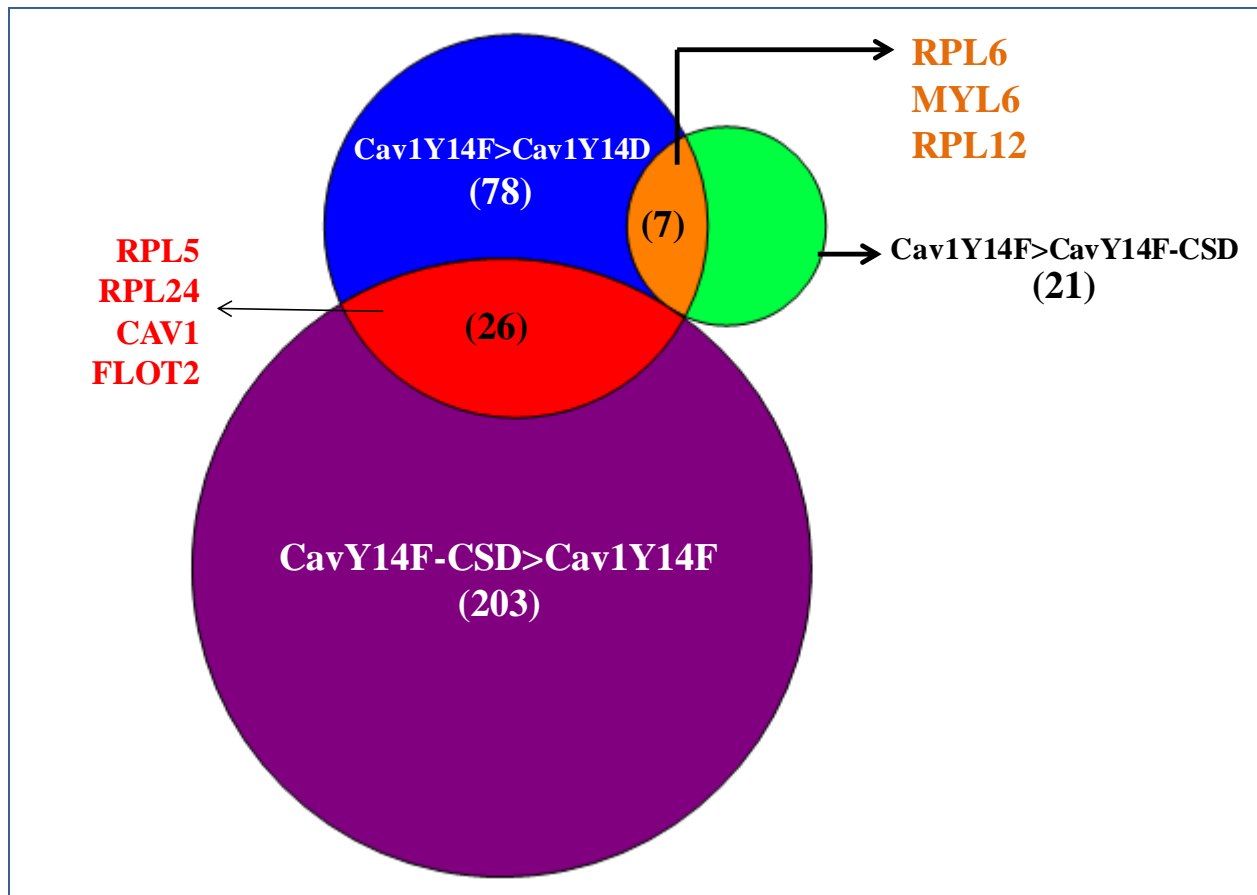
Figure 3.16: Comparative analysis of Cav1(1-101)Y14D and Cav1(1-101)Y14F interactome with Cav1(1-101)Y14F and Cav1(1-101)Y14F-CSD interactome. Interacting partners from Cav1(1-101)Y14F>Cav1(1-101)Y14D (78 proteins) v.s Cav1(1-101)Y14F>Cav1(1-101)Y14F-CSD (7 proteins) v.s Cav1(1-101)Y14F-CSD>Cav1(1-101)Y14F (203 proteins) were analyzed and 7 proteins were found to be common between Cav1(1-101)Y14F>Cav1(1-101)Y14D and Cav1(1-101)Y14F>Cav1(1-101)Y14F-CSD, and around 26 proteins between Cav1(1-101)Y14F>Cav1(1-101)Y14D and Cav1(1-101)Y14F-CSD>Cav1(1-101)Y14F.

3.3 TO DETERMINE WHETHER pCAV1-SPECIFIC INTERACTION WITH HSP90 IMPACTS CAV1 FUNCTION IN CANCER CELL MIGRATION

3.3.1 Validations

Quantitative Proteomics of GST alone, Cav1(1-101)Y14D and Cav1(1-101)Y14F showed pCav1 specific interaction with HSP90 (**Figure 3.17A**). pCav1-HSP90 interaction was validated through GST pull down followed by western blotting in vitro. Pulldown was followed by separation on SDS-PAGE and western blotting. The blot was probed using anti HSP90 antibody and revealed that Cav1(1-101)Y14D pulled down HSP90 confirming the pCav1-HSP90 interaction (**Figure 3.17B**). Multiple validations, upon quantification, rendered statistically significant data of pCav1 speacific interaction with HSP90 (**Figure 3.17C**). Next we asked, wheather this pCav1-HSP90 interaction impacting Cav1 function in cancer cell migration or not.

(A)

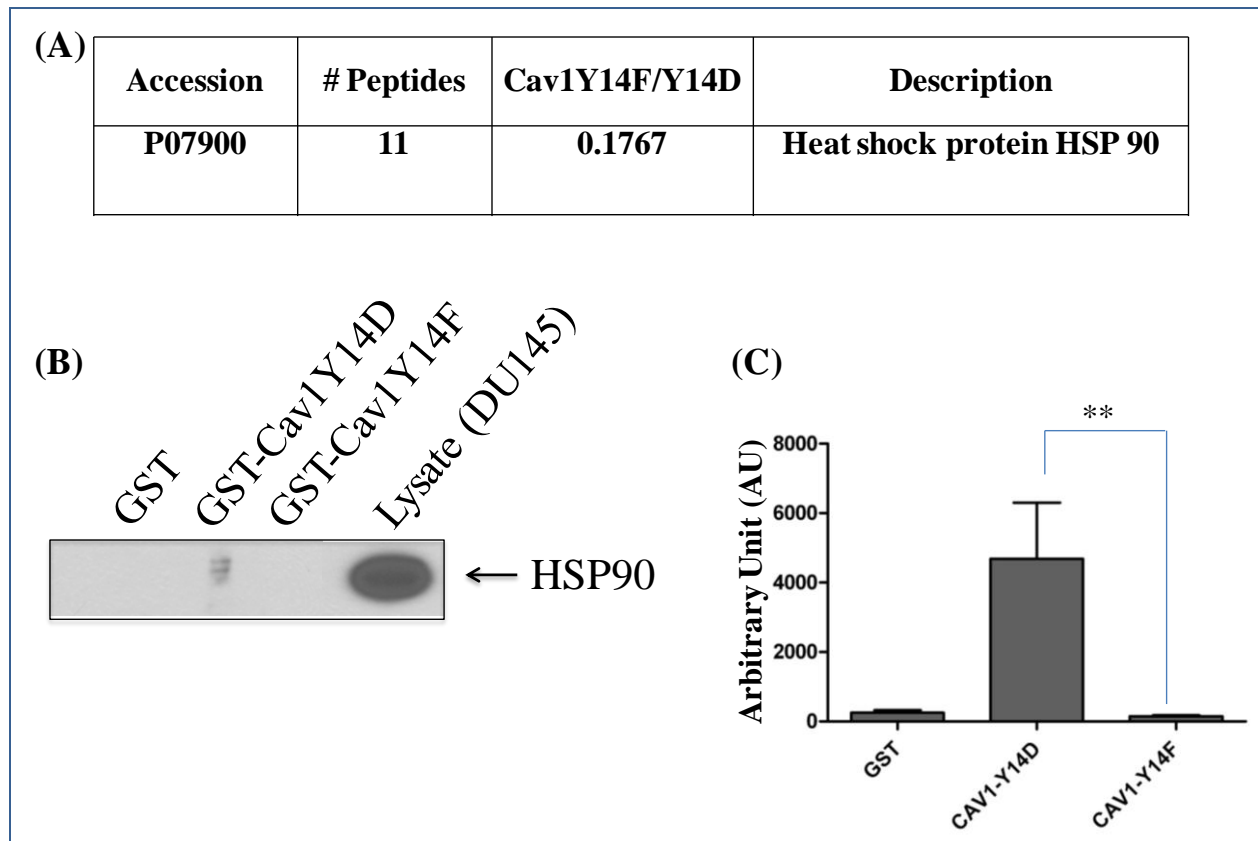| Accession	# Peptides	Cav1Y14F/Y14D	Description
P07900	11	0.1767	Heat shock protein HSP 90

(B)

(C)

*Figure 3.17: Validation of Cav1(1-101)Y14D interaction with HSP90 by GST pull down and western blotting (number of experiments=3). (A) Quantitative proteomics data for HSP90 showing more binding with Cav1(1-101)Y14D compared to Cav1(1-101)Y14F. (B) pCav1 specific interaction of HSP90 was validated by GST pull down followed by western blotting and probed for HSP90. (C) Western blots were analyzed for statistical significance of pCav1-HSP90 interaction through One-way ANNOVA where ** means P<0.01.*

3.3.2 Expression analysis of HSP90, Cav1 and AKT after drug treatment

HSP90 is a well-known chaperone and cells express it in excess quantity during stress. HSP90 is responsible for proper folding and maturation of various client proteins (AKT, EGFR, IGFR, C-RAF etc) that help in cancer cell survival and proliferation (**Calderwood et al, 2006**). HSP90 has an ATP binding pocket, which regulates its functionality (**Stebbins et. al, 1997**). We therefore used 17 AAG (HSP90 inhibitor), which binds to the ATP binding pocket of HSP90 and makes it non-functional. This promotes degradation of its client proteins and hampers cancer cell survival and proliferation (**Imai et. al, 2003**). It has been shown that after 17 AAG treatments, expression of HSP90 goes up whereas the expression of AKT, p-AKT and other client proteins goes down (**Kamal et. al, 2003**).

We have used human prostate cancer cell lines, DU145 and its stables (DU145-YD, DU145-YF, DU145-WT and DU145-DSRed) and also PC3. Normal DU145, DU145-YF and DU145-DSred have low pCav1 levels whereas DU145-YD, DU145-WT and PC3 have high pCav1 levels.

Since proteomics analysis showed that HSP90 interacts more with GST-Cav1(1-101)Y14D, we decided to test the effect of 17AAG on this interaction. DU145 and its stable cell lines were treated with different concentrations of 17AAG for 24 h in a dose dependent manner (5nM, 10nM, 25nM); 0.01% DMSO and no treatment were used as controls. siCav1 knockdown was performed in PC3 cell lines for 48 h. siCtrl was used as a control. 24 h post siRNA transfection, cells were treated with 17 AAG (5nM, 10nM, 25nM) or 0.01% DMSO. The treated cell lysates were prepared and separated on SDS-PAGE, transferred on to nitrocellulose membrane and western blotted. **Figure 3.18A** and **Figure 3.18B** show western blots probed with anti-HSP90 and β-Actin for DU145 and its stables and PC3 (+/- siCav1) respectively.

HSP90 expressions were normalized against β-Actin and quantified. As shown, the expression of HSP90, consistent with previously published results, increases after 17AAG treatment (**Figure 3.18C**). Western blot experiments are semi-quantitative and to have better accuracy, we could have biological replicates as well as technical replicates. To obtain the statistical analysis, we have to normalize our protein of interest with loading control (here β-Actin). As, in our case, we have two biological replicates and multiple cell lines so we performed grouped analysis having Mean with SEM (standard error mean). Range of HSP90 expression (western blot band quantitation normalized with β-Actin) between two biological replicate was used to partially conclude the results. This could be sufficient for western blot data to see the differential expression, but it is always preferred to have n=3 as the variation between the experiments will impact our overall conclusion. 25nM concentration of 17 AAG showed the highest expression of HSP90 in almost all the cell models used (except PC3-siCav1). Therefore, we used this concentration for further experiments (i.e. cell viability and cell migration assays). As predicted, Cav1 expression went down post siCav1 (**Figure 3.18D).** 17AAG treatment was in agreement with published result and showed an increased expression in siCtrl but an opposite effect in siCav1, which could be due to the lack of Cav1 expression (**Figure 3.18D)**.
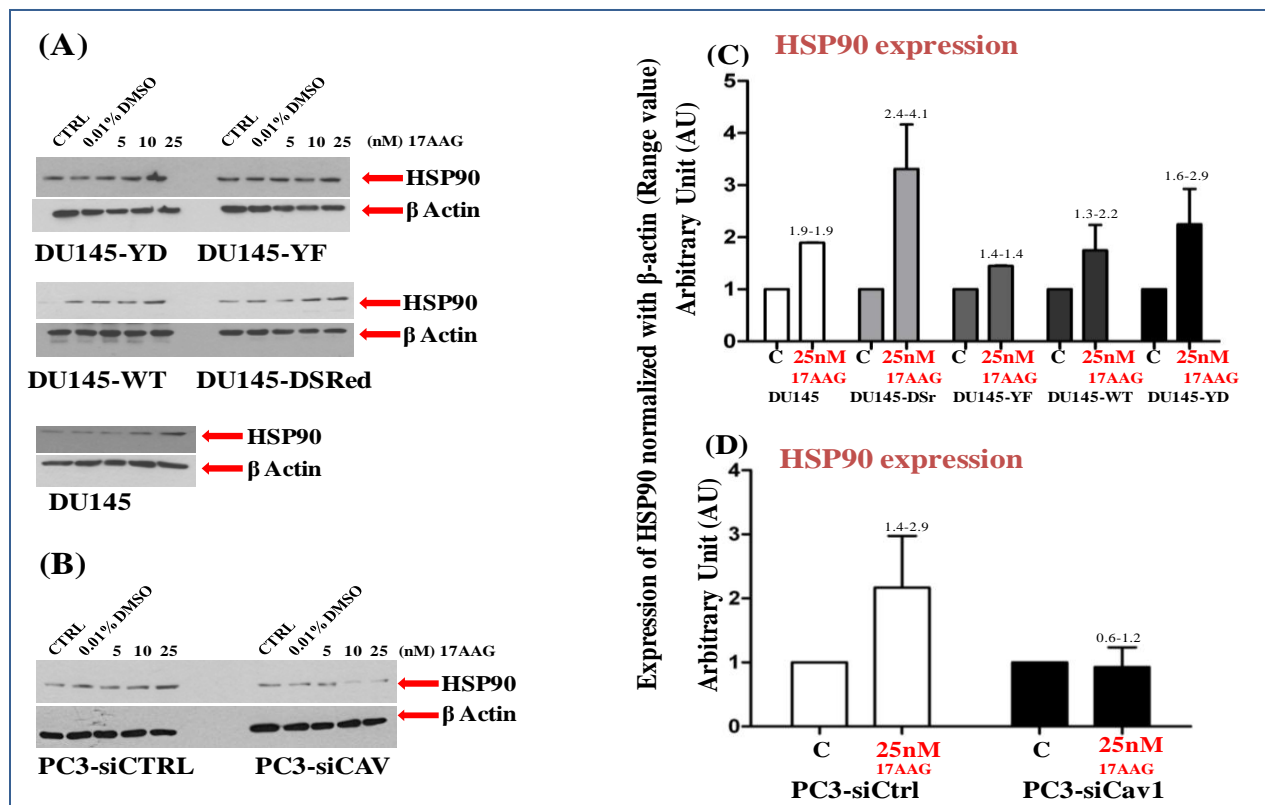
Figure 3.18: Expression analysis of HSP90 normalized with β-Actin after 17 AAG treatment in DU145 & its stables and PC3 (+/-siCav1) cell lines (Number of experiment=2). (A) & (B) DU145 and its stables and PC3 (+/-siCav1) were treated with 17AAG in dose dependent manner (5nM, 10nM, 25nM), and 0.01% DMSO and no treatment were used as controls for 24 h. Equal amount of proteins from different cell lysates were used for western blotting and probed for HSP90 and β-Actin (for normalization). (C) & (D) Western blots images were analyzed for 25nM which was best concentration for our cell models as it was already shown in literature that HSP90 expression goes up after 17AAG treatment. Range of HSP90 expression (western blot band quantitation normalized with β-Actin) between two biological replicate was shown above the bar.

We also probed the blots for Cav1 to check its expression level after treatment. DU145 and its stables (**Figure 3.19A)** and PC3 (+/- siCav1) (**Figure 3.19B)** were probed for Cav1. Expression of Cav1 was normalized for β-Actin in DU145 and its stables (**Figure 3.19C)** and PC3 (+/- siCav1) cell lines (**Figure 3.19D)** after 25nM of 17 AAG treatments. This showed that after treatment, DU145, DU145-Y14F and DU145-DSred had lower expression level of Cav1 whereas DU145-Y14D, DU145-WT and PC3-siCtrl had higher expression of Cav1.
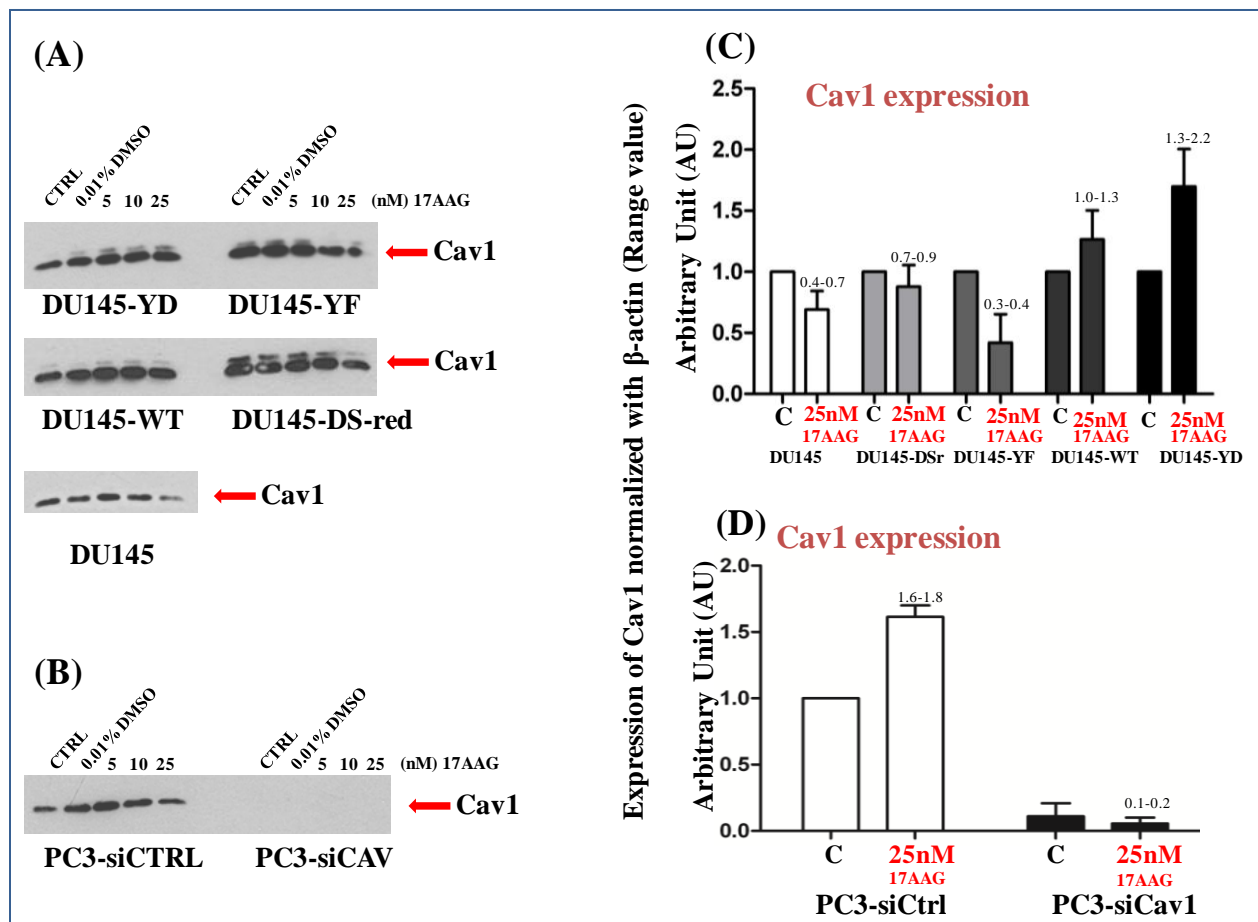
Figure 3.19: Expression analysis of Cav1 normalized with β-Actin after 17 AAG treatment in DU145 & its stables and PC3 (+/-siCav1) cell lines (Number of experiment=2). *(A) & (B) The previously 17 AAG treated blots were probed for Cav1 to check its expression. (C) & (D) Western blots images were analyzed and we saw that expression of Cav1 was higher in cell models containing pCav1. Range of Cav1 expression (western blot band quantitation normalized with β-Actin) between two biological replicate was shown above the bar.*

AKT expression was assessed after treatment with 17 AAG in DU145 and its stables (**Figure 3.20A)** and PC3 (+/- siCav1) (**Figure 3.20B).** Expression was normalized against β-Actin and quantified, as shown for DU145 and its stables (**Figure 3.20C)** and PC3 (+/- siCav1) cell lines (**Figure 3.20D).** 17AAG treatment showed negative effect on DU145, DU145-YF and DU145-DSred cells reducing the expression level of AKT while DU145-YD, DU145-WT and PC3-siCtrl had an opposite effect with an increase in expression level of AKT.
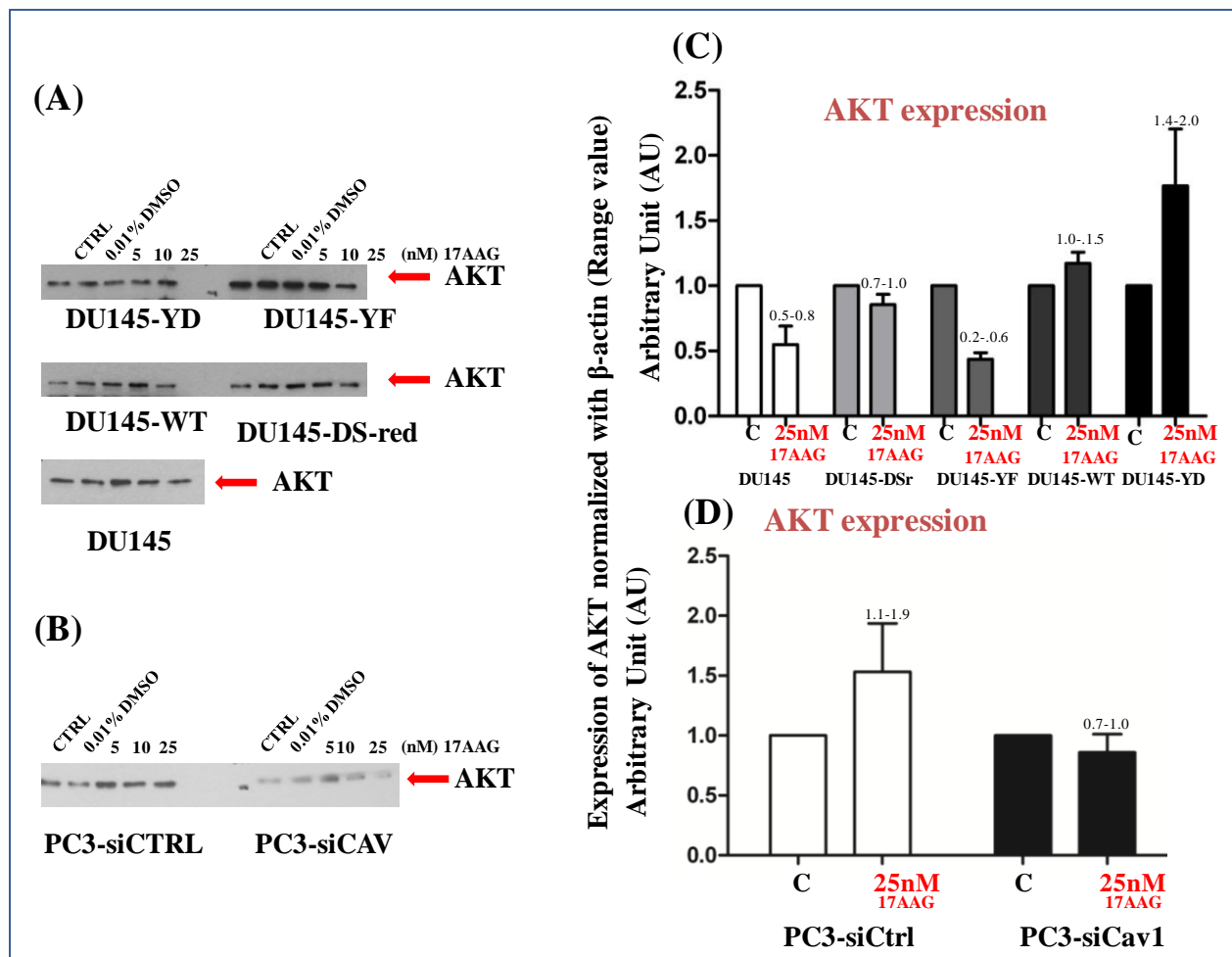
Figure 3.20: Expression analysis of AKT normalized with β-Actin after 17 AAG treatment in DU145 & its stables and PC3 (+/-siCav1) cell lines (Number of experiment=2). *(A) & (B) The previously 17 AAG treated blots were probed for AKT to check its expression. (C) & (D) Western blots images were analyzed and we saw that expression of AKT was higher in cell models containing pCav1. Range of AKT expression (western blot band quantitation normalized with β-Actin) between two biological replicate was shown above the bar.*

The present data shows that phosphorylation of Cav1 has an impact over non-functional HSP90. Previous studies have shown that 17 AAG treatment results in a non-functional HSP90 that in turn down regulates AKT expression and inhibits the growth of prostate cancer xenografts (**Solit et. al, 2002; Kamal et. al, 2003**). Our results show that cell lines lacking p-Cav1 follow the same pattern after 17 AAG treatment (with decreased AKT expression) while cell lines having pCav1 show increased expression of AKT and pCav1 overcomes the effect of non functional HSP90.

3.3 Cell viability after 17 AAG treatment

Cell viability assays were performed for all the cell models after 17 AAG treatment. 17 AAG treatments were previously shown to decrease cell proliferation and growth. We used MTT assay, a calorimetric assay for measuring metabolic activity of cell. The metabolic enzyme, NAD(P)H-dependent cellular oxidoreductase measures cells viability. It reduces the tetrazolium dye MTT{3-(4,5-dimethylthiazol-2-yl)-2,5-diphenyltetrazolium bromide} to its insoluble formazan and gives a purple color. Cells were treated with MTT for about 4 h in 37 ºC CO_2 incubator and purple formazan crystals were solubilized in the buffer. The OD was measured at 570nm.

DU145 and its stables were treated with 25nM 17 AAG for 24, 48 and 72 h in 96-well plate and just before the completion set time MTT was added for 4 h. Formazan crystals were solubilized and resulting color was measured. Obtained OD was normalized against DMSO and the graph was generated post data analysis as shown in **Figure 3.21A.** In PC3 (+/-siCav1) knockdown cells were treated with 17 AAG after 12 h for 24 and 48 h respectively and similarly before the

time completion, treated with MTT for 4 h, crystals solubilized and OD was measured. The graph was generated after normalizing with DMSO (**Figure 3.21B**).
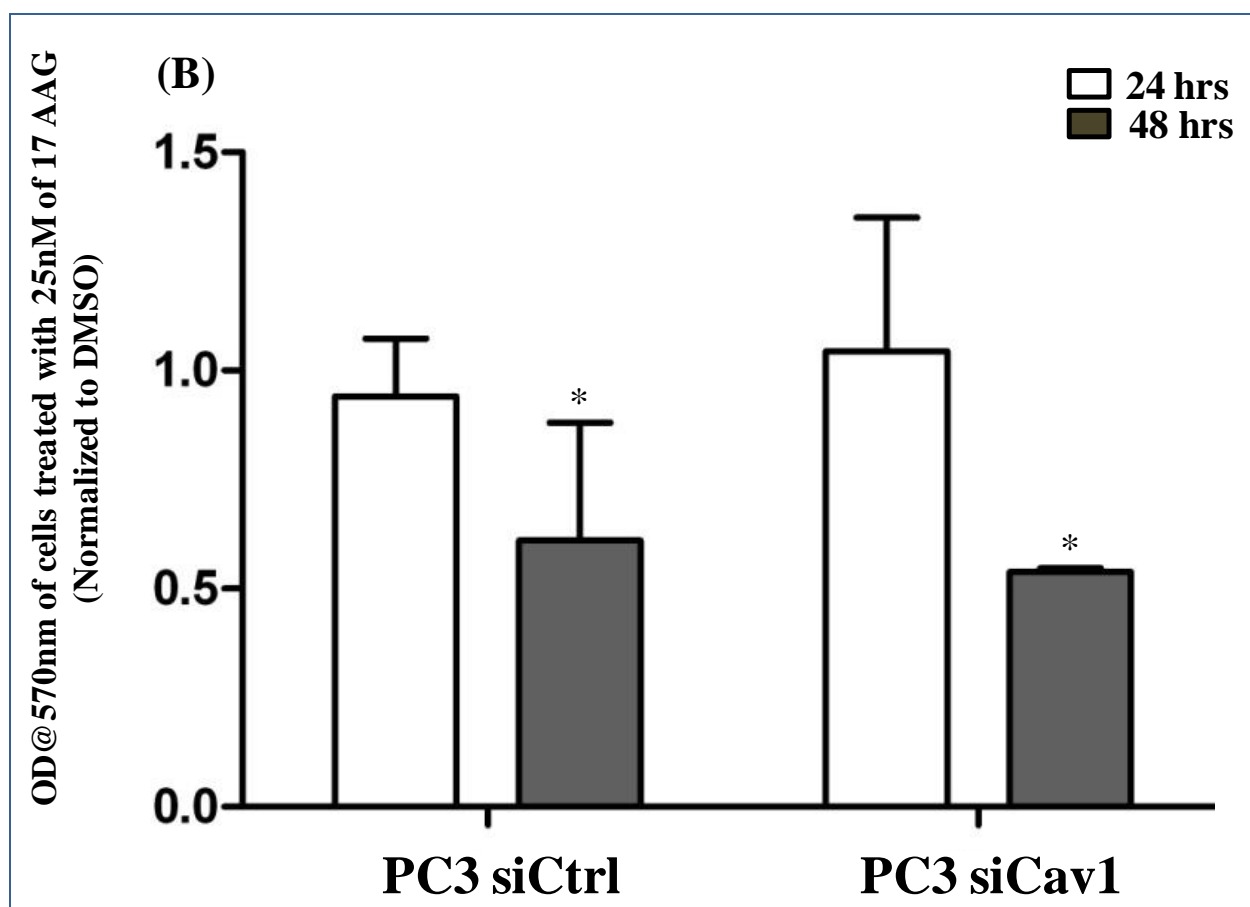
(A)
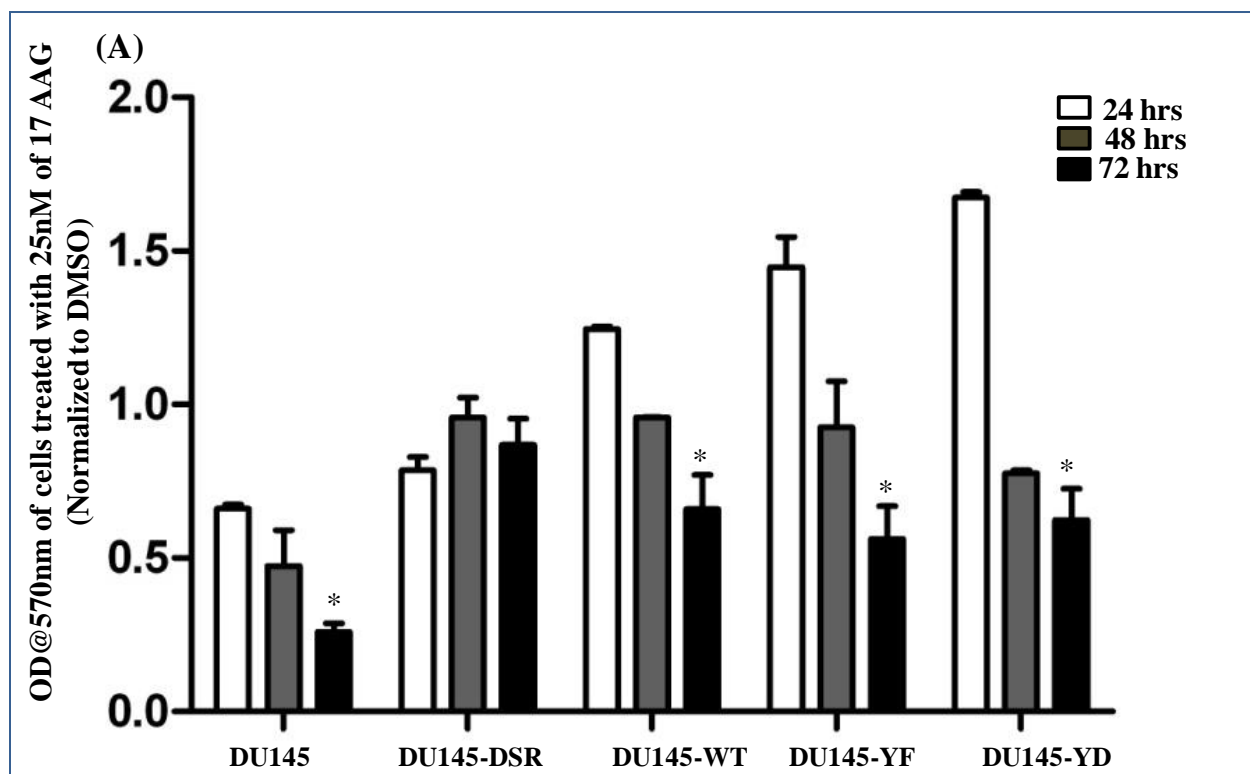
*Figure 3.21: Cell viability assay using MTT for DU145 and its stables and PC3 (+/-siCav1) cell lines after 17 AAG treatment (number of experiment=3). Cell viability assays using MTT were performed for DU145 and its stables and PC3 (+/-siCav1) after 17 AAG treatment. (A) Viability for DU145 and its stables were checked for 24, 48 and 72 h and (B) 24 h and 48 h for PC3 (+/-siCav1) which is statistical significant by Two-way ANNOVA where * means P<0.05.*

As evident from the graphs, the results showed that the cell viability decreased over the time for all the cell models except DU145-DSred.

3.3.4 Cell migration assay after 17 AAG treatment

The cell migration assays were performed for 8 h in Transwell chambers with 8 micron size filters. Cells were seeded in insert with serum free media and while complete media was added in the 24 well base. Cells were treated with 17 AAG for 24 h and after 16 h the cells were transferred onto the filters for 8 h (with 17 AAG added in both 24 well and insert). The migrated cells were fixed, stained with 0.05% crystal violet prepared in 70% EtOH, scored manually and graph was generated.

The graph shows decreased cell migration in DU145 & its stables (**Figure 3.22A)** as well as in PC3 (+/-siCav1) **(Figure 3.22B)** after 17 AAG. In DU145 & its stables, the DU145-YD cells were more migratory compared to DU145-YF irrespective of the treatment (+/-17AAG). Also, PC3(-siCav1) cells migrate more compared to PC3(+siCav1) depicting the role of pCav1 in cancer cell migration. The present data suggests a pCav1-dependent function of HSP90 in regulating cancer cell migration.
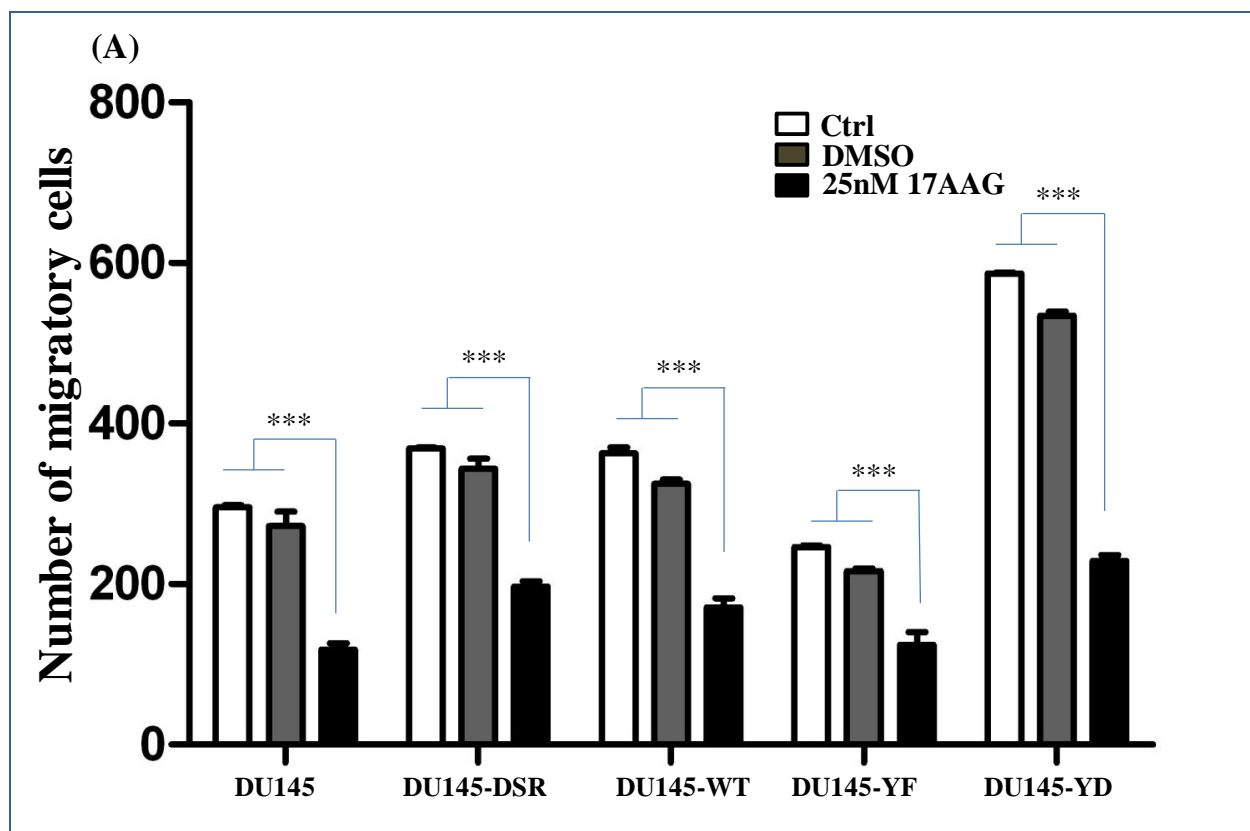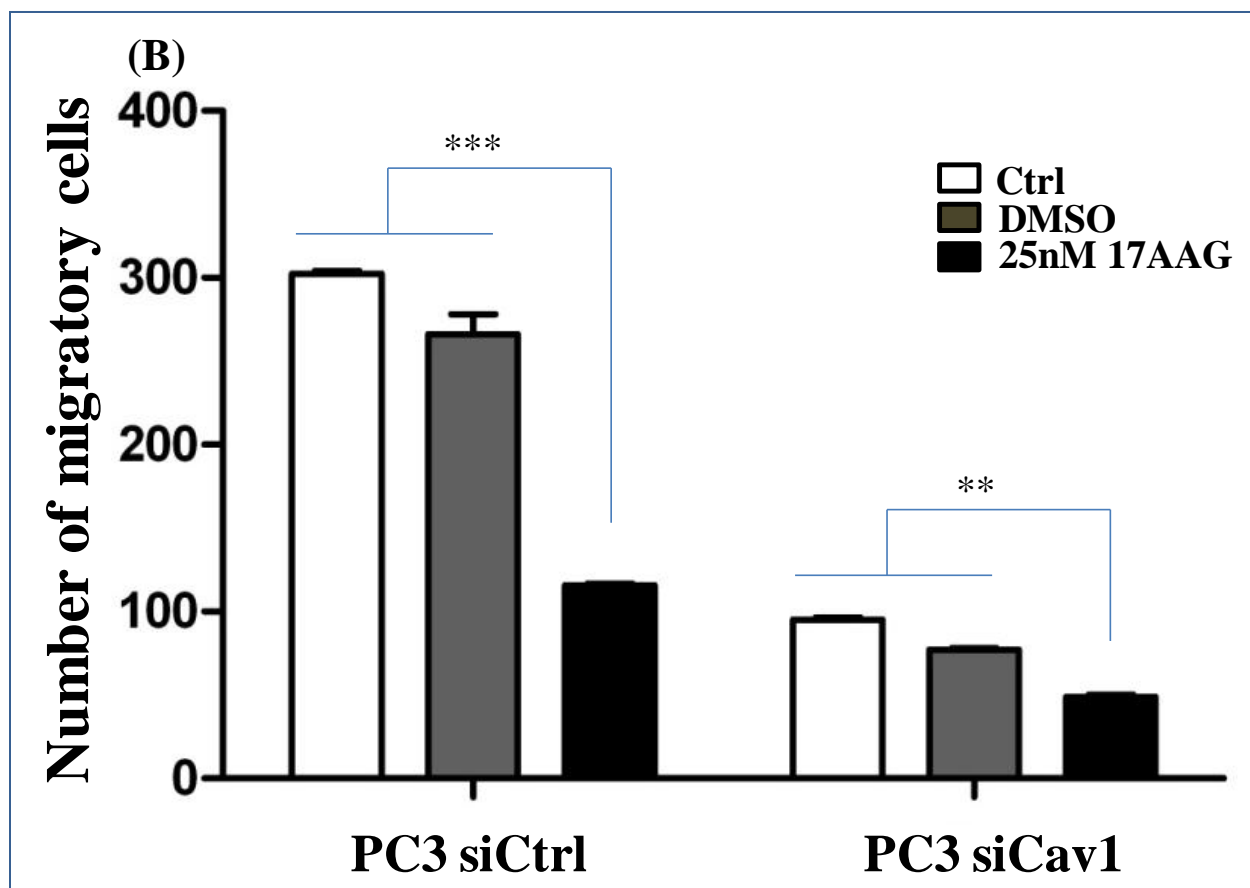
*Figure 3.22: Cell migration assay for DU145 and its stables and PC3 (+/-siCav1) after treatment of 17 AAG (number of experiment=3). Cell migration assays were performed for DU145 & its stables and PC3 (+/-siCav1) cells after 17 AAG treatment. The cells were transferred on transwell chambers (0.8 micron pore size) for 8 h during 24 h treatment with 17 AAG. The migrated cells were counted manually and graph was generated depicting statistical significance for treated and non-treated cell models by Two-way ANNOVA where ** means P<0.01 and *** means P<0.001.*

CHAPTER 4: DISCUSSION

4.1 pCAV1 AND PSEUDOPOD IN CANCER CELL MIGRATION

In cancer, tumor cells migrate and invade distant locations from the primary site through extra- and intra- vasation and niche in to various parts of the body causing secondary tumors. This process is called metastasis (**Guan, 2015**). Epithelial-Mesenchymal Transition (EMT) is a phenomenon where epithelial cells transform into a more migratory, mesenchymal or fibroblastic cells and is strongly associated with tumor metastasis (**Heerboth et. al, 2015**). Thus, it is this ability of tumor cells of undergoing EMT, which promotes secondary tumor formation making the disease more deadly. During EMT, the migratory cell gains polarity and elongates to form actin rich pseudopod protrusions (**Saykali and El-Sibai, 2014**). These pseudopod protrusions have been shown to play an important role in mesenchymal type of cell migration eventually causing metastasis (**Nurnberg et. al, 2011**).

Proteomic analysis study of metastatic cancer cell pseudopodia previously published from our lab has revealed a variety of classes and groups of proteins that are involved in actin-regulation, adhesion, glycolysis, protein and RNA translation, ubiquitin-mediated protein degradation, chaperones and signaling which are predominantly pseudopod enriched (**Jia et. al, 2005**). Another proteomic and microarray analysis of actin-rich pseudopodia from our lab revealed around 384 mRNAs and 64 proteins are similar in six metastatic cancer cell lines and around 19 of these proteins are pseudopod specific. It was further shown that out of the 19 proteins the knockdown of AHNAK, septin-9, eIF4E, and S100A11 proteins decreased actin cytoskeleton dynamics and had MET features which were prevented by stabilizing the actin cytoskeleton (**Shankar et. al, 2010**).

Cav1 is present usually in the terminally differentiated cells such as smooth muscle, endothelial cells, adipocytes, and also, type-I pneumocytes **(Chen and Che, 2014)**. Cav1 expression is linked to cancer cell migration, invasion and metastasis. In some cancer types it is highly expressed, for instance in prostate, bladder cancers and multiple myeloma whereas in some others like breast, cervical and ovarian cancers it has a low expression **(Hehlgans and Cordes, 2011)**. Cav1 contains a Src-dependent tyrosine 14 phosphorylation site. Our lab has previously shown that pCav1 that is highly expressed in metastatic, migratory and invasive cancer cells, is predominantly localized in the actin rich ruffles or protrusions at the leading edge of migration. We have also shown that the phosphorylation event involves Rho/ROCK signaling pathway promoting increased cell migration and regulating the FAs dynamics with the help of pCav1 **(Joshi et. al, 2008)**. Recent (unpublished results) show that the pCav1 interaction with PKM2 (metabolic enzyme) regulates various cellular processes such as cell cycle progression, metabolic pathways etc thereby playing a major role in tumor progression **(Submitted to elife, Shankar et al, 2016)**.

We decided to test the binding partners of Y14 phosphorylated pCav1. GST or GST-Cav1 (1-101) variant beads were generated and this was followed by GST pull down assays and quantitative proteomics. MaxQuant software package was used for analyzing the quantitative MS data.

As shown **in Figure 3.5 and 3.6**, PANTHER search analysis showed that according to GO biological process Cav1(1-101)Y14D appeared to be interact more with proteins involved in regulation of cellular stress (HSP70, HSPA9), cell proliferation (ITGB1, IQGAP1), signal transduction, metabolic process (PKM2, PPIA) and apoptosis (HSP90) whereas Cav1(1-101)Y14F showed MORE interaction with proteins regulating actin cytoskeleton (MYH10,

MYO18A) and RNA processing (RPS11, RPS14 and RPS17). PANTHER search analysis also confirmed that based on GO Cellular Process, Cav1(1-101)Y14D interacts more with proteins involved in the regulation of focal adhesion (Vinculin), cell junction, microtubule cytoskeleton and chromosome, supporting our previously published **(Joshi et. al, 2008; Goetz et. al, 2008)** and recent **(unpublished, Meng et.al, 2016)** results. Cav1(1-101)Y14F interacts more with proteins that regulate the actomyosin complex, actin filament bundle and ribonucleoprotein. Also, comparing the Cav1(1-101)Y14D and Cav1(1-101)Y14F interactome with DU145 pseudopod proteomics list gave some interesting results. 84 differentially interacting proteins from Cav1(1-101)Y14D were enriched in pseudopod proteome while only 24 proteins are enriched from Cav1(1-101)Y14F (**Figure 3.7**). This showed that various proteins interacting with Cav1(1-101)Y14D interactome were indeed enriched in pseudopod. These data are in dovetail confirming previous reports from our lab **(Jia et al, 2005; Shankar et al, 2010)**. Thus, globally looking at our bioinformatics analysis, it seems safe to predict that Cav1 phosphorylation, through its interactome, perhaps has a crucial role to play in stabilizing and recruiting various proteins that are involved in cancer cell metabolism, proliferation and migration.

4.2 pCAV1 INTERACTION: DOES IT REUIRES INTACT CSD OR NOT?

Cav1 contains a highly Conserved Scaffolding Domain (CSD) located from 82-101 AA that is known to physically interact with multiple proteins and play a role in regulating signal transduction **(Bucci et al., 2000)**. Studies have shown that the proteins that physically interact with Cav1 carry a motif, called Caveolin Binding Motif (CBM) **(Collins et al., 2012)**. Conversely, structural and bioinformatics analysis has shown that these CBMs are buried inside the protein and rather inapproachable for interaction **(Collins et. al, 2012)**. Another group

proposes CBM as a typical linear motif, which is present in 30% of human proteins but does not have a statistically significant enrichment in Cav1 interactome **(Byrne et. al, 2012)**. Also, sequence and structure-based studies have shown no characteristics properties present in CBM, which should have been there in any interaction motif.

Further, various other studies have also shown that many Cav1 binding partners lack CBM. For instance, Sproutyprotein-1, hepatocyte Cell Adhesion Molecule (hepaCAM), Protein Kinase A (PKAcat), nerve growth factor receptor and sterol carrier protein lack CBM and yet interact with Cav **(Cabrita et. al, 2006; Moh et. al, 2009; Zhang et. al, 2007)**.

Our proteomics data shows that only 40-45% of the binding partners of Cav1(1-101)Y14D and Cav1(1-101)Y14F have CBM domains. This data does not clarify the importance of the presence or absence of CBM in the binding partners. For instance, on one hand we have HSP90, whose physical interaction with pCav1 affects cancer cell migration, that does have a CBM (**F**IG**Y**PITL**Y**) and on the other hand, we have PKM2 that lacks a CBM and yet interacts with pCav1. PKM2 regulates various cellular and metabolic processes required for cancer cell survival and tumor progression. Therefore, it can be argued that the binding of different proteins with Cav1 might not be affected through our CSD double point mutations F92A and V94A. Also, we cannot discard the possibility that other residues of CSD might hamper these binding interactions.

We decided to investigate whether CSD domain of Cav1 has any importance in Y14 phosphorylation mediated interactions. In order to do this we mutated the CSD domain and performed pull down assays and proteomics. Double point mutations (F92A/V94A) in CSD domain of Cav1 have been well characterized that shows the role of CSD in Cav1 binding with

other proteins **(Kimura et al., 2002)**. PCR as well as site-directed mutagenesis was employed to create CSD mutants (F92A/V94A) from previously generated GST-Y14D-CSD and GST-Y14F-CSD and GST beads were prepared. Pull down assay and quantitative proteomics of two separate sets of samples: one set with GST, GST-Cav1(1-101)Y14D and GST-Cav1(1-101)Y14D-CSD beads and the other set with GST, GST-Cav1(1-101)Y14F and GST-Cav1(1-101)Y14F-CSD. Proteomics data analysis inferred that it is the Y14 site of Cav1 that plays a more critical role compared to the CSD domain in our cell model **(Figure 3.15 and 3.16)**. It is possible that the phosphorylation at Y14 and CSD may work in concert in determining the selective binding of Cav1. In absence of phosphorylation or an intact CSD may influence specificity of Cav1 interaction (perhaps due to structural alteration) and perhaps increase the number of proteins binding to YF-CSD **(Figure 3.16)**. It would be interesting to future investigate this and perform some structural analysis of Cav1-CSD mutant using both experimental (NMR) and bioinformatics approach which could provide some clues and give clearer picture.

4.3 pCAV1-SPECIFIC INTERACTION IMPACTS ON CAV1 FUNCTION IN CANCER CELL MIGRATION

We know pCav1 plays an important role in promoting tumor cell migration, invasion and metastasis **(Joshi et. al, 2008)**. So we were interested in understanding how pCav1-specific interaction with pseudopod enriched protein could influence on Cav1 function in cancer cell migration. Our proteomics study of Cav1(1-101)Y14D and Cav1(1-101)Y14F revealed pCav1 interaction with HSP90, which is also enriched in pseudopodia **(Figure 3.17(A))**. HSP90 is a molecular chaperone that helps in the proper folding, assembly, maturation, and stabilization of a variety of client proteins such as AKT, EGFR, and IGFR and also, enhances the cancer cell survival and proliferation **(Sawai et al., 2008)**. It also degrades misfolded protein through

proteasomal degradation pathway **(Amm et. al, 2014)**. Blocking HSP90 function has long been associated with anti-tumor effects and therefore, various HSP90 inhibitors such as Geldanamycin, 17 AAG and Derrubone have been explored as potential anti-cancer drugs **(Stebbins et al., 1997; Clarke et al., 2006; Hadden et al., 2006)**. It was shown that 17 AAG binds to the ATP binding pocket of HSP90 which makes it non functional and leads to the proteosomal degradation of accumulated proteins **(Kamal and Burrows, 2009)**. It was also shown that 17 AAG decreases the expression of various growth and proliferation related signaling molecules, like AKT, p-AKT, Her2 and also retards the growth of xenografted prostate cancer cell model **(Solit et. al, 2002; Ma et. al, 2014)**.

We used human prostate cancer cell lines, DU145 and its stables (DU145-YD, DU145-YF, DU145-WT and DU145-DSRed) and highly metastatic, migratory, invasive pCav1 positive, PC3. We know from our previously published work **(Joshi et. al, 2008)** and some of the recent unpublished data **(under preparation: Meng et. al 2016)** that DU145, DU145-YF and DU145-DSred have no pCav1 whereas DU145-YD (as phosphomimetic) and PC3 have high pCav1 levels **(Joshi et al, 2008)**. Our data showed that 17 AAG treatment induces the expression of AKT as well as Cav1 in the cell lines that have higher pCav1 levels **(Figure 3.19 & 3.20)**. Previous studies have shown that AKT expression goes down after 17AAG treatment **(Solit et. al, 2002)** similar to our cell models containing less pCav1 level wheras the cell models with high pCav1 have high AKT expression. This data suggests the impact of pCav1 over non functional HSP90.

Furthermore, after 17 AAG treatment, the number of viable and migratory cells decreased in DU145 & its stables as well as for PC3 (+/-siCav1). Interestingly, DU145-YD and PC3 (-siCav1) cells having high pCav1 levels were more migratory compared to low pCav1 containing

DU145-YF and PC3 (+siCav1) cells irrespective of the treatment (+/-17AAG) **(Figure 3.22)**. This suggests a pCav1-dependent function of HSP90 in regulating cancer cell migration.

So, it suggests a pCav1-dependent function of HSP90 in regulating cancer cell migration. So, we propose a model for this **(Figure 4.1)**.
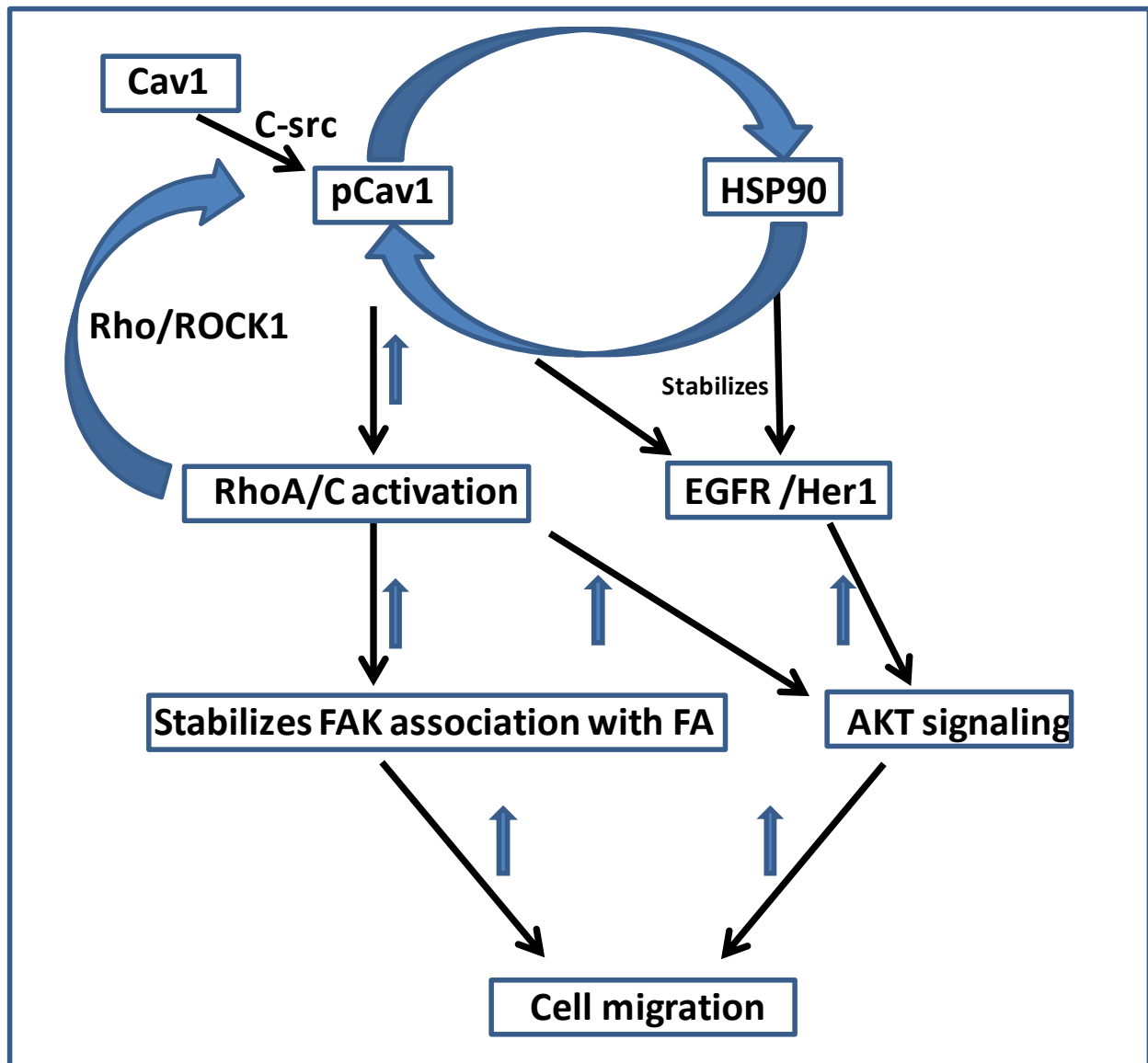
Figure 4.1 Model for impact pCav1-speacific interaction on Cav1 function in cancer cell migration

Actin rich protrusions (pseudopods) are important regulators of cancer cell migration (**Joyce and Pollard, 2009**). Proteomic and bioinformatics analysis has shown a large number of protein groups enriched in pseudopod, which includes groups of proteins related to actin-regulation, adhesion, glycolysis, protein translation, chaperones (HSP90) and signaling. These groups are involved in maintaining and promoting cell migration (**Shankar et. al, 2010; Jia et. al, 2005**). pCav1 is involved in regulating FAK stability and FA dynamics. Through proteomics we have found a direct physical interaction between pCav1 and HSP90 that was validated by GST pull down (**Figure 3.17**). We have also found increased expression HSP90 in DU145 cells stably transfected with Cav1(1-101)Y14D. We propose that this pCav1 specific interaction with HSP90 helps stabilize pCav1 at the protrusions. It is known that pCav1 activates RhoA GTPase through Rho/ROCK signaling, which in turn induces pCav1 and functions as a feedback loop. This leads to FAK stabilization and regulation of FA turnover, which eventually promotes cell migration (**Joshi et. al, 2008; Arpaia et. al, 2012**). RhoC-GTPase is also activated by pCav1, which activates AKT signaling and promotes cell motility and invasion (**Lehman et. al, 2012**).

pCav1 activates EGFR under mechanical stress whereas HSP90 stabilizes EGFR and Her1 expression (**Sawai et al., 2008; Zhang et. al, 2007**). Thus, HSP90 and pCav1, together or individually could alter the downstream signaling through the activation of AKT and promote cell migration (**Zhang et. al, 2007**).

As a future direction, we could explore how pCav1 and its interaction with HSP90 impacts cell cycle progression and cell proliferation by exposing cell lines (differentially expressing pCav1) to 17AAG. One of the important roles of pCav1 is to regulate FA dynamics, which also has a role in promoting tumor cell migration. Vinculin, being the predominant candidate of FA, and PKM2, a metabolic enzyme, have been found interacting with pCav1 and both are enriched in

pseudopod in our cell model **(unpublished Meng et. al, 2016)**. Presence of pCav1 and its interaction with HSP90 in pseudopod could have significant impact on the stability of other focal adhesion proteins as chaperones play vital role in stabilizing and proper folding of various proteins. Exposing the cells to 17AAG could help us understand how the colocalization of HSP90, pCav1 and other pseudopod-enriched candidates would get influenced. pCav1 has been linked to caveolae biogenesis under various stress conditions **(Joshi et al, 2012)** and whether stress responsive HSP90 has any role to play in this could also be explored in future using 17AAG and Electron Microscopy (EM). Together these attempts can help further clarify the dual role of Cav1 in signaling events driving tumor suppression or promotion.

CHAPTER 5: CONCLUSIONS

5.1 Proteomics data and bioinformatics analysis suggest that the Y14 phosphorylation impacts Cav1 interaction with different proteins. The Cav1(1-101)Y14D interactome, enriched in pseudopodia has different classes of interacting proteins compared to Cav1(1-101)Y14F.

Caveats and Contingencies:

In this aim, we have compared Cav1(1-101)Y14D mutant to the Cav1(1-101)Y14F mutant. The modification with phenylalanine, 'F' could change the conformation of Cav1, which could in turn influence the binding of different proteins to Cav1. Hence it is imperative to compare Cav1(1-101)Y14D interactome with Cav1WT to get a clearer picture.

GST pull down has some limitations. For example, the buffer used in the assay is non-physiological and the entire binding experiments are performed in vitro. Moreover, GST itself could non-specifically bind with many proteins which calls for stringent washing protocols. An alternate approach could be to transiently transfect DU145 or HEK-293 cells with myc-tagged Cav1WT or its mutants followed by co-IP with myc antibody and finally perform western blotting or proteomic analysis to validate in vivo interactions. In addition to this large data sets could be analyzed with protein arrays and other screening assays.

5.2 Proteomics analysis data suggest that double point mutation (F92A/V94A) in the CSD domain disrupts binding of one-third of both Cav1(1-101)Y14D and Cav1(1-101)Y14F interactome. Phosphorylation of Y14 and CSD domain may also function in concert in determining the selective binding of Cav1. In the absence of phosphorylation or intact CSD, Cav1 binding specificity may get influenced leading to increased number of proteins binding to Cav1(1-101)Y14F-CSD perhaps.

Caveats and Contingencies:

In Aim2, to explore the role of CSD on pCav1 interactome, double point mutations of CSD (F92A/V94A) were used which may not have been effective enough in altering the binding of CSD. This could be addressed by comparing the data with Cav1-1-78 AA mutants (w/o CSD domain) to get a better idea about the dependency of intact CSD on Cav1(1-101)Y14D while binding with proteins. Using this mutant in vivo (CoIP) or GST pull down validation can be done, followed by western blotting and proteomics analysis.

5.3 HSP90 is abundantly present in pseudopods and our data suggest that a functional HSP90 is required for cell migration. It also reveals the pCav1-dependent function of HSP90 in regulating cell migration.

Caveats and Contingencies:

GST pull down followed by western blotting was performed to investigate pCav1-specific interaction with HSP90. In addition to this FRET approach can be used to detect this interaction in vivo. Transient transfection of cells with pCav1 and HSP90 FRET plasmids and further analysis can confirm in vivo interactions.

17 AAG (HSP90 inhibitor) was used to explore whether or not pCav1-specific interaction with HSP90 impacts Cav1 function during cancer cell migration. Alternatively, siRNA knockdown approach targeting HSP90 or CRISPER/Cas9 HSP90 knockout cell models can be used to for this purpose.

Significance

This study reveals that Y14 phosphorylation impacts on Cav1 interaction with different proteins and partially affected by the CSD mutation (F92/V94) used for our study. Also, pCav1 specific interaction with HSP90 decreases prostate cancer cell migration.

References

Aebersold, R., and Mann, M. (2003). Mass spectrometry-based proteomics. Nature 422, 198-207.

Ahmed, S.N., Brown, D.A., and London, E. (1997). On the origin of sphingolipid/cholesterol-rich detergent-insoluble cell membranes: physiological concentrations of cholesterol and sphingolipid induce formation of a detergent-insoluble, liquid-ordered lipid phase in model membranes. Biochemistry 36, 10944-10953.

Amm, I., Sommer, T., and Wolf, D.H. (2014). Protein quality control and elimination of protein waste: the role of the ubiquitin-proteasome system. Biochimica et biophysica acta 1843, 182-196.

Anderson, R.G. (1998). The caveolae membrane system. Annual review of biochemistry 67, 199-225.

Arpaia, E., Blaser, H., Quintela-Fandino, M., Duncan, G., Leong, H.S., Ablack, A., Nambiar, S.C., Lind, E.F., Silvester, J., Fleming, C.K., et al. (2012). The interaction between caveolin-1 and Rho-GTPases promotes metastasis by controlling the expression of alpha5-integrin and the activation of Src, Ras and Erk. Oncogene 31, 884-896.

Ashburner, M., Ball, C.A., Blake, J.A., Botstein, D., Butler, H., Cherry, J.M., Davis, A.P., Dolinski, K., Dwight, S.S., Eppig, J.T., et al. (2000). Gene ontology: tool for the unification of biology. The Gene Ontology Consortium. Nature genetics 25, 25-29.

Bantscheff, M., Lemeer, S., Savitski, M.M., and Kuster, B. (2007). Quantitative mass spectrometry in proteomics: critical review update from 2007 to the present. Analytical and bioanalytical chemistry 404, 939-965.

Bertucci, F., Araujo, J., and Giovannini, M. (2013). Pancreatic metastasis from osteosarcoma and Ewing sarcoma: literature review. Scandinavian journal of gastroenterology 48, 4-8.

Betapudi, V. (2009). Myosin II motor proteins with different functions determine the fate of lamellipodia extension during cell spreading. PloS one 5, e8560.

Bickel, P.E., Scherer, P.E., Schnitzer, J.E., Oh, P., Lisanti, M.P., and Lodish, H.F. (1997). Flotillin and epidermal surface antigen define a new family of caveolae-associated integral membrane proteins. The Journal of biological chemistry 272, 13793-13802.

Boersema, P.J., Aye, T.T., van Veen, T.A., Heck, A.J., and Mohammed, S. (2008). Triplex protein quantification based on stable isotope labeling by peptide dimethylation applied to cell and tissue lysates. Proteomics 8, 4624-4632.

Brown, D.A., and Rose, J.K. (1992). Sorting of GPI-anchored proteins to glycolipid-enriched membrane subdomains during transport to the apical cell surface. Cell 68, 533-544.

Bucci, M., Gratton, J.P., Rudic, R.D., Acevedo, L., Roviezzo, F., Cirino, G., and Sessa, W.C. (2000). In vivo delivery of the caveolin-1 scaffolding domain inhibits nitric oxide synthesis and reduces inflammation. Nature medicine 6, 1362-1367.

Byrne, D.P., Dart, C., and Rigden, D.J. (2012). Evaluating caveolin interactions: do proteins interact with the caveolin scaffolding domain through a widespread aromatic residue-rich motif? PloS one 7, e44879.

Cabrita, M.A., Jaggi, F., Widjaja, S.P., and Christofori, G. (2006). A functional interaction between sprouty proteins and caveolin-1. The Journal of biological chemistry 281, 29201-29212.

Calderwood, S.K., Khaleque, M.A., Sawyer, D.B., and Ciocca, D.R. (2006). Heat shock proteins in cancer: chaperones of tumorigenesis. Trends in biochemical sciences 31, 164-172.

Campbell, I.D., and Humphries, M.J. (2011). Integrin structure, activation, and interactions. Cold Spring Harbor perspectives in biology 3.

Caselli, A., Mazzinghi, B., Camici, G., Manao, G., and Ramponi, G. (2002). Some protein tyrosine phosphatases target in part to lipid rafts and interact with caveolin-1. Biochemical and biophysical research communications 296, 692-697.

Chaffer, C.L., and Weinberg, R.A. (2011). A perspective on cancer cell metastasis. Science (New York, NY 331, 1559-1564.

Chatr-aryamontri, A., Ceol, A., Palazzi, L.M., Nardelli, G., Schneider, M.V., Castagnoli, L., and Cesareni, G. (2007). MINT: the Molecular INTeraction database. Nucleic acids research 35, D572-574.

Chen, D., and Che, G. (2014). Value of caveolin-1 in cancer progression and prognosis: Emphasis on cancer-associated fibroblasts, human cancer cells and mechanism of caveolin-1 expression (Review). Oncology letters 8, 1409-1421.

Chen, D., Shah, A., Nguyen, H., Loo, D., Inder, K.L., and Hill, M.M. (2014). Online quantitative proteomics p-value calculator for permutation-based statistical testing of peptide ratios. Journal of proteome research 13, 4184-4191.

Chidlow, J.H., Jr., and Sessa, W.C. (2010). Caveolae, caveolins, and cavins: complex control of cellular signalling and inflammation. Cardiovascular research 86, 219-225.

Chodniewicz, D., and Klemke, R.L. (2004). Guiding cell migration through directed extension and stabilization of pseudopodia. Experimental cell research 301, 31-37.

Chun, M., Liyanage, U.K., Lisanti, M.P., and Lodish, H.F. (1994). Signal transduction of a G protein-coupled receptor in caveolae: colocalization of endothelin and its receptor with caveolin. Proceedings of the National Academy of Sciences of the United States of America 91, 11728-11732.

Ciobanasu, C., Faivre, B., and Le Clainche, C. (2013). Actomyosin-dependent formation of the mechanosensitive talin-vinculin complex reinforces actin anchoring. Nature communications 5, 3095.

Clark, A.G., and Vignjevic, D.M. (2015). Modes of cancer cell invasion and the role of the microenvironment. Current opinion in cell biology 36, 13-22.

Cohen, A.W., Hnasko, R., Schubert, W., and Lisanti, M.P. (2004). Role of caveolae and caveolins in health and disease. Physiological reviews 84, 1341-1379.

Cohen, A.W., Park, D.S., Woodman, S.E., Williams, T.M., Chandra, M., Shirani, J., Pereira de Souza, A., Kitsis, R.N., Russell, R.G., Weiss, L.M., et al. (2003). Caveolin-1 null mice develop cardiac hypertrophy with hyperactivation of p42/44 MAP kinase in cardiac fibroblasts. Am J Physiol Cell Physiol 284, C457-474.

Collins, B.M., Davis, M.J., Hancock, J.F., and Parton, R.G. (2012). Structure-based reassessment of the caveolin signaling model: do caveolae regulate signaling through caveolin-protein interactions? Developmental cell 23, 11-20.

Costello, L.C., and Franklin, R.B. (2006). The clinical relevance of the metabolism of prostate cancer; zinc and tumor suppression: connecting the dots. Molecular cancer 5, 17.

Couet, J., Li, S., Okamoto, T., Ikezu, T., and Lisanti, M.P. (1997). Identification of peptide and protein ligands for the caveolin-scaffolding domain. Implications for the interaction of caveolin with caveolae-associated proteins. The Journal of biological chemistry 272, 6525-6533.

Croft, D., O'Kelly, G., Wu, G., Haw, R., Gillespie, M., Matthews, L., Caudy, M., Garapati, P., Gopinath, G., Jassal, B., et al. (2011). Reactome: a database of reactions, pathways and biological processes. Nucleic acids research 39, D691-697.

Csermely, P., Schnaider, T., Soti, C., Prohaszka, Z., and Nardai, G. (1998). The 90-kDa molecular chaperone family: structure, function, and clinical applications. A comprehensive review. Pharmacology & therapeutics 79, 129-168.

Deb, M., Sengupta, D., Kar, S., Rath, S.K., Roy, S., Das, G., and Patra, S.K. (2016). Epigenetic drift towards histone modifications regulates CAV1 gene expression in colon cancer. Gene 581, 75-84.

Dengjel, J., Jakobsen, L., and Andersen, J.S. (2010). Organelle proteomics by label-free and SILAC-based protein correlation profiling. Methods in molecular biology (Clifton, NJ 658, 255-265.

Dennis, J.W., Nabi, I.R., and Demetriou, M. (2009). Metabolism, cell surface organization, and disease. Cell 139, 1229-1241.

Dietzen, D.J., Hastings, W.R., and Lublin, D.M. (1995). Caveolin is palmitoylated on multiple cysteine residues. Palmitoylation is not necessary for localization of caveolin to caveolae. The Journal of biological chemistry 270, 6838-6842.

Dimopoulos, M.A., Mitsiades, C.S., Anderson, K.C., and Richardson, P.G. (2011). Tanespimycin as antitumor therapy. Clinical lymphoma, myeloma & leukemia 11, 17-22.

Dorsam, R.T., and Gutkind, J.S. (2007). G-protein-coupled receptors and cancer. Nat Rev Cancer 7, 79-94.

Doucey, M.A., Bender, F.C., Hess, D., Hofsteenge, J., and Bron, C. (2006). Caveolin-1 interacts with the chaperone complex TCP-1 and modulates its protein folding activity. Cell Mol Life Sci 63, 939-948.

Engelman, J.A., Chu, C., Lin, A., Jo, H., Ikezu, T., Okamoto, T., Kohtz, D.S., and Lisanti, M.P. (1998). Caveolin-mediated regulation of signaling along the p42/44 MAP kinase cascade in vivo. A role for the caveolin-scaffolding domain. FEBS letters 428, 205-211.

Engelman, J.A., Lee, R.J., Karnezis, A., Bearss, D.J., Webster, M., Siegel, P., Muller, W.J., Windle, J.J., Pestell, R.G., and Lisanti, M.P. (1998). Reciprocal regulation of neu tyrosine kinase activity and caveolin-1 protein expression in vitro and in vivo. Implications for human breast cancer. The Journal of biological chemistry 273, 20448-20455.

Epand, R.M., Sayer, B.G., and Epand, R.F. (2005). Caveolin scaffolding region and cholesterol-rich domains in membranes. Journal of molecular biology 345, 339-350.

Faltermeier, C.M., Drake, J.M., Clark, P.M., Smith, B.A., Zong, Y., Volpe, C., Mathis, C., Morrissey, C., Castor, B., Huang, J., et al. (2015). Functional screen identifies kinases driving prostate cancer visceral and bone metastasis. Proceedings of the National Academy of Sciences of the United States of America 113, E172-181.

Feng, S., Wang, Y., Wang, X., Wang, Z., Cui, Y., Liu, J., Zhao, C., Jin, M., and Zou, W. (2010). Caveolin-1 gene silencing promotes the activation of PI3K/AKT dependent on Eralpha36 and the transformation of MCF10ACE. Science China 53, 598-605.

Fenn, J.B., Mann, M., Meng, C.K., Wong, S.F., and Whitehouse, C.M. (1989). Electrospray ionization for mass spectrometry of large biomolecules. Science (New York, NY 246, 64-71.

Ferraldeschi, R., Nava Rodrigues, D., Riisnaes, R., Miranda, S., Figueiredo, I., Rescigno, P., Ravi, P., Pezaro, C., Omlin, A., Lorente, D., et al. (2015). PTEN protein loss and clinical outcome from castration-resistant prostate cancer treated with abiraterone acetate. European urology 67, 795-802.

Ferraldeschi, R., Nava Rodrigues, D., Riisnaes, R., Miranda, S., Figueiredo, I., Rescigno, P., Ravi, P., Pezaro, C., Omlin, A., Lorente, D., et al. (2015). PTEN protein loss and clinical outcome from castration-resistant prostate cancer treated with abiraterone acetate. European urology 67, 795-802.

Foster, L.J., De Hoog, C.L., and Mann, M. (2003). Unbiased quantitative proteomics of lipid rafts reveals high specificity for signaling factors. Proceedings of the National Academy of Sciences of the United States of America 100, 5813-5818.

Franceschini, A., Szklarczyk, D., Frankild, S., Kuhn, M., Simonovic, M., Roth, A., Lin, J., Minguez, P., Bork, P., von Mering, C., et al. (2013). STRING v9.1: protein-protein interaction networks, with increased coverage and integration. Nucleic acids research 41, D808-815.

Friedl, P., and Gilmour, D. (2009). Collective cell migration in morphogenesis, regeneration and cancer. Nat Rev Mol Cell Biol 10, 445-457.

Friedl, P., and Wolf, K. (2003). Tumour-cell invasion and migration: diversity and escape mechanisms. Nat Rev Cancer 3, 362-374.

Friedman, D.B., Hoving, S., and Westermeier, R. (2009). Isoelectric focusing and two-dimensional gel electrophoresis. Methods in enzymology 463, 515-540.

Garcia-Cardena, G., Martasek, P., Masters, B.S., Skidd, P.M., Couet, J., Li, S., Lisanti, M.P., and Sessa, W.C. (1997). Dissecting the interaction between nitric oxide synthase (NOS) and caveolin. Functional significance of the nos caveolin binding domain in vivo. The Journal of biological chemistry 272, 25437-25440.

Gaus, K., Le Lay, S., Balasubramanian, N., and Schwartz, M.A. (2006). Integrin-mediated adhesion regulates membrane order. The Journal of cell biology 174, 725-734.

Gevaert, K., Impens, F., Ghesquiere, B., Van Damme, P., Lambrechts, A., and Vandekerckhove, J. (2008). Stable isotopic labeling in proteomics. Proteomics 8, 4873-4885.

Glenney, J.R., Jr., and Soppet, D. (1992). Sequence and expression of caveolin, a protein component of caveolae plasma membrane domains phosphorylated on tyrosine in Rous sarcoma virus-transformed fibroblasts. Proceedings of the National Academy of Sciences of the United States of America 89, 10517-10521.

Goetz, J.G., Joshi, B., Lajoie, P., Strugnell, S.S., Scudamore, T., Kojic, L.D., and Nabi, I.R. (2008). Concerted regulation of focal adhesion dynamics by galectin-3 and tyrosine-phosphorylated caveolin-1. The Journal of cell biology 180, 1261-1275.

Goetz, J.G., Lajoie, P., Wiseman, S.M., and Nabi, I.R. (2008). Caveolin-1 in tumor progression: the good, the bad and the ugly. Cancer metastasis reviews 27, 715-735.

Gratton, J.P., Fontana, J., O'Connor, D.S., Garcia-Cardena, G., McCabe, T.J., and Sessa, W.C. (2000). Reconstitution of an endothelial nitric-oxide synthase (eNOS), hsp90, and caveolin-1 complex in vitro. Evidence that hsp90 facilitates calmodulin stimulated displacement of eNOS from caveolin-1. The Journal of biological chemistry 275, 22268-22272.

Grzegrzolka, J., Biala, M., Wojtyra, P., Kobierzycki, C., Olbromski, M., Gomulkiewicz, A., Piotrowska, A., Rys, J., Podhorska-Okolow, M., and Dziegiel, P. (2015). Expression of EMT Markers SLUG and TWIST in Breast Cancer. Anticancer research 35, 3961-3968.

Guan, X. (2015). Cancer metastases: challenges and opportunities. Acta pharmaceutica Sinica 5, 402-418.

Guirguis, R., Margulies, I., Taraboletti, G., Schiffmann, E., and Liotta, L. (1987). Cytokine-induced pseudopodial protrusion is coupled to tumour cell migration. Nature 329, 261-263.

Gumbiner, B.M. (1996). Cell adhesion: the molecular basis of tissue architecture and morphogenesis. Cell 84, 345-357.

Guo, T., Wang, W., Rudnick, P.A., Song, T., Li, J., Zhuang, Z., Weil, R.J., DeVoe, D.L., Lee, C.S., and Balgley, B.M. (2007). Proteome analysis of microdissected formalin-fixed and paraffin-embedded tissue specimens. J Histochem Cytochem 55, 763-772.

Guo, W.H., and Wang, Y.L. (2007). Retrograde fluxes of focal adhesion proteins in response to cell migration and mechanical signals. Molecular biology of the cell 18, 4519-4527.

Gupton, S.L., and Waterman-Storer, C.M. (2006). Spatiotemporal feedback between actomyosin and focal-adhesion systems optimizes rapid cell migration. Cell 125, 1361-1374.

Hailstones, D., Sleer, L.S., Parton, R.G., and Stanley, K.K. (1998). Regulation of caveolin and caveolae by cholesterol in MDCK cells. Journal of lipid research 39, 369-379.

Hakim, D.N., Pelly, T., Kulendran, M., and Caris, J.A. (2015). Benign tumours of the bone: A review. Journal of bone oncology 4, 37-41.

Hammond, D.E., Hyde, R., Kratchmarova, I., Beynon, R.J., Blagoev, B., and Clague, M.J. (2009). Quantitative analysis of HGF and EGF-dependent phosphotyrosine signaling networks. Journal of proteome research 9, 2734-2742.

Han, F., Gu, D., Chen, Q., and Zhu, H. (2009). Caveolin-1 acts as a tumor suppressor by down-regulating epidermal growth factor receptor-mitogen-activated protein kinase signaling pathway in pancreatic carcinoma cell lines. Pancreas 38, 766-774.

Han, F., Zhang, L., Zhou, Y., and Yi, X. (2015). Caveolin-1 regulates cell apoptosis and invasion ability in paclitaxel-induced multidrug-resistant A549 lung cancer cells. International journal of clinical and experimental pathology 8, 8937-8947.

Hanahan, D., and Weinberg, R.A. (2000). The hallmarks of cancer. Cell 100, 57-70.

Hanahan, D., and Weinberg, R.A. (2011). Hallmarks of cancer: the next generation. Cell 144, 646-674.

Hansen, C.G., Shvets, E., Howard, G., Riento, K., and Nichols, B.J. (2013). Deletion of cavin genes reveals tissue-specific mechanisms for morphogenesis of endothelial caveolae. Nature communications 4, 1831.

Hayashi, K., Matsuda, S., Machida, K., Yamamoto, T., Fukuda, Y., Nimura, Y., Hayakawa, T., and Hamaguchi, M. (2001). Invasion activating caveolin-1 mutation in human scirrhous breast cancers. Cancer research 61, 2361-2364.

Heerboth, S., Housman, G., Leary, M., Longacre, M., Byler, S., Lapinska, K., Willbanks, A., and Sarkar, S. (2015). EMT and tumor metastasis. Clinical and translational medicine 4, 6.

Hehlgans, S., and Cordes, N. (2011). Caveolin-1: an essential modulator of cancer cell radio-and chemoresistance. American journal of cancer research 1, 521-530.

Hishiya, A., and Takayama, S. (2008). Molecular chaperones as regulators of cell death. Oncogene 27, 6489-6506.

Huang, C., Qiu, Z., Wang, L., Peng, Z., Jia, Z., Logsdon, C.D., Le, X., Wei, D., Huang, S., and Xie, K. (2011). A novel FoxM1-caveolin signaling pathway promotes pancreatic cancer invasion and metastasis. Cancer research 72, 655-665.

Huang, C.H., Kuo, C.J., Liang, S.S., Chi, S.W., Hsi, E., Chen, C.C., Lee, K.T., and Chiou, S.H. (2015). Onco-proteogenomics identifies urinary S100A9 and GRN as potential combinatorial biomarkers for early diagnosis of hepatocellular carcinoma. BBA clinical 3, 205-213.

Huang da, W., Sherman, B.T., and Lempicki, R.A. (2009). Bioinformatics enrichment tools: paths toward the comprehensive functional analysis of large gene lists. Nucleic acids research 37, 1-13.

Huertas-Martinez, J., Rello-Varona, S., Herrero-Martin, D., Barrau, I., Garcia-Monclus, S., Sainz-Jaspeado, M., Lagares-Tena, L., Nunez-Alvarez, Y., Mateo-Lozano, S., Mora, J., et al. (2014). Caveolin-1 is down-regulated in alveolar rhabdomyosarcomas and negatively regulates tumor growth. Oncotarget 5, 9744-9755.

Hurlstone, A.F., Reid, G., Reeves, J.R., Fraser, J., Strathdee, G., Rahilly, M., Parkinson, E.K., and Black, D.M. (1999). Analysis of the CAVEOLIN-1 gene at human chromosome 7q31.1 in primary tumours and tumour-derived cell lines. Oncogene 18, 1881-1890.

Imai, J., Maruya, M., Yashiroda, H., Yahara, I., and Tanaka, K. (2003). The molecular chaperone Hsp90 plays a role in the assembly and maintenance of the 26S proteasome. The EMBO journal 22, 3557-3567.

Isshiki, M., and Anderson, R.G. (1999). Calcium signal transduction from caveolae. Cell calcium 26, 201-208.

Ito, A., Mimae, T., Yamamoto, Y.S., Hagiyama, M., Nakanishi, J., Ito, M., Hosokawa, Y., Okada, M., Murakami, Y., and Kondo, T. (2012). Novel application for pseudopodia proteomics using excimer laser ablation and two-dimensional difference gel electrophoresis. Laboratory investigation; a journal of technical methods and pathology 92, 1374-1385.

Iwanicki, M.P., Vomastek, T., Tilghman, R.W., Martin, K.H., Banerjee, J., Wedegaertner, P.B., and Parsons, J.T. (2008). FAK, PDZ-RhoGEF and ROCKII cooperate to regulate adhesion movement and trailing-edge retraction in fibroblasts. Journal of cell science 121, 895-905.

Jang, M., Kim, S.S., and Lee, J. (2013). Cancer cell metabolism: implications for therapeutic targets. Experimental & molecular medicine 45, e45.

Jia, Z., Barbier, L., Stuart, H., Amraei, M., Pelech, S., Dennis, J.W., Metalnikov, P., O'Donnell, P., and Nabi, I.R. (2005). Tumor cell pseudopodial protrusions. Localized signaling domains coordinating cytoskeleton remodeling, cell adhesion, glycolysis, RNA translocation, and protein translation. The Journal of biological chemistry 280, 30564-30573.

Jolly, M.K., Boareto, M., Huang, B., Jia, D., Lu, M., Ben-Jacob, E., Onuchic, J.N., and Levine, H. (2015). Implications of the Hybrid Epithelial/Mesenchymal Phenotype in Metastasis. Frontiers in oncology 5, 155.

Joshi, B., Bastiani, M., Strugnell, S.S., Boscher, C., Parton, R.G., and Nabi, I.R. (2012). Phosphocaveolin-1 is a mechanotransducer that induces caveola biogenesis via Egr1 transcriptional regulation. The Journal of cell biology 199, 425-435.

Joshi, B., Strugnell, S.S., Goetz, J.G., Kojic, L.D., Cox, M.E., Griffith, O.L., Chan, S.K., Jones, S.J., Leung, S.P., Masoudi, H., et al. (2008). Phosphorylated caveolin-1 regulates Rho/ROCK-dependent focal adhesion dynamics and tumor cell migration and invasion. Cancer research 68, 8210-8220.

Kamal, A., and Burrows, F.J. (2004). Hsp90 inhibitors as selective anticancer drugs. Discovery medicine 4, 277-280.

Kanehisa, M., Goto, S., Sato, Y., Furumichi, M., and Tanabe, M. (2012). KEGG for integration and interpretation of large-scale molecular data sets. Nucleic acids research 40, D109-114.

Kang, J., Park, J.H., Lee, H.J., Jo, U., Park, J.K., Seo, J.H., Kim, Y.H., Kim, I., and Park, K.H. (2015). Caveolin-1 Modulates Docetaxel-Induced Cell Death in Breast Cancer Cell Subtypes through Different Mechanisms. Cancer Res Treat 48, 715-726.

Kannan, A., Krishnan, A., Ali, M., Subramaniam, S., Halagowder, D., and Sivasithamparam, N.D. (2014). Caveolin-1 promotes gastric cancer progression by up-regulating epithelial to mesenchymal transition by crosstalk of signalling mechanisms under hypoxic condition. Eur J Cancer 50, 204-215.

Karam, J.A., Lotan, Y., Roehrborn, C.G., Ashfaq, R., Karakiewicz, P.I., and Shariat, S.F. (2007). Caveolin-1 overexpression is associated with aggressive prostate cancer recurrence. The Prostate 67, 614-622.

Karas, M., and Kruger, R. (2003). Ion formation in MALDI: the cluster ionization mechanism. Chemical reviews 103, 427-440.

Kawauchi, T. (2012). Cell adhesion and its endocytic regulation in cell migration during neural development and cancer metastasis. International journal of molecular sciences 13, 4564-4590.

Kerrien, S., Aranda, B., Breuza, L., Bridge, A., Broackes-Carter, F., Chen, C., Duesbury, M., Dumousseau, M., Feuermann, M., Hinz, U., et al. (2012). The IntAct molecular interaction database in 2012. Nucleic acids research 40, D841-846.

Kimura, A., Mora, S., Shigematsu, S., Pessin, J.E., and Saltiel, A.R. (2002). The insulin receptor catalyzes the tyrosine phosphorylation of caveolin-1. The Journal of biological chemistry 277, 30153-30158.

Koike, S., Kodera, Y., Nakao, A., Iwata, H., and Yatabe, Y. (2010). Absence of the caveolin-1 P132L mutation in cancers of the breast and other organs. J Mol Diagn 12, 712-717.

Koivisto, P.A., and Rantala, I. (1999). Amplification of the androgen receptor gene is associated with P53 mutation in hormone-refractory recurrent prostate cancer. The Journal of pathology 187, 237-241.

Kolch, W., and Pitt, A. (2010). Functional proteomics to dissect tyrosine kinase signalling pathways in cancer. Nat Rev Cancer 10, 618-629.

Koomen, J.M., Haura, E.B., Bepler, G., Sutphen, R., Remily-Wood, E.R., Benson, K., Hussein, M., Hazlehurst, L.A., Yeatman, T.J., Hildreth, L.T., et al. (2008). Proteomic contributions to personalized cancer care. Mol Cell Proteomics 7, 1780-1794.

Kovanich, D., Cappadona, S., Raijmakers, R., Mohammed, S., Scholten, A., and Heck, A.J. (2012). Applications of stable isotope dimethyl labeling in quantitative proteomics. Analytical and bioanalytical chemistry 404, 991-1009.

Kuo, K.K., Kuo, C.J., Chiu, C.Y., Liang, S.S., Huang, C.H., Chi, S.W., Tsai, K.B., Chen, C.Y., Hsi, E., Cheng, K.H., et al. (2016). Quantitative Proteomic Analysis of Differentially Expressed Protein Profiles Involved in Pancreatic Ductal Adenocarcinoma. Pancreas 45, 71-83.

Kurzchalia, T.V., Dupree, P., Parton, R.G., Kellner, R., Virta, H., Lehnert, M., and Simons, K. (1992). VIP21, a 21-kD membrane protein is an integral component of trans-Golgi-network-derived transport vesicles. The Journal of cell biology 118, 1003-1014.

Kyriazi, S., Kaye, S.B., and deSouza, N.M. (2010). Imaging ovarian cancer and peritoneal metastases--current and emerging techniques. Nature reviews 7, 381-393.

Lajoie, P., Goetz, J.G., Dennis, J.W., and Nabi, I.R. (2009). Lattices, rafts, and scaffolds: domain regulation of receptor signaling at the plasma membrane. The Journal of cell biology 185, 381-385.

Lajoie, P., and Nabi, I.R. (2010). Lipid rafts, caveolae, and their endocytosis. International review of cell and molecular biology 282, 135-163.

Lajoie, P., Partridge, E.A., Guay, G., Goetz, J.G., Pawling, J., Lagana, A., Joshi, B., Dennis, J.W., and Nabi, I.R. (2007). Plasma membrane domain organization regulates EGFR signaling in tumor cells. The Journal of cell biology 179, 341-356.

Laude, A.J., and Prior, I.A. (2004). Plasma membrane microdomains: organization, function and trafficking. Molecular membrane biology 21, 193-205.

Lauffenburger, D.A., and Horwitz, A.F. (1996). Cell migration: a physically integrated molecular process. Cell 84, 359-369.

Lecharpentier, A., Vielh, P., Perez-Moreno, P., Planchard, D., Soria, J.C., and Farace, F. (2011). Detection of circulating tumour cells with a hybrid (epithelial/mesenchymal) phenotype in patients with metastatic non-small cell lung cancer. British journal of cancer 105, 1338-1341.

Lee, H., Park, D.S., Razani, B., Russell, R.G., Pestell, R.G., and Lisanti, M.P. (2002). Caveolin-1 mutations (P132L and null) and the pathogenesis of breast cancer: caveolin-1 (P132L) behaves in a dominant-negative manner and caveolin-1 (-/-) null mice show mammary epithelial cell hyperplasia. The American journal of pathology 161, 1357-1369.

Lee, H., Park, D.S., Wang, X.B., Scherer, P.E., Schwartz, P.E., and Lisanti, M.P. (2002). Src-induced phosphorylation of caveolin-2 on tyrosine 19. Phospho-caveolin-2 (Tyr(P)19) is localized near focal adhesions, remains associated with lipid rafts/caveolae, but no longer forms a high molecular mass hetero-oligomer with caveolin-1. The Journal of biological chemistry 277, 34556-34567.

Lee, H., Volonte, D., Galbiati, F., Iyengar, P., Lublin, D.M., Bregman, D.B., Wilson, M.T., Campos-Gonzalez, R., Bouzahzah, B., Pestell, R.G., et al. (2000). Constitutive and growth factor-regulated phosphorylation of caveolin-1 occurs at the same site (Tyr-14) in vivo:

identification of a c-Src/Cav-1/Grb7 signaling cassette. Molecular endocrinology (Baltimore, Md 14, 1750-1775.

Lee, S.W., Reimer, C.L., Oh, P., Campbell, D.B., and Schnitzer, J.E. (1998). Tumor cell growth inhibition by caveolin re-expression in human breast cancer cells. Oncogene 16, 1391-1397.

Levental, I., Lingwood, D., Grzybek, M., Coskun, U., and Simons, K. (2010). Palmitoylation regulates raft affinity for the majority of integral raft proteins. Proceedings of the National Academy of Sciences of the United States of America 107, 22050-22054.

Li, L., Ren, C.H., Tahir, S.A., Ren, C., and Thompson, T.C. (2003). Caveolin-1 maintains activated Akt in prostate cancer cells through scaffolding domain binding site interactions with and inhibition of serine/threonine protein phosphatases PP1 and PP2A. Molecular and cellular biology 23, 9389-9404.

Li, S., Couet, J., and Lisanti, M.P. (1996). Src tyrosine kinases, Galpha subunits, and H-Ras share a common membrane-anchored scaffolding protein, caveolin. Caveolin binding negatively regulates the auto-activation of Src tyrosine kinases. The Journal of biological chemistry 271, 29182-29190.

Li, S., Seitz, R., and Lisanti, M.P. (1996). Phosphorylation of caveolin by src tyrosine kinases. The alpha-isoform of caveolin is selectively phosphorylated by v-Src in vivo. The Journal of biological chemistry 271, 3863-3868.

Liang, H., Cheung, L.W., Li, J., Ju, Z., Yu, S., Stemke-Hale, K., Dogruluk, T., Lu, Y., Liu, X., Gu, C., et al. (2012). Whole-exome sequencing combined with functional genomics reveals novel candidate driver cancer genes in endometrial cancer. Genome research 22, 2120-2129.

Lichty, J.J., Malecki, J.L., Agnew, H.D., Michelson-Horowitz, D.J., and Tan, S. (2005). Comparison of affinity tags for protein purification. Protein expression and purification 41, 98-105.

Lin, B., Yin, T., Wu, Y.I., Inoue, T., and Levchenko, A. (2015). Interplay between chemotaxis and contact inhibition of locomotion determines exploratory cell migration. Nature communications 6, 6619.

Lisanti, M.P., Sargiacomo, M., and Scherer, P.E. (1999). Purification of caveolae-derived membrane microdomains containing lipid-anchored signaling molecules, such as GPI-anchored proteins, H-Ras, Src-family tyrosine kinases, eNOS, and G-protein alpha-, beta-, and gamma-subunits. Methods in molecular biology (Clifton, NJ 116, 51-60.

Lisanti, M.P., Scherer, P.E., Tang, Z., and Sargiacomo, M. (1994). Caveolae, caveolin and caveolin-rich membrane domains: a signalling hypothesis. Trends in cell biology 4, 231-235.

Liu, L., and Pilch, P.F. (2008). A critical role of cavin (polymerase I and transcript release factor) in caveolae formation and organization. The Journal of biological chemistry 283, 4314-4322.

Liu, P., and Anderson, R.G. (1995). Compartmentalized production of ceramide at the cell surface. The Journal of biological chemistry 270, 27179-27185.

Liu, P., Rudick, M., and Anderson, R.G. (2002). Multiple functions of caveolin-1. The Journal of biological chemistry 277, 41295-41298.

Liu, P., Ying, Y., Ko, Y.G., and Anderson, R.G. (1996). Localization of platelet-derived growth factor-stimulated phosphorylation cascade to caveolae. The Journal of biological chemistry 271, 10299-10303.

Liu, Y.J., Le Berre, M., Lautenschlaeger, F., Maiuri, P., Callan-Jones, A., Heuze, M., Takaki, T., Voituriez, R., and Piel, M. (2015). Confinement and low adhesion induce fast amoeboid migration of slow mesenchymal cells. Cell 160, 659-672.

Lock, J.G., Wehrle-Haller, B., and Stromblad, S. (2008). Cell-matrix adhesion complexes: master control machinery of cell migration. Seminars in cancer biology 18, 65-76.

Luan, T.Y., Zhu, T.N., Cui, Y.J., Zhang, G., Song, X.J., Gao, D.M., Zhang, Y.M., Zhao, Q.L., Liu, S., Su, T.Y., et al. (2015). Expression of caveolin-1 is correlated with lung adenocarcinoma proliferation, migration, and invasion. Medical oncology (Northwood, London, England) 32, 207.

Luo, L., King, N.P., Yeo, J.C., Jones, A., and Stow, J.L. (2014). Single-step protease cleavage elution for identification of protein-protein interactions from GST pull-down and mass spectrometry. Proteomics 14, 19-23.

Ma, L., Sato, F., Sato, R., Matsubara, T., Hirai, K., Yamasaki, M., Shin, T., Shimada, T., Nomura, T., Mori, K., et al. (2014). Dual targeting of heat shock proteins 90 and 70 promotes cell death and enhances the anticancer effect of chemotherapeutic agents in bladder cancer. Oncology reports 31, 2482-2492.

Mahmood, T., and Yang, P.C. (2012). Western blot: technique, theory, and trouble shooting. North American journal of medical sciences 4, 429-434.

Malik, R., Dulla, K., Nigg, E.A., and Korner, R. (2010). From proteome lists to biological impact--tools and strategies for the analysis of large MS data sets. Proteomics 10, 1270-1283.

Martinez-Outschoorn, U.E., Sotgia, F., and Lisanti, M.P. (2015). Caveolae and signalling in cancer. Nat Rev Cancer 15, 225-237.

McCubrey, J.A., Abrams, S.L., Fitzgerald, T.L., Cocco, L., Martelli, A.M., Montalto, G., Cervello, M., Scalisi, A., Candido, S., Libra, M., et al. (2015). Roles of signaling pathways in drug resistance, cancer initiating cells and cancer progression and metastasis. Advances in biological regulation 57, 75-101.

McMahon, K.A., Zajicek, H., Li, W.P., Peyton, M.J., Minna, J.D., Hernandez, V.J., Luby-Phelps, K., and Anderson, R.G. (2009). SRBC/cavin-3 is a caveolin adapter protein that regulates caveolae function. The EMBO journal 28, 1001-1015.

Meng, W., and Takeichi, M. (2009). Adherens junction: molecular architecture and regulation. Cold Spring Harbor perspectives in biology 1, a002899.

Mesri, M. (2014). Advances in Proteomic Technologies and Its Contribution to the Field of Cancer. Advances in medicine 2014, 238045.

Mi, H., Muruganujan, A., Casagrande, J.T., and Thomas, P.D. (2013). Large-scale gene function analysis with the PANTHER classification system. Nature protocols 8, 1551-1566.

Mineo, C., James, G.L., Smart, E.J., and Anderson, R.G. (1996). Localization of epidermal growth factor-stimulated Ras/Raf-1 interaction to caveolae membrane. The Journal of biological chemistry 271, 11930-11935.

Moh, M.C., Lee, L.H., Zhang, T., and Shen, S. (2009). Interaction of the immunoglobulin-like cell adhesion molecule hepaCAM with caveolin-1. Biochemical and biophysical research communications 378, 755-760.

Morgan, T.M., Lange, P.H., Porter, M.P., Lin, D.W., Ellis, W.J., Gallaher, I.S., and Vessella, R.L. (2009). Disseminated tumor cells in prostate cancer patients after radical prostatectomy and without evidence of disease predicts biochemical recurrence. Clin Cancer Res 15, 677-683.

Morrissey, C., Vessella, R.L., Lange, P.H., and Lam, H.M. (2016). The biology and clinical implications of prostate cancer dormancy and metastasis. Journal of molecular medicine (Berlin, Germany) 94, 259-265.

Mougeolle, A., Poussard, S., Decossas, M., Lamaze, C., Lambert, O., and Dargelos, E. (2015). Oxidative stress induces caveolin 1 degradation and impairs caveolae functions in skeletal muscle cells. PloS one 10, e0122654.

Muller, P.A., and Vousden, K.H. (2013). p53 mutations in cancer. Nature cell biology 15, 2-8.

Nabi, I.R. (2009). Cavin fever: regulating caveolae. Nature cell biology 11, 789-791.

Nam, K.H., Lee, B.L., Park, J.H., Kim, J., Han, N., Lee, H.E., Kim, M.A., Lee, H.S., and Kim, W.H. (2012). Caveolin 1 expression correlates with poor prognosis and focal adhesion kinase expression in gastric cancer. Pathobiology 80, 87-94.

Nicolson, G.L. (2014). The Fluid-Mosaic Model of Membrane Structure: still relevant to understanding the structure, function and dynamics of biological membranes after more than 40 years. Biochimica et biophysica acta 1838, 1451-1466.

Nurnberg, A., Kitzing, T., and Grosse, R. (2011). Nucleating actin for invasion. Nat Rev Cancer 11, 177-187.

Okamoto, T., Schlegel, A., Scherer, P.E., and Lisanti, M.P. (1998). Caveolins, a family of scaffolding proteins for organizing "preassembled signaling complexes" at the plasma membrane. The Journal of biological chemistry 273, 5419-5422.

Ong, S.E., and Mann, M. (2005). Mass spectrometry-based proteomics turns quantitative. Nature chemical biology 1, 252-262.

Osman, I., Drobnjak, M., Fazzari, M., Ferrara, J., Scher, H.I., and Cordon-Cardo, C. (1999). Inactivation of the p53 pathway in prostate cancer: impact on tumor progression. Clin Cancer Res 5, 2082-2088.

Ostermeyer, A.G., Paci, J.M., Zeng, Y., Lublin, D.M., Munro, S., and Brown, D.A. (2001). Accumulation of caveolin in the endoplasmic reticulum redirects the protein to lipid storage droplets. The Journal of cell biology 152, 1071-1078.

Panaretou, B., Prodromou, C., Roe, S.M., O'Brien, R., Ladbury, J.E., Piper, P.W., and Pearl, L.H. (1998). ATP binding and hydrolysis are essential to the function of the Hsp90 molecular chaperone in vivo. The EMBO journal 17, 4829-4836.

Pancotti, F., Roncuzzi, L., Maggiolini, M., and Gasperi-Campani, A. (2012). Caveolin-1 silencing arrests the proliferation of metastatic lung cancer cells through the inhibition of STAT3 signaling. Cellular signalling 24, 1390-1397.

Pani, B., and Singh, B.B. (2009). Lipid rafts/caveolae as microdomains of calcium signaling. Cell calcium 45, 625-633.

Park, D.S., Razani, B., Lasorella, A., Schreiber-Agus, N., Pestell, R.G., Iavarone, A., and Lisanti, M.P. (2001). Evidence that Myc isoforms transcriptionally repress caveolin-1 gene expression via an INR-dependent mechanism. Biochemistry 40, 3354-3362.

Parri, M., Buricchi, F., Giannoni, E., Grimaldi, G., Mello, T., Raugei, G., Ramponi, G., and Chiarugi, P. (2007). EphrinA1 activates a Src/focal adhesion kinase-mediated motility response leading to rho-dependent actino/myosin contractility. The Journal of biological chemistry 282, 19619-19628.

Parri, M., and Chiarugi, P. (2010). Rac and Rho GTPases in cancer cell motility control. Cell Commun Signal 8, 23.

Parton, R.G., and del Pozo, M.A. (2013). Caveolae as plasma membrane sensors, protectors and organizers. Nat Rev Mol Cell Biol 14, 98-112.

Parton, R.G., Hanzal-Bayer, M., and Hancock, J.F. (2006). Biogenesis of caveolae: a structural model for caveolin-induced domain formation. Journal of cell science 119, 787-796.

Patel, V.J., Thalassinos, K., Slade, S.E., Connolly, J.B., Crombie, A., Murrell, J.C., and Scrivens, J.H. (2009). A comparison of labeling and label-free mass spectrometry-based proteomics approaches. Journal of proteome research 8, 3752-3759.

Pattabiraman, D.R., Bierie, B., Kober, K.I., Thiru, P., Krall, J.A., Zill, C., Reinhardt, F., Tam, W.L., and Weinberg, R.A. (2016). Activation of PKA leads to mesenchymal-to-epithelial transition and loss of tumor-initiating ability. Science (New York, NY 351, aad3680.

Pearl, L.H., and Prodromou, C. (2000). Structure and in vivo function of Hsp90. Current opinion in structural biology 10, 46-51.

Pike, L.J. (2004). Lipid rafts: heterogeneity on the high seas. The Biochemical journal 378, 281-292.

Podar, K., Tai, Y.T., Cole, C.E., Hideshima, T., Sattler, M., Hamblin, A., Mitsiades, N., Schlossman, R.L., Davies, F.E., Morgan, G.J., et al. (2003). Essential role of caveolae in interleukin-6- and insulin-like growth factor I-triggered Akt-1-mediated survival of multiple myeloma cells. The Journal of biological chemistry 278, 5794-5801.

Popper, H.H. (2016). Progression and metastasis of lung cancer. Cancer metastasis reviews 35, 75-91.

Porter, J.R., Fritz, C.C., and Depew, K.M. (2010). Discovery and development of Hsp90 inhibitors: a promising pathway for cancer therapy. Current opinion in chemical biology 14, 412-420.

Quann, K., Gonzales, D.M., Mercier, I., Wang, C., Sotgia, F., Pestell, R.G., Lisanti, M.P., and Jasmin, J.F. (2013). Caveolin-1 is a negative regulator of tumor growth in glioblastoma and modulates chemosensitivity to temozolomide. Cell cycle (Georgetown, Tex 12, 1510-1520.

Razani, B., Combs, T.P., Wang, X.B., Frank, P.G., Park, D.S., Russell, R.G., Li, M., Tang, B., Jelicks, L.A., Scherer, P.E., et al. (2002). Caveolin-1-deficient mice are lean, resistant to diet-induced obesity, and show hypertriglyceridemia with adipocyte abnormalities. The Journal of biological chemistry 277, 8635-8647.

Razani, B., Woodman, S.E., and Lisanti, M.P. (2002). Caveolae: from cell biology to animal physiology. Pharmacological reviews 54, 431-467.

Reymond, M.A., and Schlegel, W. (2007). Proteomics in cancer. Advances in clinical chemistry 44, 103-142.

Ridley, A.J., Schwartz, M.A., Burridge, K., Firtel, R.A., Ginsberg, M.H., Borisy, G., Parsons, J.T., and Horwitz, A.R. (2003). Cell migration: integrating signals from front to back. Science (New York, NY 302, 1704-1709.

Rothberg, K.G., Heuser, J.E., Donzell, W.C., Ying, Y.S., Glenney, J.R., and Anderson, R.G. (1992). Caveolin, a protein component of caveolae membrane coats. Cell 68, 673-682.

Sagynaliev, E., Steinert, R., Nestler, G., Lippert, H., Knoch, M., and Reymond, M.A. (2005). Web-based data warehouse on gene expression in human colorectal cancer. Proteomics 5, 3066-3078.

Sallam, R.M. (2015). Proteomics in cancer biomarkers discovery: challenges and applications. Disease markers 2015, 321370.

Salomonis, N., Hanspers, K., Zambon, A.C., Vranizan, K., Lawlor, S.C., Dahlquist, K.D., Doniger, S.W., Stuart, J., Conklin, B.R., and Pico, A.R. (2007). GenMAPP 2: new features and resources for pathway analysis. BMC bioinformatics 8, 217.

Sargiacomo, M., Sudol, M., Tang, Z., and Lisanti, M.P. (1993). Signal transducing molecules and glycosyl-phosphatidylinositol-linked proteins form a caveolin-rich insoluble complex in MDCK cells. The Journal of cell biology 122, 789-807.

Sawai, A., Chandarlapaty, S., Greulich, H., Gonen, M., Ye, Q., Arteaga, C.L., Sellers, W., Rosen, N., and Solit, D.B. (2008). Inhibition of Hsp90 down-regulates mutant epidermal growth factor receptor (EGFR) expression and sensitizes EGFR mutant tumors to paclitaxel. Cancer research 68, 589-596.

Saykali, B.A., and El-Sibai, M. (2014). Invadopodia, regulation, and assembly in cancer cell invasion. Cell communication & adhesion 21, 207-212.

Schaab, C., Geiger, T., Stoehr, G., Cox, J., and Mann, M. (2012). Analysis of high accuracy, quantitative proteomics data in the MaxQB database. Mol Cell Proteomics 11, M111 014068.

Scherer, P.E., Okamoto, T., Chun, M., Nishimoto, I., Lodish, H.F., and Lisanti, M.P. (1996). Identification, sequence, and expression of caveolin-2 defines a caveolin gene family. Proceedings of the National Academy of Sciences of the United States of America 93, 131-135.

Schlegel, A., Arvan, P., and Lisanti, M.P. (2001). Caveolin-1 binding to endoplasmic reticulum membranes and entry into the regulated secretory pathway are regulated by serine phosphorylation. Protein sorting at the level of the endoplasmic reticulum. The Journal of biological chemistry 276, 4398-4408.

Schmitt, E., Gehrmann, M., Brunet, M., Multhoff, G., and Garrido, C. (2007). Intracellular and extracellular functions of heat shock proteins: repercussions in cancer therapy. Journal of leukocyte biology 81, 15-27.

Shankar, J., Messenberg, A., Chan, J., Underhill, T.M., Foster, L.J., and Nabi, I.R. (2010). Pseudopodial actin dynamics control epithelial-mesenchymal transition in metastatic cancer cells. Cancer research 70, 3780-3790.

Shaul, P.W., Smart, E.J., Robinson, L.J., German, Z., Yuhanna, I.S., Ying, Y., Anderson, R.G., and Michel, T. (1996). Acylation targets emdothelial nitric-oxide synthase to plasmalemmal caveolae. The Journal of biological chemistry 271, 6518-6522.

Shenoy-Scaria, A.M., Dietzen, D.J., Kwong, J., Link, D.C., and Lublin, D.M. (1994). Cysteine3 of Src family protein tyrosine kinase determines palmitoylation and localization in caveolae. The Journal of cell biology 126, 353-363.

Shi, Y., Tan, S.H., Ng, S., Zhou, J., Yang, N.D., Koo, G.B., McMahon, K.A., Parton, R.G., Hill, M.M., Del Pozo, M.A., et al. (2015). Critical role of CAV1/caveolin-1 in cell stress responses in human breast cancer cells via modulation of lysosomal function and autophagy. Autophagy 11, 769-784.

Simons, K., and Ehehalt, R. (2002). Cholesterol, lipid rafts, and disease. The Journal of clinical investigation 110, 597-603.

Simons, K., and Sampaio, J.L. (2011). Membrane organization and lipid rafts. Cold Spring Harbor perspectives in biology 3, a004697.

Simons, K., and Toomre, D. (2000). Lipid rafts and signal transduction. Nat Rev Mol Cell Biol 1, 31-39.

Simons, K., and van Meer, G. (1988). Lipid sorting in epithelial cells. Biochemistry 27, 6197-6202.

Singer, S.J., and Nicolson, G.L. (1972). The fluid mosaic model of the structure of cell membranes. Science (New York, NY 175, 720-731.

Sinha, B., Koster, D., Ruez, R., Gonnord, P., Bastiani, M., Abankwa, D., Stan, R.V., Butler-Browne, G., Vedie, B., Johannes, L., et al. (2011). Cells respond to mechanical stress by rapid disassembly of caveolae. Cell 144, 402-413.

Smart, E.J., Graf, G.A., McNiven, M.A., Sessa, W.C., Engelman, J.A., Scherer, P.E., Okamoto, T., and Lisanti, M.P. (1999). Caveolins, liquid-ordered domains, and signal transduction. Molecular and cellular biology 19, 7289-7304.

Solit, D.B., Zheng, F.F., Drobnjak, M., Munster, P.N., Higgins, B., Verbel, D., Heller, G., Tong, W., Cordon-Cardo, C., Agus, D.B., et al. (2002). 17-Allylamino-17-demethoxygeldanamycin induces the degradation of androgen receptor and HER-2/neu and inhibits the growth of prostate cancer xenografts. Clin Cancer Res 8, 986-993.

Song, K.S., Li, S., Okamoto, T., Quilliam, L.A., Sargiacomo, M., and Lisanti, M.P. (1996). Co-purification and direct interaction of Ras with caveolin, an integral membrane protein of caveolae microdomains. Detergent-free purification of caveolae microdomains. The Journal of biological chemistry 271, 9690-9697.

Sotgia, F., Martinez-Outschoorn, U.E., Howell, A., Pestell, R.G., Pavlides, S., and Lisanti, M.P. (2012). Caveolin-1 and cancer metabolism in the tumor microenvironment: markers, models, and mechanisms. Annual review of pathology 7, 423-467.

Stark, C., Breitkreutz, B.J., Chatr-Aryamontri, A., Boucher, L., Oughtred, R., Livstone, M.S., Nixon, J., Van Auken, K., Wang, X., Shi, X., et al. (2006). The BioGRID Interaction Database: 2011 update. Nucleic acids research 39, D698-704.

Stebbins, C.E., Russo, A.A., Schneider, C., Rosen, N., Hartl, F.U., and Pavletich, N.P. (1997). Crystal structure of an Hsp90-geldanamycin complex: targeting of a protein chaperone by an antitumor agent. Cell 89, 239-250.

Stula, M., Orzechowski, H.D., Gschwend, S., Vetter, R., von Harsdorf, R., Dietz, R., and Paul, M. (2000). Influence of sustained mechanical stress on Egr-1 mRNA expression in cultured human endothelial cells. Molecular and cellular biochemistry 210, 101-108.

Takaguri, A., Kamato, M., Satoh, Y., Ohtsuki, K., and Satoh, K. (2015). Effect of alteration of caveolin-1 expression on doxorubicin-induced apoptosis in H9c2 cardiac cells. Cell biology international 39, 1053-1060.

Takeuchi, K., Morizane, Y., Kamami-Levy, C., Suzuki, J., Kayama, M., Cai, W., Miller, J.W., and Vavvas, D.G. (2013). AMP-dependent kinase inhibits oxidative stress-induced caveolin-1 phosphorylation and endocytosis by suppressing the dissociation between c-Abl and Prdx1 proteins in endothelial cells. The Journal of biological chemistry 288, 20581-20591.

Tang, B., Li, Y., Zhao, L., Yuan, S., Wang, Z., Li, B., and Chen, Q. (2013). Stable isotope dimethyl labeling combined with LTQ mass spectrometric detection, a quantitative proteomics technology used in liver cancer research. Biomedical reports 1, 549-554.

Tang, Z., Okamoto, T., Boontrakulpoontawee, P., Katada, T., Otsuka, A.J., and Lisanti, M.P. (1997). Identification, sequence, and expression of an invertebrate caveolin gene family from the nematode Caenorhabditis elegans. Implications for the molecular evolution of mammalian caveolin genes. The Journal of biological chemistry 272, 2437-2445.

Teodorczyk, M., and Martin-Villalba, A. (2010). Sensing invasion: cell surface receptors driving spreading of glioblastoma. Journal of cellular physiology 222, 1-10.

Tew, K.D., Manevich, Y., Grek, C., Xiong, Y., Uys, J., and Townsend, D.M. (2011). The role of glutathione S-transferase P in signaling pathways and S-glutathionylation in cancer. Free radical biology & medicine 51, 299-313.

Tsai, J.H., and Yang, J. (2013). Epithelial-mesenchymal plasticity in carcinoma metastasis. Genes & development 27, 2192-2206.

Van Aelst, L., and D'Souza-Schorey, C. (1997). Rho GTPases and signaling networks. Genes & development 11, 2295-2322.

Vanneman, M., and Dranoff, G. (2012). Combining immunotherapy and targeted therapies in cancer treatment. Nat Rev Cancer 12, 237-251.

Vanneman, M., and Dranoff, G. (2012). Combining immunotherapy and targeted therapies in cancer treatment. Nat Rev Cancer 12, 237-251.

Vereb, G., Szollosi, J., Matko, J., Nagy, P., Farkas, T., Vigh, L., Matyus, L., Waldmann, T.A., and Damjanovich, S. (2003). Dynamic, yet structured: The cell membrane three decades after the Singer-Nicolson model. Proceedings of the National Academy of Sciences of the United States of America 100, 8053-8058.

Vo, B.T., Morton, D., Jr., Komaragiri, S., Millena, A.C., Leath, C., and Khan, S.A. (2013). TGF-beta effects on prostate cancer cell migration and invasion are mediated by PGE2 through activation of PI3K/AKT/mTOR pathway. Endocrinology 154, 1768-1779.

Volonte, D., Galbiati, F., Pestell, R.G., and Lisanti, M.P. (2001). Cellular stress induces the tyrosine phosphorylation of caveolin-1 (Tyr(14)) via activation of p38 mitogen-activated protein

kinase and c-Src kinase. Evidence for caveolae, the actin cytoskeleton, and focal adhesions as mechanical sensors of osmotic stress. The Journal of biological chemistry 276, 8094-8103.

Wang, R., Li, Z., Guo, H., Shi, W., Xin, Y., Chang, W., and Huang, T. (2014). Caveolin 1 knockdown inhibits the proliferation, migration and invasion of human breast cancer BT474 cells. Molecular medicine reports 9, 1723-1728.

Weisser, J., Lai, Z.W., Bronsert, P., Kuehs, M., Drendel, V., Timme, S., Kuesters, S., Jilg, C.A., Wellner, U.F., Lassmann, S., et al. (2015). Quantitative proteomic analysis of formalin-fixed, paraffin-embedded clear cell renal cell carcinoma tissue using stable isotopic dimethylation of primary amines. BMC genomics 16, 559.

Weng, L., Enomoto, A., Ishida-Takagishi, M., Asai, N., and Takahashi, M. (2009). Girding for migratory cues: roles of the Akt substrate Girdin in cancer progression and angiogenesis. Cancer science 101, 836-842.

Whitmarsh, A.J. (2013). A new regulator of caveolae signalling. eLife 2, e01428.

Wiechen, K., Sers, C., Agoulnik, A., Arlt, K., Dietel, M., Schlag, P.M., and Schneider, U. (2001). Down-regulation of caveolin-1, a candidate tumor suppressor gene, in sarcomas. The American journal of pathology 158, 833-839.

Williams, T.M., Lee, H., Cheung, M.W., Cohen, A.W., Razani, B., Iyengar, P., Scherer, P.E., Pestell, R.G., and Lisanti, M.P. (2004). Combined loss of INK4a and caveolin-1 synergistically enhances cell proliferation and oncogene-induced tumorigenesis: role of INK4a/CAV-1 in mammary epithelial cell hyperplasia. The Journal of biological chemistry 279, 24745-24756.

Williams, T.M., and Lisanti, M.P. (2004). The caveolin proteins. Genome biology 5, 214.

Wolf, K., Wu, Y.I., Liu, Y., Geiger, J., Tam, E., Overall, C., Stack, M.S., and Friedl, P. (2007). Multi-step pericellular proteolysis controls the transition from individual to collective cancer cell invasion. Nature cell biology 9, 893-904.

Wong, I.Y., Javaid, S., Wong, E.A., Perk, S., Haber, D.A., Toner, M., and Irimia, D. (2014). Collective and individual migration following the epithelial-mesenchymal transition. Nature materials 13, 1063-1071.

Worth, D.C., and Parsons, M. (2008). Adhesion dynamics: mechanisms and measurements. The international journal of biochemistry & cell biology 40, 2397-2409.

Yamada, E. (1955). The fine structure of the gall bladder epithelium of the mouse. The Journal of biophysical and biochemical cytology 1, 445-458.

Yamamoto, M., Toya, Y., Jensen, R.A., and Ishikawa, Y. (1999). Caveolin is an inhibitor of platelet-derived growth factor receptor signaling. Experimental cell research 247, 380-388.

Yang, J., Mani, S.A., Donaher, J.L., Ramaswamy, S., Itzykson, R.A., Come, C., Savagner, P., Gitelman, I., Richardson, A., and Weinberg, R.A. (2004). Twist, a master regulator of morphogenesis, plays an essential role in tumor metastasis. Cell 117, 927-939.

Yang, J., and Weinberg, R.A. (2008). Epithelial-mesenchymal transition: at the crossroads of development and tumor metastasis. Developmental cell 14, 818-829.

Yao, D., Dai, C., and Peng, S. (2011). Mechanism of the mesenchymal-epithelial transition and its relationship with metastatic tumor formation. Mol Cancer Res 9, 1608-1620.

Zajchowski, L.D., and Robbins, S.M. (2002). Lipid rafts and little caves. Compartmentalized signalling in membrane microdomains. European journal of biochemistry / FEBS 269, 737-752.

Zeichner, S.B., Terawaki, H., and Gogineni, K. (2016). A Review of Systemic Treatment in Metastatic Triple-Negative Breast Cancer. Breast Cancer (Auckl) 10, 25-36.

Zhan, Y., Wang, L., Liu, J., Ma, K., Liu, C., Zhang, Y., and Zou, W. (2013). Choline plasmalogens isolated from swine liver inhibit hepatoma cell proliferation associated with caveolin-1/Akt signaling. PloS one 8, e77387.

Zhang, H., and Burrows, F. (2004). Targeting multiple signal transduction pathways through inhibition of Hsp90. Journal of molecular medicine (Berlin, Germany) 82, 488-499.

Zhang, W., Razani, B., Altschuler, Y., Bouzahzah, B., Mostov, K.E., Pestell, R.G., and Lisanti, M.P. (2000). Caveolin-1 inhibits epidermal growth factor-stimulated lamellipod extension and cell migration in metastatic mammary adenocarcinoma cells (MTLn3). Transformation suppressor effects of adenovirus-mediated gene delivery of caveolin-1. The Journal of biological chemistry 275, 20717-20725.

Zhang, X., Ling, M.T., Wang, Q., Lau, C.K., Leung, S.C., Lee, T.K., Cheung, A.L., Wong, Y.C., and Wang, X. (2007). Identification of a novel inhibitor of differentiation-1 (ID-1) binding partner, caveolin-1, and its role in epithelial-mesenchymal transition and resistance to apoptosis in prostate cancer cells. The Journal of biological chemistry 282, 33284-33294.

Zhao, R., and Houry, W.A. (2005). Hsp90: a chaperone for protein folding and gene regulation. Biochemistry and cell biology = Biochimie et biologie cellulaire 83, 703-710.

Zheng, Y.Z., Boscher, C., Inder, K.L., Fairbank, M., Loo, D., Hill, M.M., Nabi, I.R., and Foster, L.J. (2011). Differential impact of caveolae and caveolin-1 scaffolds on the membrane raft proteome. Mol Cell Proteomics 10, M110 007146.

Zhu, H., Bilgin, M., Bangham, R., Hall, D., Casamayor, A., Bertone, P., Lan, N., Jansen, R., Bidlingmaier, S., Houfek, T., et al. (2001). Global analysis of protein activities using proteome chips. Science (New York, NY 293, 2101-2105.

Zhu, H., Klemic, J.F., Chang, S., Bertone, P., Casamayor, A., Klemic, K.G., Smith, D., Gerstein, M., Reed, M.A., and Snyder, M. (2000). Analysis of yeast protein kinases using protein chips. Nature genetics 26, 283-289.

Zhu, X., Zhang, Y., Li, Q., Yang, L., Zhang, N., Ma, S., Zhang, K., Song, J., and Guan, F. (2016). beta-Carotene Induces Apoptosis in Human Esophageal Squamous Cell Carcinoma Cell Lines via the Cav-1/AKT/NF-kappaB Signaling Pathway. Journal of biochemical and molecular toxicology 30, 148-157.

Zou, Y., and Wang, Y. (2007). Mass spectrometric analysis of high-mobility group proteins and their post-translational modifications in normal and cancerous human breast tissues. Journal of proteome research 6, 2304-2314.

Zundel, W., Swiersz, L.M., and Giaccia, A. (2000). Caveolin 1-mediated regulation of receptor tyrosine kinase-associated phosphatidylinositol 3-kinase activity by ceramide. Molecular and cellular biology 20, 1507-1514.